

~~72168~~

N84-27730

NASA CR-165592

PWA 5594-167



LOW-PRESSURE TURBINE SUBSONIC CASCADE
TECHNOLOGY REPORT

ENERGY EFFICIENT ENGINE
COMPONENT DEVELOPMENT AND INTEGRATION PROGRAM

by

Om P. Sharma, et al.

UNITED TECHNOLOGIES CORPORATION
Pratt & Whitney Aircraft
Commercial Products Division

Because of their possible significant early commercial value, these data

ed

data. This legend shall be marked on any reproduction of these data in whole or in part.

Prepared for

NATIONAL AERONAUTICS AND SPACE ADMINISTRATION
Lewis Research Center
Cleveland, Ohio 44135
Contract NAS3-20646



.

)



400 Main Street
East Hartford, Connecticut 06108

Commercial Products Division

In reply please refer to:
WBG:WS - E1M3 (4872n)
LC--82-11

8 February 1982

To: National Aeronautics and Space Administration
Lewis Research Center
21000 Brookpark Road
Cleveland, OH 44135

Attention: Mr. Carl C. Ciepluch, Mail Stop 301-4

Subject: Energy Efficient Engine Low-Pressure Turbine Subsonic
Cascade Technology Report (PWA-5594-167)

References: (a) Letter, Carl C. Ciepluch to W.B. Gardner,
"Contract NAS3-20646 - Low-Pressure Turbine
Subsonic Cascade Technology Report
(WBS 4.2.6.2.2), "dated January 29, 1982,
ref. 2321

(b) Contract No. NAS3-20646

Enclosures: 20 Copies of the subject report

Gentlemen:

Enclosed are twenty (20) copies of the subject report, revised in accordance with the requirements of reference (a). Distribution is being made in compliance with reference (b).

Sincerely yours,

UNITED TECHNOLOGIES CORPORATION
Pratt & Whitney Aircraft Group
Commercial Products Division

A handwritten signature in cursive script, appearing to read "W B Gardner".

W. B. Gardner
Program Manager

cc: Administrative Contracting Officer (Letter Only)
Air Force Plant Representative Office
Pratt & Whitney Aircraft Group
East Hartford, CT 06108

1. REPORT NO. NASA CR-165592	2. GOVERNMENT AGENCY	3. RECIPIENT'S CATALOG NO.	
4. TITLE AND SUBTITLE ENERGY EFFICIENT ENGINE LOW-PRESSURE TURBINE SUBSONIC CASCADE COMPONENT DEVELOPMENT AND INTEGRATION PROGRAM		5. REPORT DATE January 1982	6. PERFORMING ORG. CODE
		8. PERFORMING ORG. REPT. NO. PWA-5594-167	
7. AUTHOR(S) O.P. Sharma, F.C. Kopper, L.K. Knudsen, J.B. Yustinich		10. WORK UNIT NO.	
9. PERFORMING ORG. NAME AND ADDRESS UNITED TECHNOLOGIES CORPORATION Pratt & Whitney Aircraft Group Commercial Products Division		11. CONTRACT OR GRANT NO. NAS3-20646	
		13. TYPE REPT./PERIOD COVERED TECHNOLOGY REPORT	
12. SPONSORING AGENCY NAME AND ADDRESS National Aeronautics and Space Administration Lewis Research Center 21000 Brookpark Road, Cleveland, Ohio 44135		14. SPONSORING AGENCY CODE	
		15. SUPPLEMENTARY NOTES Prepared in cooperation with NASA Project Manager, C. C. Ciepluch NASA Lewis Research Center, Cleveland, Ohio	
16. ABSTRACT A subsonic cascade test program was conducted to provide technical data for optimizing the blade and vane airfoil designs for the Energy Efficient Engine Low-Pressure Turbine component. The program consisted of three parts. The first involved an evaluation of the low-camber inlet guide vane. The second, was an evaluation of two candidate aerodynamic loading philosophies for the fourth blade root section. The third part consisted of an evaluation of three candidate airfoil geometries for the fourth blade mean section. The performance of each candidate airfoil was evaluated in a linear cascade configuration. The overall results of this study indicate that the 'aft-loaded' airfoil designs resulted in lower losses which substantiated Pratt & Whitney Aircraft's design philosophy for the Energy Efficient Engine low-pressure turbine component.			
17. KEY WORDS (SUGGESTED BY AUTHOR(S)) Aft-Loaded Airfoils Squared-Off Airfoils Energy Efficient Engine Low Turbine Subsonic Cascade Airfoil Test		[REDACTED]	
19. SECURITY CLASS THIS (REPT) UNCLASSIFIED	20. SECURITY CLASS THIS (PAGE) UNCLASSIFIED	21. NO. PGS	22. PRICE *

FOREWORD

The Energy Efficient Engine Component Development and Integration Program is being conducted under parallel National Aeronautics and Space Administration contracts to Pratt & Whitney Aircraft Group and General Electric Company. The overall project is under the direction of Mr. Carl C. Ciepluch. Mr. John W. Schaefer is the NASA assistant project manager for the Pratt & Whitney Aircraft effort under NASA Contract NAS3-20646. The NASA project engineer responsible for the portion of the project described in this report is Mr. Michael Vanco. Mr. William B. Gardner is manager of the Energy Efficient Engine Program at Pratt & Whitney Aircraft Group. Principal contributors to this report were Dr. Om P. Sharma and Mr. Frederick C. Kopper.

TABLE OF CONTENTS

<u>Section</u>	<u>Page</u>
1.0 SUMMARY	1
2.0 INTRODUCTION	3
3.0 ANALYSIS AND DESIGN	5
3.1 Low Camber Vane Cascade	5
3.2 Blade Cascades	6
3.2.1 Alternate Loading Cascades	11
3.2.2 Airfoil Design Concept Cascades	13
4.0 FABRICATION AND ASSEMBLY	17
5.0 TESTING	18
5.1 General Description	18
5.2 Test Facility and Instrumentation	18
5.2.1 Test Facility	18
5.2.2 Test Instrumentation	18
5.3 Test Procedures	22
5.3.1 Establishing Test Conditions	22
5.3.2 Shakedown Testing	22
5.3.3 Performance Testing	22
5.3.4 Performance Test Plans	23
5.4 Data Reduction and Analysis	26
6.0 RESULTS	28
6.1 Low Camber Vane Cascade Performance	28
6.1.1 Flow Visualization	28
6.1.2 Performance Results	30
6.1.2.1 Airfoil Pressure Distributions	30
6.1.2.2 Design Point Loss	34
6.1.2.3 Off-Design Profile Loss	37
6.2 Fourth Stage Blade Cascade Performance	38
6.2.1 Flow Visualization	38
6.2.2 Airfoil Pressure Distributions	40
6.2.3 Design Point Loss	40
6.2.4 Off-Design Loss	51
6.3 Design Concept Verification	52
6.3.1 Airfoil Pressure Distributions	52
6.3.2 Design Point Loss	52
6.3.3 Off-Design Loss	68
6.4 Cascade Vs. Boundary Layer Tunnel Tests	71

Table Of Contents (continued)

7.0	SUMMARY OF RESULTS	72
7.1	Surface Static Pressure Data vs. Pratt & Whitney Aircraft Potential Flow Prediction Method	72
7.2	Loss Assessment	72
7.2.1	Low Camber Vane	72
7.2.2	Transonic 'Aft-loaded' Versus Subsonic 'Squared-off' for Root Section	72
7.2.3	'Aft-loaded' Versus 'Heavyweight' and 'Lightweight' Design for the Mean Section	73
APPENDIX A - AIRFOIL COORDINATES		
A-1	Coordinates for Low Camber Vane Airfoil	74
A-2	Coordinates for Subsonic 'Squared-off' Airfoil	75
A-3	Coordinates for Transonic 'Aft-loaded' Airfoil	76
A-4	Coordinates for Heavyweight Airfoil	77
A-5	Coordinates for Lightweight Airfoil	78
APPENDIX B - REFERENCES		79
APPENDIX C - LIST OF SYMBOLS		80

LIST OF ILLUSTRATIONS

<u>Number</u>	<u>Title</u>	<u>Page</u>
2-1	Low-Pressure Turbine Subsonic Cascade Program Logic Diagram	4
3-1	Low-Pressure Turbine Inlet Vane Flow	6
3-2	Low Camber Vane Shape and Predicted Pressure Distribution	7
3-3	Low Camber Vane Cascade Pack Details	9
3-4	Alternate Loading Distribution for Two Airfoils Having the Same Load Coefficient and Velocity Triangle	10
3-5	Alternate Loading Distribution for Fourth Blade Root Section 'Aft-Loaded' Transonic Versus 'Squared-Off' Subsonic	12
3-6	Cascade Pack Dimensions	14
3-7	'Aft-Loaded' Versus 'Heavyweight' Versus 'Lightweight' Designs	15
5-1	Cascade Test Facility	19
5-2	Low Camber Vane Cascade Nominal Static Pressure Tap Locations	20
5-3	Blade Cascade Typical Static Pressure Tap Locations	21
5-4	Wake Mixing Control Volume	27
6-1	Flow Visualization at -13.0 Degrees Incidence Showing Pressure Surface Separation Bubble	29
6-2	Endwall Flow Schematic	30
6-3 (a)	Predicted Versus Measured Airfoil Surface Static Pressure Distribution at -4.3 Degrees Incidence	31
6-3 (b)	Predicted Versus Measured Airfoil Surface Static Pressure Distribution at -7.9 Degrees Incidence	31

LIST OF ILLUSTRATIONS (Continued)

<u>Number</u>	<u>Title</u>	<u>Page</u>
6-3 (c)	Predicted Versus Measured Airfoil Surface Static Pressure Distribution at -11.1 Degrees Incidence	32
6-3 (d)	Predicted Versus Measured Airfoil Surface Static Pressure Distribution at -13.0 Degrees Incidence	32
6-3 (e)	Predicted Versus Measured Airfoil Surface Static Pressure Distribution at +2.4 Degrees Incidence	33
6-3 (f)	Predicted Versus Measured Airfoil Surface Static Pressure Distribution at +5.9 Degrees Incidence	33
6-3 (g)	Predicted Versus Measured Airfoil Surface Static Pressure Distribution at +9.3 Degrees Incidence	34
6-4	Bubble Simulation at +9.3 Degrees Incidence	35
6-5	Loss Contours for -4.3 Degrees Incidence Data Point	36
6-6	Design Point Spanwise Loss Profile	37
6-7	Loss Versus Incidence for the Low Camber Vane	38
6-8	Subsonic 'Squared-Off' Suction Surface Flow Visualization	39
6-9	Transonic 'Aft-Loaded' Suction Surface Flow Visualization	39
6-10 (a)	'Aft-Loaded' Airfoil - Predicted Versus Measured Pressure Distribution at -4.72 Degrees Incidence, Mach Number 0.784	41
6-10 (b)	'Aft-Loaded' Airfoil - Predicted Versus Measured Pressure Distribution at -4.72 Degrees Incidence, Mach Number 0.852	41
6-10 (c)	'Aft-Loaded' Airfoil - Predicted Versus Measured Pressure Distribution at -4.72 Degrees Incidence, Mach Number 0.881	42
6-10 (d)	'Aft-Loaded' Airfoil - Predicted Versus Measured Pressure Distribution at -4.72 Degrees Incidence, Mach Number 0.937	42

LIST OF ILLUSTRATIONS (Continued)

<u>Number</u>	<u>Title</u>	<u>Page</u>
6-10 (e)	'Aft-Loaded' Airfoil - Predicted Versus Measured Pressure Distribution at -4.72 Degrees Incidence, Mach Number 0.969	43
6-10 (f)	'Aft-Loaded' Airfoil - Predicted Versus Measured Pressure Distribution at +5.28 Degrees Incidence, Mach Number 0.770	43
6-10 (g)	'Aft-Loaded' Airfoil - Predicted Versus Measured Pressure Distribution at +0.28 Degrees Incidence, Mach Number 0.776	44
6-10 (h)	'Aft-Loaded' Airfoil - Predicted Versus Measured Pressure Distribution at -9.72 Degrees Incidence, Mach Number 0.778	44
6-10 (i)	'Aft-Loaded' Airfoil - Predicted Versus Measured Pressure Distribution at -14.72 Degrees Incidence, Mach Number 0.777	45
6-11 (a)	'Squared-Off' Airfoil - Predicted Versus Measured Pressure Distribution at -4.71 Degrees Incidence, Mach Number 0.779	45
6-11 (b)	'Squared-Off' Airfoil - Predicted Versus Measured Pressure Distribution at -4.71 Degrees Incidence, Mach Number 0.845	46
6-11 (c)	'Squared-Off' Airfoil - Predicted Versus Measured Pressure Distribution at -4.71 Degrees Incidence, Mach Number 0.891	46
6-11 (d)	'Squared-Off' Airfoil - Predicted Versus Measured Pressure Distribution at -4.71 Degrees Incidence, Mach Number 0.940	47
6-11 (e)	'Squared-Off' Airfoil - Predicted Versus Measured Pressure Distribution at +0.29 Degrees Incidence, Mach Number 0.777	47
6-11 (f)	'Squared-Off' Airfoil - Predicted Versus Measured Pressure Distribution at +3.3 Degrees Incidence, Mach Number 0.773	48

LIST OF ILLUSTRATIONS (Continued)

<u>Number</u>	<u>Title</u>	<u>Page</u>
6-11 (g)	'Squared-Off' Airfoil - Predicted Versus Measured Pressure Distribution at -9.71 Degrees Incidence, Mach Number 0.776	48
6-11 (h)	'Squared-Off' Airfoil - Predicted Versus Measured Pressure Distribution at -11.71 Degrees Incidence, Mach Number 0.779	49
6-11 (i)	'Squared-Off' Airfoil - Predicted Versus Measured Pressure Distribution at -16.71 Degrees Incidence, Mach Number 0.776	49
6-12	'Squared-Off' and 'Aft-Loaded' Airfoils Predicted Versus Measured Mixed-Out, Mid-Span Losses	50
6-13	'Squared-Off' and 'Aft-Loaded' Airfoils Measured Gap-Averaged Secondary Losses	50
6-14	Subsonic 'Squared-Off' and Transonic 'Aft-Loaded' Airfoils Predicted Versus Measured Profile Loss Data	51
6-15 (a)	'Aft-Loaded' Baseline - Predicted Versus Measured Pressure Distribution at -4.72 Degrees Incidence, Mach Number 0.724	53
6-15 (b)	'Aft-Loaded' Baseline - Predicted Versus Measured Pressure Distribution at -4.72 Degrees Incidence, Mach Number 0.633	53
6-15 (c)	'Aft-Loaded' Baseline - Predicted Versus Measured Pressure Distribution at -4.72 Degrees Incidence, Mach Number 0.837	54
6-15 (d)	'Aft-Loaded' Baseline - Predicted Versus Measured Pressure Distribution at -4.72 Degrees Incidence, Mach Number 0.887	54
6-15 (e)	'Aft-Loaded' Baseline - Predicted Versus Measured Pressure Distribution at -4.72 Degrees Incidence, Mach Number 0.939	55

LIST OF ILLUSTRATIONS (Continued)

<u>Number</u>	<u>Title</u>	<u>Page</u>
6-15 (f)	'Aft-Loaded' Baseline - Predicted Versus Measured Pressure Distribution at +0.282 Degrees Incidence, Mach Number 0.724	55
6-15 (g)	'Aft-Loaded' Baseline - Predicted Versus Measured Pressure Distribution at +5.282 Degrees Incidence, Mach Number 0.718	56
6-15 (h)	'Aft-Loaded' Baseline - Predicted Versus Measured Pressure Distribution at -9.72 Degrees Incidence, Mach Number 0.729	56
6-15 (i)	'Aft-Loaded' Baseline - Predicted Versus Measured Pressure Distribution at -14.72 Degrees Incidence, Mach Number 0.731	57
6-15 (j)	'Aft-Loaded' Baseline - Predicted Versus Measured Pressure Distribution at -19.72 Degrees Incidence, Mach Number 0.728	57
6-16 (a)	'Heavyweight' - Predicted Versus Measured Pressure Distribution at -4.72 Degrees Incidence, Mach Number 0.721	58
6-16 (b)	'Heavyweight' - Predicted Versus Measured Pressure Distribution at -4.72 Degrees Incidence, Mach Number 0.631	58
6-16 (c)	'Heavyweight' - Predicted Versus Measured Pressure Distribution at -4.72 Degrees Incidence, Mach Number 0.82	59
6-16 (d)	'Heavyweight' - Predicted Versus Measured Pressure Distribution at -4.72 Degrees Incidence, Mach Number 0.87	59
6-16 (e)	'Heavyweight' - Predicted Versus Measured Pressure Distribution at -4.72 Degrees Incidence, Mach Number 0.91	60
6-16 (f)	'Heavyweight' - Predicted Versus Measured Pressure Distribution at +0.285 Degrees Incidence, Mach Number 0.715	60

LIST OF ILLUSTRATIONS (Continued)

<u>Number</u>	<u>Title</u>	<u>Page</u>
6-16 (g)	'Heavyweight' - Predicted Versus Measured Pressure Distribution at +5.28 Degrees Incidence, Mach Number 0.716	61
6-16 (h)	'Heavyweight' - Predicted Versus Measured Pressure Distribution at -9.72 Degrees Incidence, Mach Number 0.723	61
6-16 (i)	'Heavyweight' - Predicted Versus Measured Pressure Distribution at -14.72 Degrees Incidence, Mach Number 0.723	62
6-16 (j)	'Heavyweight' - Predicted Versus Measured Pressure Distribution at -19.72 Degrees Incidence, Mach Number 0.727	62
6-17 (a)	'Lightweight' - Predicted Versus Measured Pressure Distribution at +0.2862 Degrees Incidence, Mach Number 0.723	63
6-17 (b)	'Lightweight' - Predicted Versus Measured Pressure Distribution at +0.2862 Degrees Incidence, Mach Number 0.632	63
6-17 (c)	'Lightweight' - Predicted Versus Measured Pressure Distribution at +0.2862 Degrees Incidence, Mach Number 0.836	64
6-17 (d)	'Lightweight' - Predicted Versus Measured Pressure Distribution at +0.2862 Degrees Incidence, Mach Number 0.883	64
6-17 (e)	'Lightweight' - Predicted Versus Measured Pressure Distribution at +0.2862 Degrees Incidence, Mach Number 0.92	65
6-17 (f)	'Lightweight' - Predicted Versus Measured Pressure Distribution at +5.2862 Degrees Incidence, Mach Number 0.75	65
6-17 (g)	'Lightweight' - Predicted Versus Measured Pressure Distribution at +10.2862 Degrees Incidence, Mach Number 0.712	66

LIST OF ILLUSTRATIONS (Continued)

<u>Number</u>	<u>Title</u>	<u>Page</u>
6-17 (h)	'Lightweight' - Predicted Versus Measured Pressure Distribution at -4.72 Degrees Incidence, Mach Number 0.726	66
6-17 (i)	'Lightweight' - Predicted Versus Measured Pressure Distribution at -9.72 Degrees Incidence, Mach Number 0.726	67
6-17 (j)	'Lightweight' - Predicted Versus Measured Pressure Distribution at -14.72 Degrees Incidence, Mach Number 0.729	67
6-18	Baseline, Heavyweight, Lightweight - Predicted Versus Measured Mixed-Out Mid-Span Losses at Design Point Incidence, Variable Mach Numbers	68
6-19	Aft-Loaded, Heavyweight, Lightweight - Predicted Versus Measured Mixed-Out Profile Loss Over Range of Incidence, Fixed Exit Mach Number	69
6-20	'Aft-Loaded' Baseline - Predicted Versus Measured Gap-Averaged Secondary Loss Over Range of Incidence, Fixed Exit Mach Number	70
6-21	Lightweight - Predicted Versus Measured Gap-Averaged Secondary Loss Over Range of Incidence, Fixed Exit Mach Number	70

SECTION 1.0 SUMMARY

This report presents results of a subsonic cascade test program whose purpose was to provide a portion of the technical input required to optimize and verify the blade and vane airfoil designs selected for the Energy Efficient Engine Low-Pressure Turbine Component.

The program was conducted in three parts; the first being an evaluation of the low-camber inlet guide vane; the second, an evaluation of two candidate aerodynamic loading philosophies for the fourth blade root section, and the third; an evaluation of three candidate airfoil geometries for the fourth blade mean section. Results from these studies are summarized below.

The first part of the study was designed to test the mean section of the first vane of the Energy Efficient Engine low-pressure turbine to evaluate the performance of the airfoil in terms of surface static pressure distribution and profile loss for a range of incidence angles. Both the airfoil surface static pressure distributions and the profile losses were found to be in good agreement with Pratt & Whitney Aircraft prediction methods. Measurements of secondary losses were also obtained at the design point and were fairly well predicted by Pratt & Whitney Aircraft cascade loss correlations. Available secondary loss correlations from literature were found to underestimate the magnitude of these losses. Airfoil surface flow visualization and measured surface static pressure distribution data indicate the presence of separation bubbles in the leading edge regions of the airfoil. These separation bubbles were found to be on the pressure surface of the airfoil for extreme negative incidence and on the suction surface for positive incidence.

In the second part of this three-part study, two candidate airfoil designs for the root section of the fourth stage blade row of the Energy Efficient Engine low-pressure turbine were tested to evaluate their relative performance in terms of airfoil surface static pressure distribution and profile losses for a range of incidence angles and Mach numbers. One of these airfoils had a transonic 'aft-loaded' pressure distribution while the other had a subsonic 'squared-off' pressure distribution. Both airfoils had the same leading and trailing edge wedge angles, same gas angles, and were designed for the same Zweifel's load coefficient. Measured data for airfoil surface static pressure distributions and profile losses for each cascade were found to be in good agreement with Pratt & Whitney Aircraft prediction methods. The 'aft-loaded' airfoil was found to have lower profile losses than the 'squared-off' airfoil over the entire range of Mach numbers. Endwall loss data were obtained at the design point for each cascade; both airfoil sections generated almost equal losses. Measured endwall loss data were found to be in good agreement with the Pratt & Whitney Aircraft cascade endwall loss correlation. Available endwall loss correlations from literature were found to be in poor agreement with the measured data by as much as ± 80 percent.

In the final part of this investigation, three airfoil sections representing the mean section of the fourth stage blade of the Energy Efficient Engine low-pressure turbine were tested in terms of airfoil surface static pressure distribution and profile losses for a range of incidence angles and Mach numbers. All three of these airfoils were designed for the same gas velocity triangles and Zweifel's load coefficient. One of these airfoils had an 'aft-loaded' pressure distribution while the other two had a 'squared-off' type of pressure distribution. One of these 'squared-off' airfoils had the same leading and trailing edge wedge angles as the 'aft-loaded' airfoil and was termed the 'heavyweight' airfoil. The other 'squared-off' airfoil had almost the same surface static pressure distribution as the 'heavyweight' airfoil but it was designed for lower inlet and exit wedge angles to yield a thin airfoil. This design is referred to as the 'lightweight' airfoil. Measured data for airfoil surface static pressure distribution and profile losses for all three airfoils were found to be in good agreement with Pratt & Whitney Aircraft prediction methods over the entire range of Mach numbers and incidence angles. The 'aft-loaded' airfoil was found to have lower profile losses than either the 'heavyweight' or the 'lightweight' airfoils. Compared to the 'aft-loaded' airfoil at the design point, the 'lightweight' and 'heavyweight' airfoils had 34 percent and 21 percent higher profile losses, respectively. High losses for the 'lightweight' airfoil were attributable to larger overspeeds in the leading edge region of the airfoil as compared to the 'heavyweight' and 'aft-loaded' airfoil designs. Secondary loss measurements were also obtained for the 'aft-loaded' and 'lightweight' airfoils at three separate incidence angles. The 'aft-loaded' airfoil was found to have lower secondary losses as compared to the 'lightweight' design. Measured secondary loss data were found to be in reasonably good agreement with the Pratt & Whitney Aircraft cascade loss correlation. Available loss correlations from literature were found to overestimate and underestimate the data by as much as + 100 percent.

The overall results of this current study indicate that the 'aft-loaded' airfoil design generates lower losses than the 'squared-off' airfoil design thus substantiating Pratt & Whitney Aircraft's "design philosophy" for the Energy Efficient Engine low-pressure turbine component.

SECTION 2.0 INTRODUCTION

The objective of the NASA Energy Efficient Engine Component Development and Integration program is to develop, evaluate, and demonstrate the technology for achieving lower installed fuel consumption and lower operating costs in future commercial turbofan engines. NASA has set minimum goals of 12 percent reduction in thrust specific fuel consumption, 5 percent reduction in direct operating cost, and 50 percent reduction in performance degradation for the Energy Efficient Engine (flight engine) relative to the JT9D-7A reference engine. In addition, environmental goals for emissions (to meet the proposed Environmental Protection Agency 1981 regulation) and noise (to meet Federal Aviation Regulation 36-1978) have been established.

The purpose of the Energy Efficient Engine low-pressure turbine subsonic cascade test program was to provide the technical input necessary to optimize the blade and vane airfoil designs of the low-pressure turbine component. The counterrotation feature of the Energy Efficient Engine's high-pressure and low-pressure turbines results in a first stage low-pressure turbine vane with a low turning level (low camber). This is a unique feature of the Energy Efficient Engine low-pressure turbine. Because of the lack of experimental data available for low turning accelerating cascades, the mean section of the low camber vane was tested in a cascade configuration. In addition, tests were also conducted to evaluate the performance of four blade cascade packs in order to substantiate the Pratt & Whitney Aircraft approach towards designing airfoil sections for the low-pressure turbine component. Data from both the vane and blade tests were collected, reduced and analysed in the post-test analysis phase.

The program was conducted to ensure timely interaction with the low-pressure turbine component effort, as summarized in Figure 2-1.

This report presents the program test procedures and results concerning the low camber vane configuration and blade configurations for the low-pressure turbine. The analysis and design effort leading to the fabrication and assembly of the test configurations is described in section 3.0. Sections 4.0 and 5.0 provide a discussion of the fabrication/assembly effort and the test programs, respectively. A detailed discussion of low-pressure turbine subsonic cascade test results is contained in section 6.0.

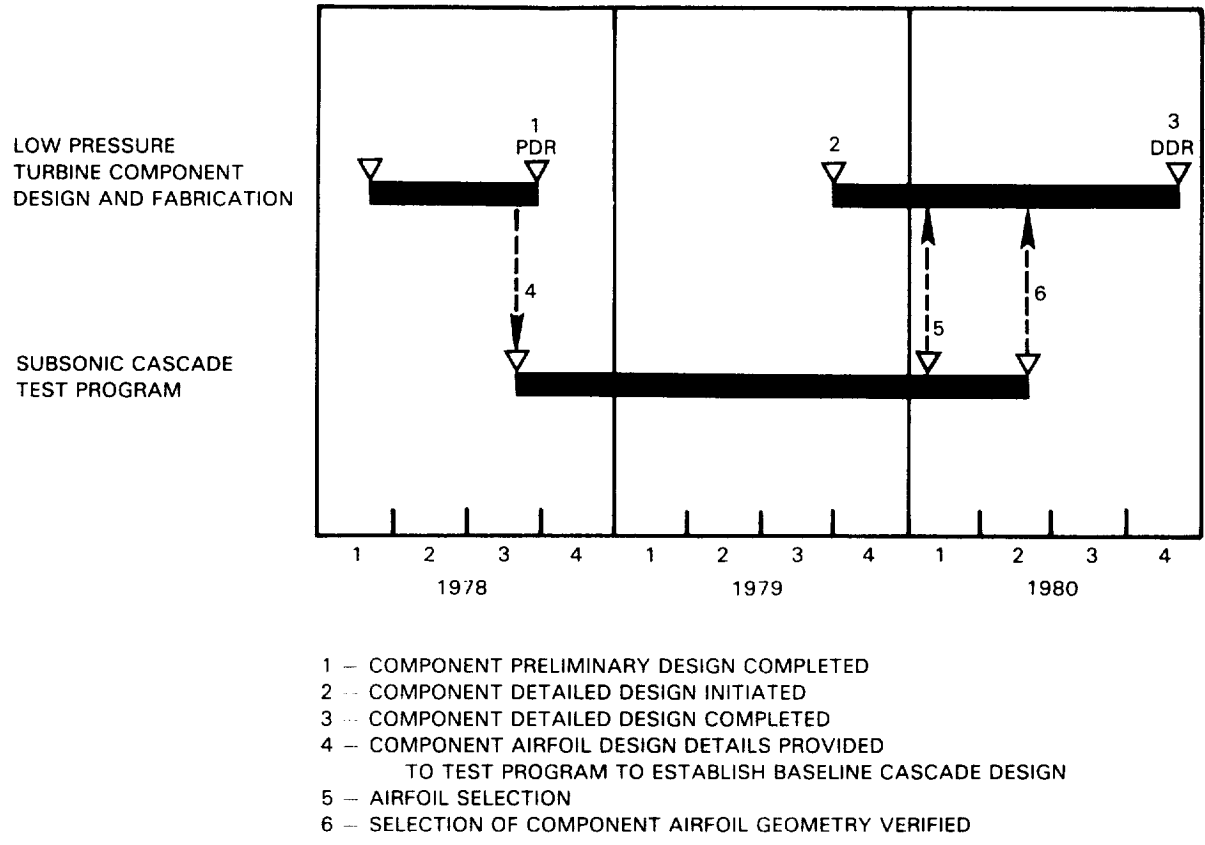


Figure 2-1 Low-Pressure Turbine Subsonic Cascade Program Logic Diagram

SECTION 3.0 ANALYSIS AND DESIGN

Two of the technology advances incorporated into the design of the Energy Efficient Engine low-pressure turbine to improve its efficiency were: (1) counterrotation of the low-pressure turbine with respect to the high-pressure turbine, and (2) reduced through-flow velocity ratio (C_x/U) coupled with 'low-loss' laminar-transitional airfoil contours. Both of these resulted in airfoil geometries sufficiently different from more conventional designs that experimental verification of their predicted performance characteristics was required.

The purpose of the analysis and design effort was to convert low-pressure turbine airfoil design characteristics into test rig cascades that would accurately simulate the component flow conditions of interest. The intent of this effort was to substantiate component design concepts and analysis methods and provide information useful to the execution of the component designs.

The design of these cascades and the basis for their design are described in the following sections.

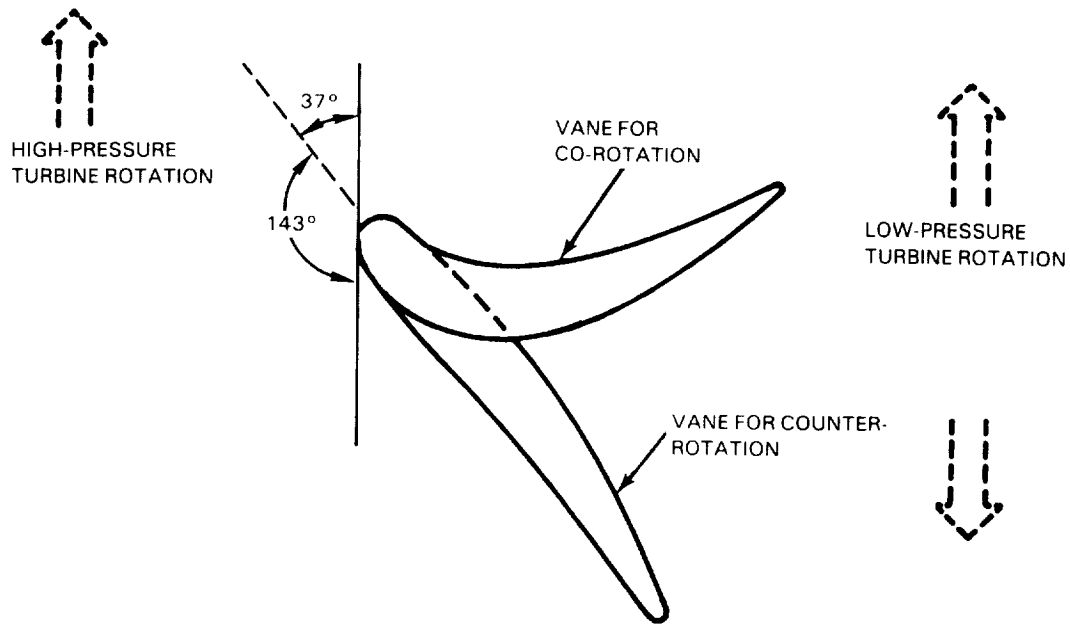
3.1 Low Camber Vane Cascade

Counterrotating high and low-pressure turbines were selected for the Energy Efficient Engine because this feature provides a potential 0.5 percent improvement in low-pressure turbine efficiency. By rotating the high and low-pressure turbine shafts in opposite directions, the swirl in the flow entering the low-pressure turbine from the high-pressure turbine is also reversed. This swirl reversal reduces the low-pressure turbine inlet vane flow turning from 100 degrees to 13 degrees as shown in Figure 3-1. The resulting low camber vane configuration is predicted to have a pressure loss nominally 55 percent that of a typical co-rotating vane design and this loss reduction translates into the component efficiency benefit noted.

In addition to the potential performance benefits associated with this vane design, the reduction in gas loads on the airfoil reduces airfoil stresses and loads transmitted to the turbine cases.

Because of the lack of experimental data available for low turning accelerating cascades, a low camber vane cascade was designed to:

- o evaluate the two-dimensional performance of the low camber vane as a function of inlet air angle (incidence) with the exit Mach number held fixed at its design value;
- o obtain secondary loss data at design incidence and Mach number in order to assess the overall performance characteristics of the vane.



	<u>CO-ROTATION</u>	<u>COUNTERROTATION</u>
VANE GAS INLET ANGLE (DEG)	37.0	143.0
VANE GAS TURNING (DEG)	100	13
COUNTERROTATION BENEFIT $\Delta\eta$ (%)	0.5	

Figure 3-1 Low-Pressure Turbine Inlet Vane Flow

The mean airfoil section of the low-pressure turbine component low camber vane was selected for cascade testing. Figure 3-2 shows the contour of this airfoil and its predicted pressure distribution at 50 percent span in the cascade configuration. Table 3-I lists the geometric and aerodynamic parameters for the low camber vane while Appendix A-1 lists the airfoil coordinates.

The resultant cascade pack based on this design is illustrated in Figure 3-3. This pack comprises twelve airfoils with a 3.126 cm (1.231 in) pitch and a 7.620 cm (3.0 in) span. The aspect ratio of the airfoils is 3.246. For rig size, the airfoil contour was scaled to 0.56 of the full-size low-pressure turbine component. Overall pack dimensions, as well as airfoil locations are also shown in Figure 3-3. Cascade pack endwalls were planar. Provisions for static pressure instrumentation are included at the mid-span in the fourth, fifth, and sixth airfoils. Details of this instrumentation are discussed in Section 5.2.2 of this report.

3.2 Blade Cascades

Extensive test data from Pratt & Whitney Aircraft rotating rig testing of various full-size low-pressure turbines has indicated that, for a given level of loading, turbine stages in which the boundary layer was predicted to be predominately laminar or transitional have measured efficiencies which are considerable higher than those turbine stages in which the boundary layer was predicted to be predominately turbulent. The total predicted benefit from using these 'low-loss' airfoils in the Energy Efficient Engine low-pressure turbine is an improvement in efficiency of 0.5 percent.

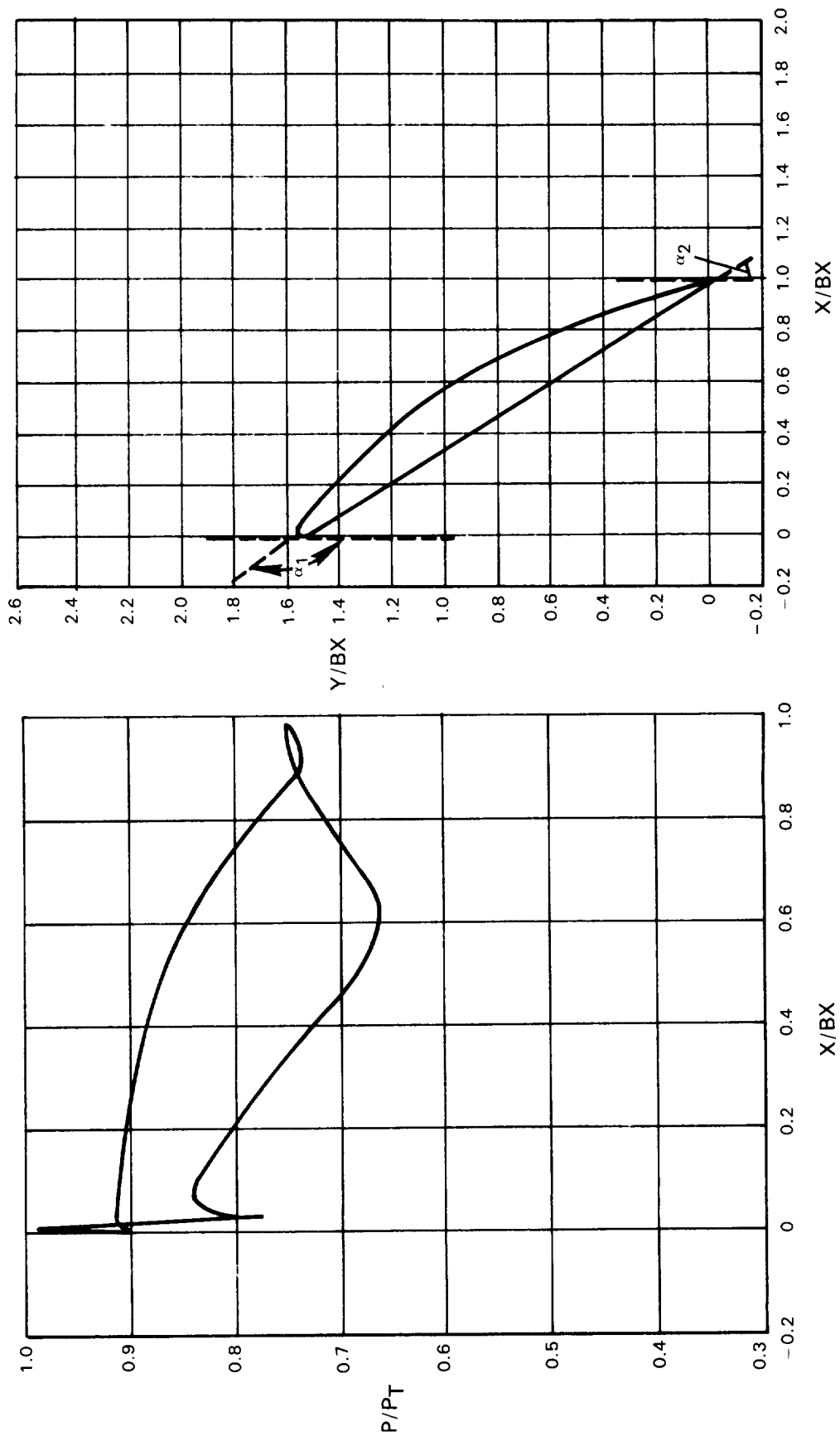


Figure 3-2 Low Camber Vane Shape and Predicted Pressure Distribution

TABLE 3-I

LOW CAMBER VANE CASCADE GEOMETRIC AND AERODYNAMIC PARAMETERSGeometric

Axial Chord - cm (inches)	2.346 (0.924)
Leading Edge Diameter - cm (inches)	0.099 (0.039)
Trailing Edge Diameter - cm (inches)	0.055 (0.022)
Uncovered Turning (deg)	15.7
Inlet Metal Angle (deg)	137.4
Exit Metal Angle (deg)	24.3
Inlet Wedge Angle (deg)	20.0
Exit Wedge Angle (deg)	10.0
Pitch - cm (inches)	3.126 (1.231)

Aerodynamic Design Point

Inlet Mach Number	0.39
Exit Mach Number	0.65
Inlet Air Angle, α_1 (deg)	142.5
Exit Air Angle, α_2 (deg)	24.3
Reynolds Number (Bx)	3.1×10^5
Turbulence Level (without grid)	~ 0.5 percent
Suction Surface Maximum Mach Number	0.82

For well designed low-pressure turbine airfoils, the pressure surface of the airfoil contributes only 10-20 percent of the total airfoil profile loss. The reason for this low-loss level is that the average velocity on the pressure surface is low and, in addition, the flow on this surface accelerates from zero velocity at the stagnation point to the exit velocity at the trailing edge and relatively low losses are generated by boundary layers developing in accelerating flows. Most of the airfoil profile losses are generated on the suction surface of the airfoil because average velocity on the suction surface is high and, in addition, flow on this surface of the airfoil accelerates from the leading edge of the airfoil to some high value and then diffuses to the trailing edge velocity. Two factors influence the growth of boundary layers developing under the influence of accelerating and diffusing flows:

1. location of the onset of transition on the airfoil surface;
2. diffusion parameter (ratio of maximum to exit velocity on the airfoil suction surface).

Delaying the onset of transition location as far as possible on the airfoil surface and reducing the diffusion parameter on the airfoil suction surface can result in reduction of losses.

In the present investigation, both the location of the transition point on the airfoil surface and the diffusion parameter were considered as potential mechanisms for controlling losses.

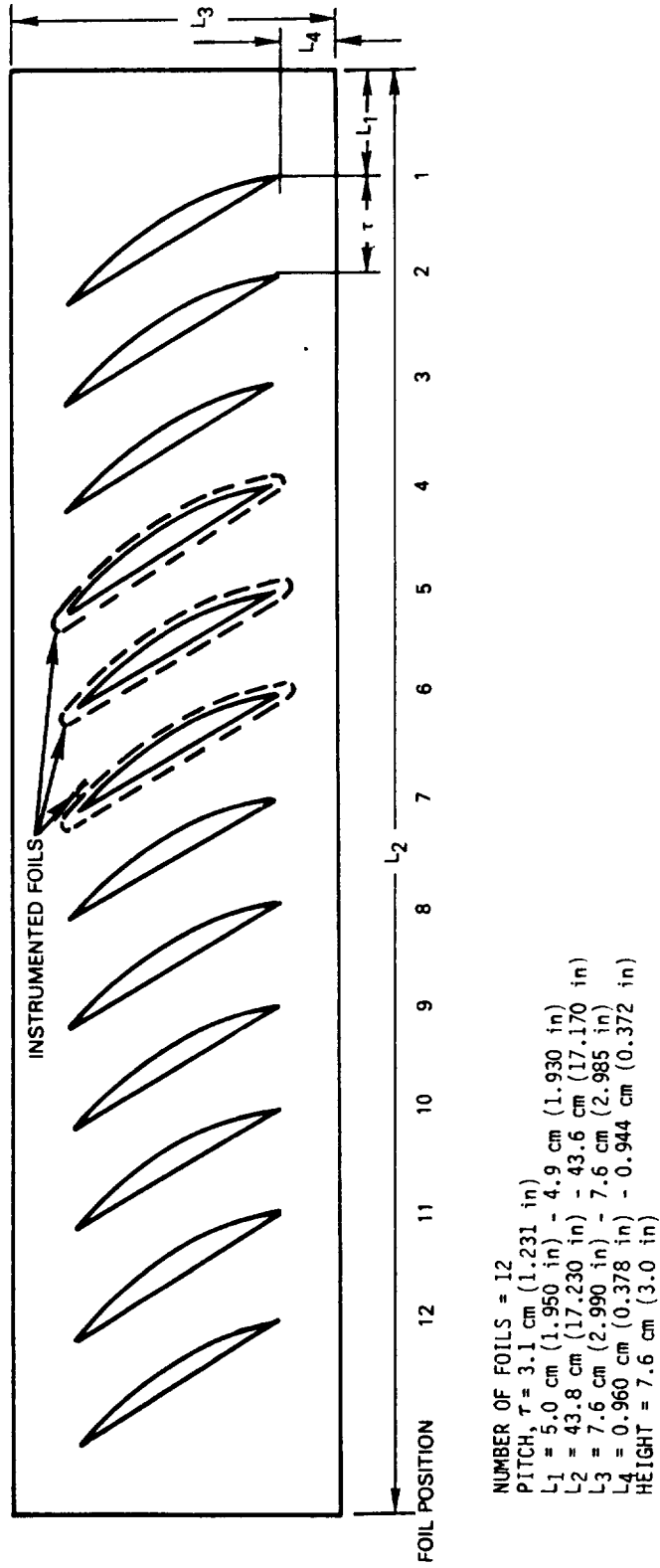


Figure 3-3 Low Camber Vane Cascade Pack Details

If the airfoil suction surface is designed to have accelerating flow up to the throat of the airfoil, while diffusion occurs in the rear part of the airfoil, then boundary layer transition is delayed to the throat. This type of airfoil is referred to as an 'aft-loaded' airfoil in this report. For a given Zweifel's load coefficient, 'aft-loaded' airfoils generally have a higher diffusion parameter, maximum Mach number, and thickness-to-chord ratio than the 'squared-off' airfoils.

As an alternative, an airfoil suction surface can be designed in a manner that the flow accelerates from the stagnation point in the front part of the airfoil, the velocity remains constant in the middle of the airfoil, with diffusion occurring in the aft part of the airfoil. This type of airfoil is referred to as a 'squared-off' airfoil in this report. These airfoils have lower diffusion parameters than 'aft-loaded' airfoils. In addition, the 'squared-off' airfoil has the potential for lower weight than the 'aft-loaded' airfoil. 'Aft-loaded' and 'squared-off' pressure distributions for two airfoils that have the same load coefficient and exit Mach number are shown in Figure 3-4.

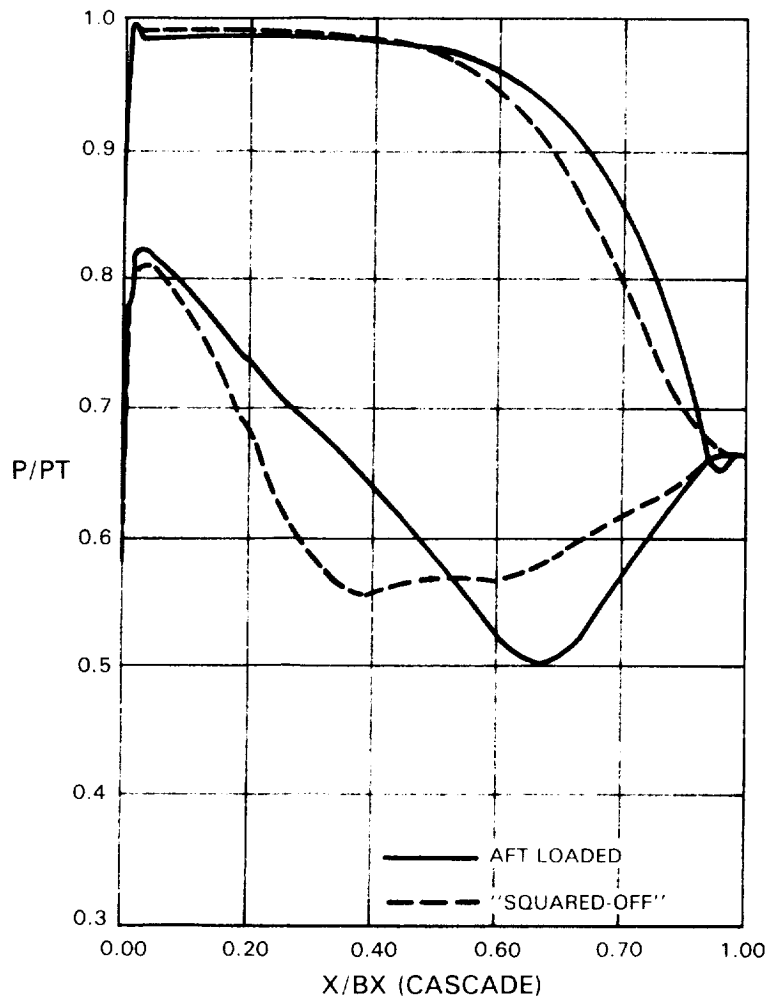


Figure 3-4 Alternate Loading Distribution for Two Airfoils Having the Same Load Coefficient and Velocity Triangle

If diffusion is considered to be the more dominating of the two mechanisms influencing losses on turbine airfoils, then 'squared-off' airfoils should result in lower losses than the 'aft-loaded' airfoils. The loss correlation of Stewart, Whitney and Wong (Appendix B - Reference 1) shows an increase in the airfoil loss with increased diffusion. This correlation would recommend the design of 'squared-off' airfoils in turbines. However, Pratt & Whitney Aircraft cascade and rotating rig test data indicate increased turbine efficiency is obtained when 'aft-loaded' airfoils are used. Therefore, specific test rigs were designed to experimentally evaluate the performance of the 'squared-off' and 'aft-loaded' airfoil designs considered as candidates for use in the Energy Efficient Engine low-pressure turbine component in order to verify the selected design philosophy. The first series of rigs was designed to evaluate the impact of alternate loading distributions on the performance of the fourth stage blade root section airfoil. The second series of rigs was designed to evaluate the performance of three potential subsonic airfoil geometries. Design details for these rigs are discussed in the following two subsections.

3.2.1 Alternate Loading Cascades

The cascades were designed to simulate the aerodynamic performance of the fourth stage blade root section because this region has the highest flow Mach number and was therefore the most critical from an aerodynamic point of view. The simulation was accomplished by designing the cascade to the turbine mean-section airfoil geometry and then adjusting the rig inlet Mach number to match predicted root flow conditions. This approach provided considerable cost savings because one of the airfoil sections designed for the alternate loading tests was also used for the design substantiation tests.

Airfoil contours and their associated surface static pressure distributions at design point for the 'squared-off' and 'aft-loaded' airfoils are shown in Figure 3-5. Table 3-II lists the geometric and aerodynamic parameters for the candidate 'squared-off' and 'aft-loaded' airfoil sections. The coordinates for the 'squared-off' airfoil are listed in Appendix A-2 and those for the 'aft-loaded' airfoil in Appendix A-3.

The resultant cascade pack based on these designs is illustrated in Figure 3-6. It comprises twelve airfoils with a 2.326 cm (0.916 in) pitch and 7.620 cm (3.0 in) span. The aspect ratio of the airfoils is also 3.0. For rig size, the airfoil contours were scaled to 0.68 of the full-size component. Overall pack dimensions, as well as airfoil locations, are shown in Figure 3-6. These dimensions are identical for each cascade. Only the airfoil geometry is different. Cascade pack endwalls are flat. Provisions for static pressure instrumentation are included in the fifth, sixth, and seventh airfoils at midspan. Details of this instrumentation are discussed in Section 5.2.2 of this report.

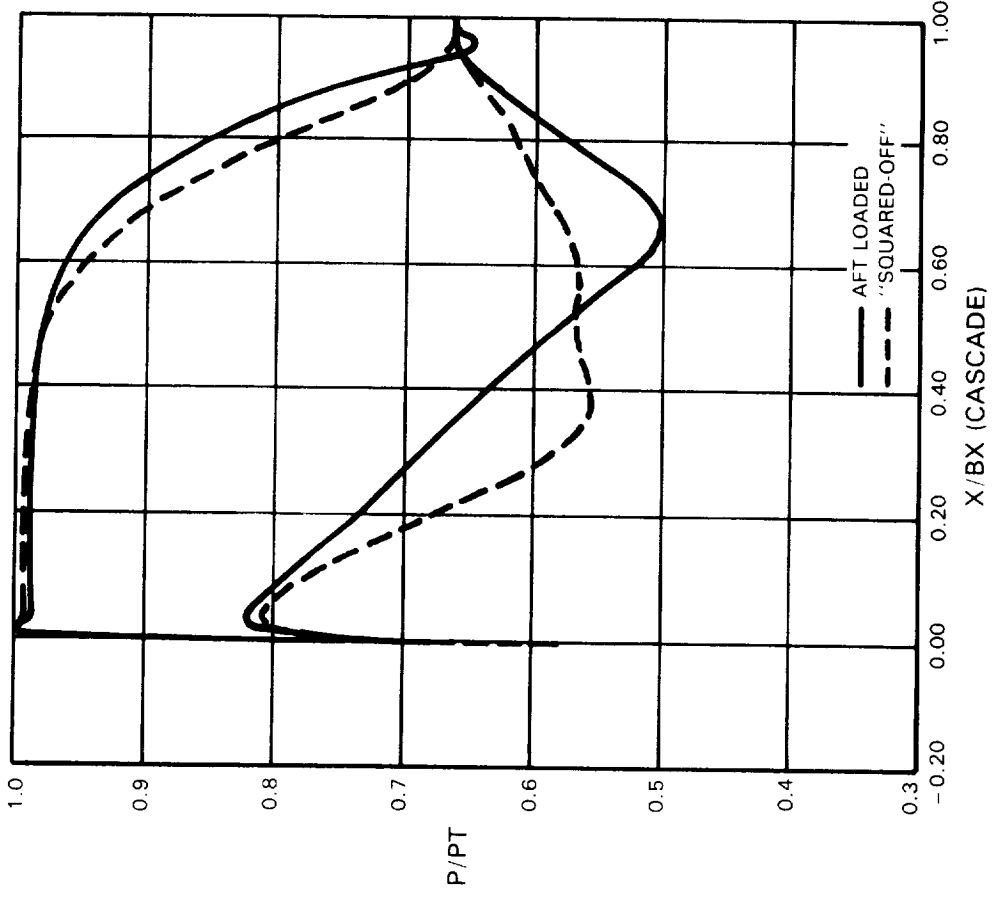
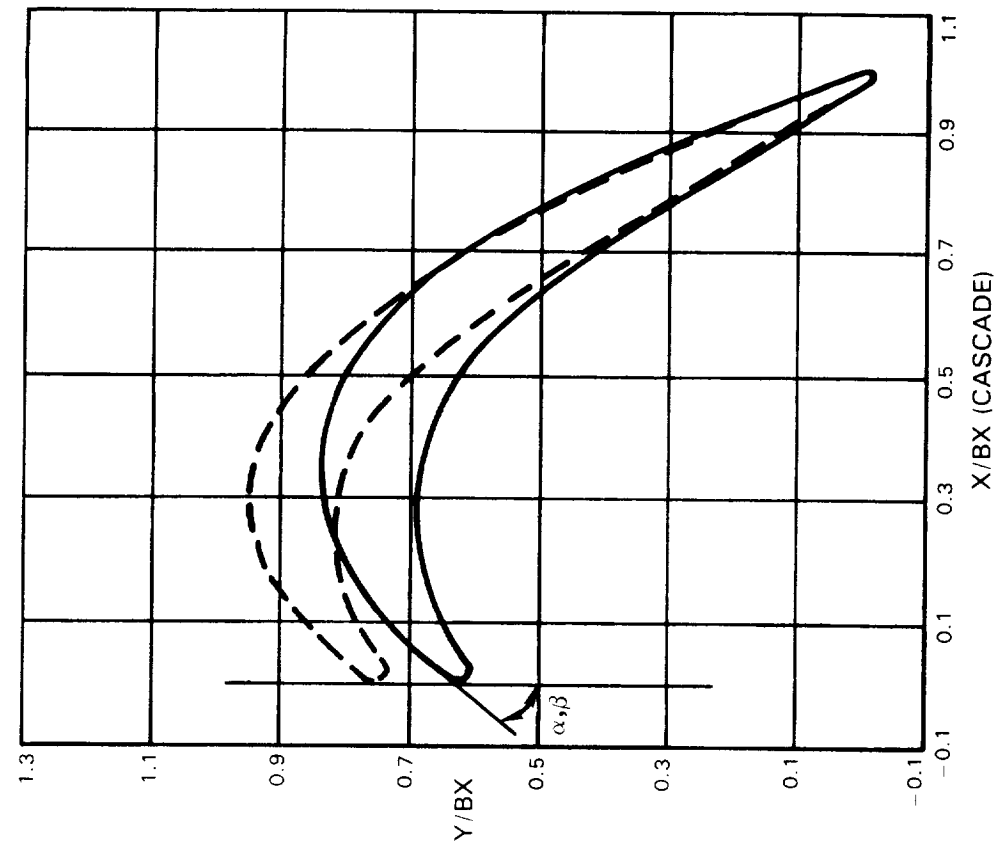


Figure 3-5 Alternate Loading Distribution for Fourth Blade Root Section 'Aft-Loaded' Transonic Versus 'Squared-Off' Subsonic

TABLE 3-II

GEOMETRIC AND AERODYNAMIC PARAMETERS FOR THE 'AFT-LOADED'
TRANSONIC AND 'SQUARED-OFF' SUBSONIC AIRFOIL SECTIONS

Cascade Pack

<u>Loading</u>	<u>Aft-Loaded</u>	<u>Squared-Off</u>
<u>Geometric</u>		
Axial Chord - cm (inches)	2.540 (1.000)	2.540 (1.000)
Leading Edge Diameter - cm (inches)	0.093 (0.037)	0.093 (0.037)
Trailing Edge Diameter - cm (inches)	0.050 (0.020)	0.050 (0.020)
Uncovered Turning (deg)	16.4	10.8
Inlet Metal Angle (deg)	44.8	44.8
Exit Metal Angle (deg)	27.5	27.5
Inlet Wedge Angle (deg)	15.0	10.0
Exit Wedge Angle (deg)	10.0	8.1
Pitch - cm (inches)	2.326 (0.916)	2.326 (0.916)
<u>Aerodynamic Design Point</u>		
Inlet Mach Number	0.37	0.37
Exit Mach Number	0.78	0.78
Inlet Air Angle, α_1 (deg)	49.8	49.8
Exit Air Angle, α_2 (deg)	27.5	27.5
Reynolds Number (Bx)	3.8×10^5	3.8×10^5
Turbulence Level (without Grid)	~ 0.5 percent	~ 0.5 percent
Suction Surface Maximum Mach Number	1.05	0.97

3.2.2 Airfoil Design Concept Cascades

These cascades were designed to simulate the aerodynamic performance of the fourth stage blade mean section for three candidate airfoil geometries: (1) the baseline 'aft-loaded' airfoil section designed for the low-pressure turbine component; (2) a squared-off 'heavyweight*' design; and (3) a squared-off 'lightweight*' design. The latter two airfoils were designed to investigate the influence of airfoil thickness distribution on the performance. In addition, the 'lightweight' airfoil reduces weight in the low-pressure turbine which results in improved component performance and lower material costs. Figure 3-7 shows the airfoil contours and their associated surface static pressure distributions at design point for the 'aft-loaded', 'heavyweight', and 'lightweight' airfoil designs used in the airfoil design substantiation tests. Table 3-III lists the geometric and aerodynamic parameters for these candidate airfoil sections. As noted earlier, the 'aft-loaded' airfoil cascade used in this test series was the same airfoil employed in the alternate loading tests. The airfoil coordinates for the 'aft-loaded' design are listed in Appendix A-3. The coordinates for the 'heavyweight' and 'lightweight' airfoil designs are listed in Appendices A-4 and A-5, respectively.

* Squared-off 'heavyweight' and squared-off 'lightweight' airfoils are hereinafter referred to as 'heavyweight' and 'lightweight' designs, respectively.

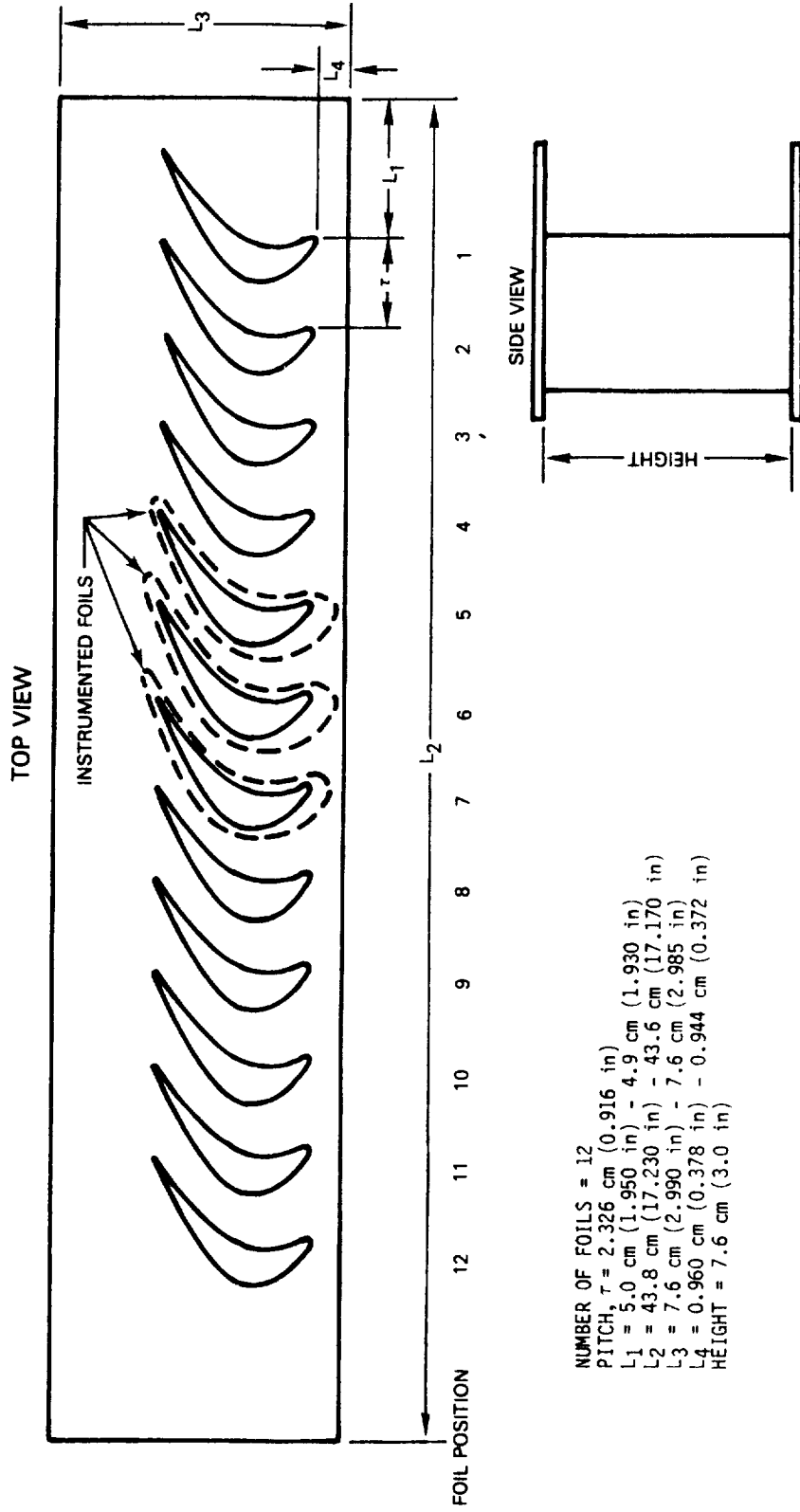


Figure 3-6 Cascade Pack Dimensions

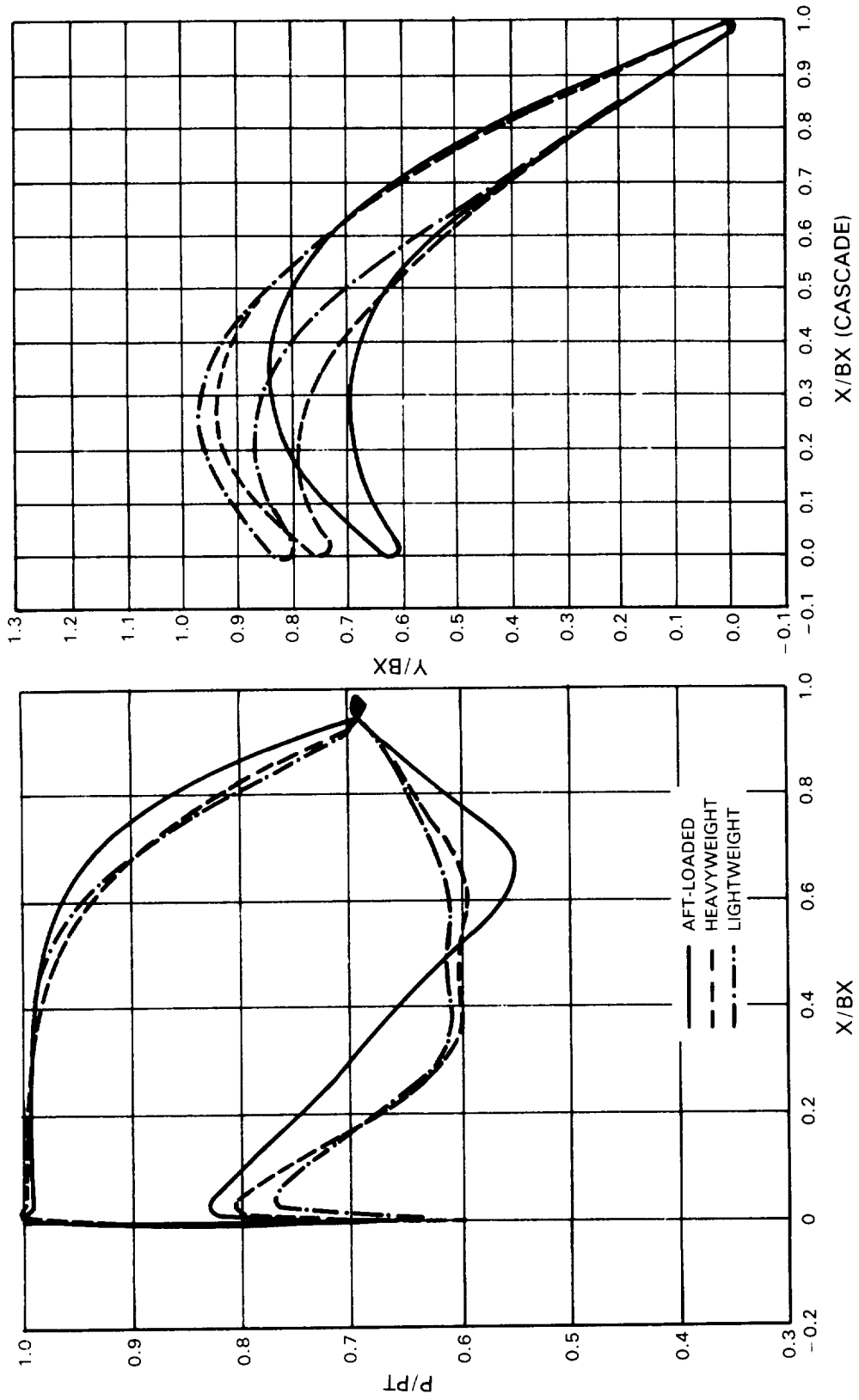


Figure 3-7 'Aft-Loaded' Versus 'Heavyweight' Versus 'Lightweight' Designs

TABLE 3-III

GEOMETRIC AND AERODYNAMIC PARAMETERS FOR THE 'AFT-LOADED,'
HEAVYWEIGHT, AND LIGHTWEIGHT AIRFOIL DESIGNS

Cascade Pack

<u>Loading</u>	<u>Aft-Loaded</u>	<u>Heavyweight</u>	<u>Lightweight</u>
<u>Geometric</u>			
Axial Chord - cm (inches)	2.540 (1.000)	2.540 (1.000)	2.540 (1.000)
Leading Edge Diameter - cm (inches)	0.093 (0.037)	0.093 (0.037)	0.093 (0.037)
Trailing Edge Diameter - cm (inches)	0.050 (0.020)	0.050 (0.020)	0.050 (0.020)
Uncovered Turning (deg)	16.4	11.9	10.6
Inlet Metal Angle (deg)	44.8	44.8	49.8
Exit Metal Angle (deg)	27.5	27.5	27.5
Inlet Wedge Angle (deg)	15.0	15.0	8.0
Exit Wedge Angle (deg)	10.0	8.0	8.0
Pitch - cm (inches)	2.326 (0.916)	2.326 (0.916)	2.326 (0.916)
<u>Aerodynamic Design Point</u>			
Inlet Mach Number	0.36	0.36	0.36
Exit Mach Number	0.74	0.74	0.74
Inlet Air Angle, α_1 (deg)	49.8	49.8	49.8
Exit Air Angle, α_2 (deg)	27.5	27.5	27.5
Reynolds Number (Bx)	3.5×10^5	3.5×10^5	3.5×10^5
Turbulence Level (with Grid)	~ 2.5%	~ 2.5%	~ 2.5%
(without Grid)	~ 0.5%	~ 0.5%	~ 0.5%
Suction Surface Maximum Mach Number	0.95	0.90	0.88

The cascade pack dimensions for these designs were identical to those for the alternate loading test series (see Figure 3-6). Only the airfoil geometry was different. Cascade pack endwalls are flat. Provisions for static pressure instrumentation are included in the fifth, sixth, and seventh airfoils at midspan. Details of this instrumentation are discussed in Section 5.2.2 of this report.

SECTION 4.0 FABRICATION AND ASSEMBLY

The cascade packs were prepared for test by standard fabrication and assembly techniques. These models were fabricated from stainless steel and provided with instrumentation to allow achievement of test objectives.

Each cascade consisted of twelve three inch sections of untwisted airfoils, which were welded to the endwalls. The complete assembly was then mounted in the test section.

SECTION 5.0 TESTING

5.1 General Description

The objective of the cascade test program was to evaluate the performance of (1) the low camber vane, (2) fourth stage blade root section transonic 'aft-loaded' and subsonic squared-off airfoils, and (3) fourth stage blade mean section 'aft-loaded', 'heavyweight' and 'lightweight' airfoils. The performance of each of the above airfoil designs were evaluated in terms of airfoil surface static pressure distributions, and profile and secondary loss.

5.2 Test Facility and Instrumentation

5.2.1 Test Facility

The Pratt & Whitney Aircraft Plane Cascade Wind Tunnel (Test Stand X-32) is a steady flow tunnel consisting of a large plenum, test section, and discharge cell. Figure 5-1 presents a schematic representation of this facility. The primary airflow enters the plenum chamber and is discharged against the plenum endwall. The flow subsequently passes through a honeycomb flow straightener and fine mesh screens, which remove swirl and make the flow uniform before it enters a rectangular bellmouth to the cascade approach duct. After passing through the cascade, the air discharges to the test cell, which is maintained at atmospheric pressure. Cascade incidence air angles are set by rotating the cascade assembly relative to the direction of the airflow in the approach duct.

5.2.2 Instrumentation

The instrumentation required for cascade testing is presented in Table 5-I.

Both the cone probe and the cobra probe were calibrated in a free jet calibration facility to develop calibration curves for total pressure, static pressure, yaw angle, and pitch angle (five-port combination probe only). This calibration was conducted at approximately the same unit Reynolds number as the cascade exit flow and over the range of the Mach numbers and angles required for the testing.

Each cascade pack had three airfoils with static pressure taps at 50 percent span bordering two airfoil passages. Two of the three airfoils had trailing edge static pressure taps. The middle of the three instrumented airfoils had static pressure taps on both sides of the airfoil for a total of 16 taps. The other two airfoils had static pressure taps only on the side facing the middle airfoil. Figure 5-2 defines the nominal static pressure tap locations for the low camber vane cascade. Figure 5-3 illustrates the typical static pressure tap locations for the other four cascades.

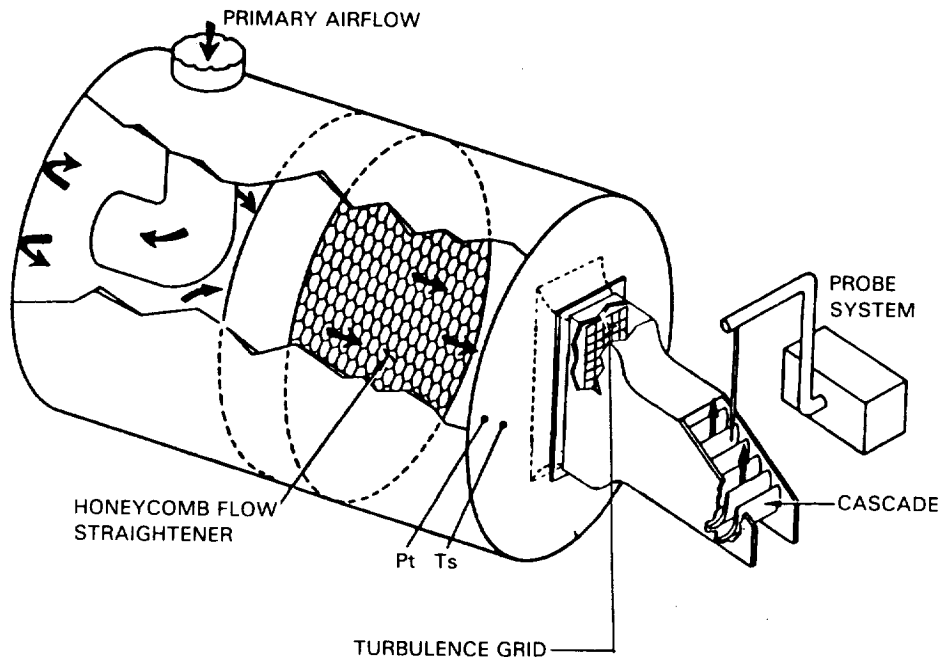


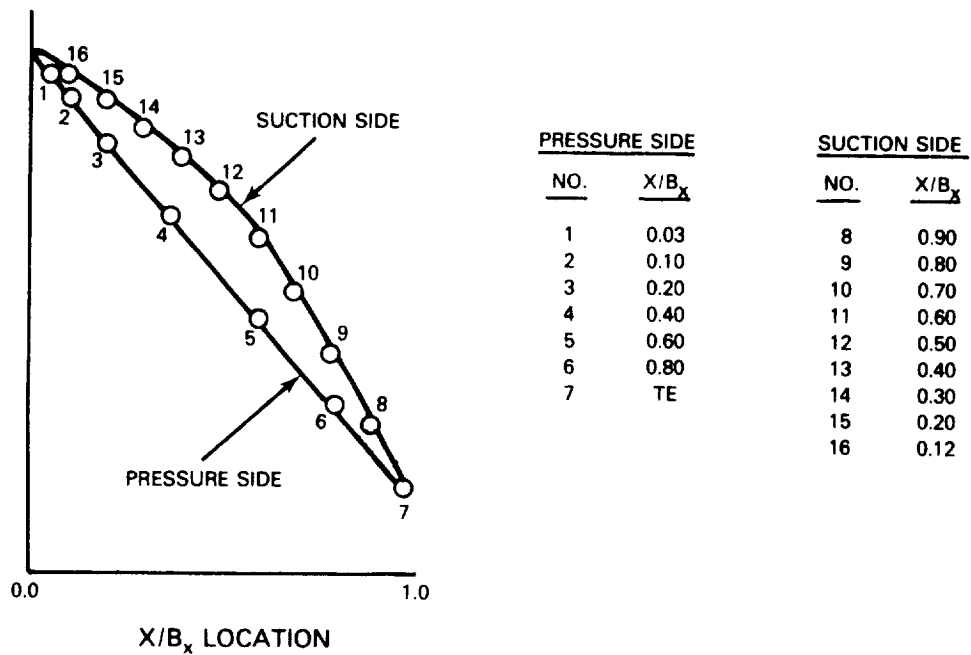
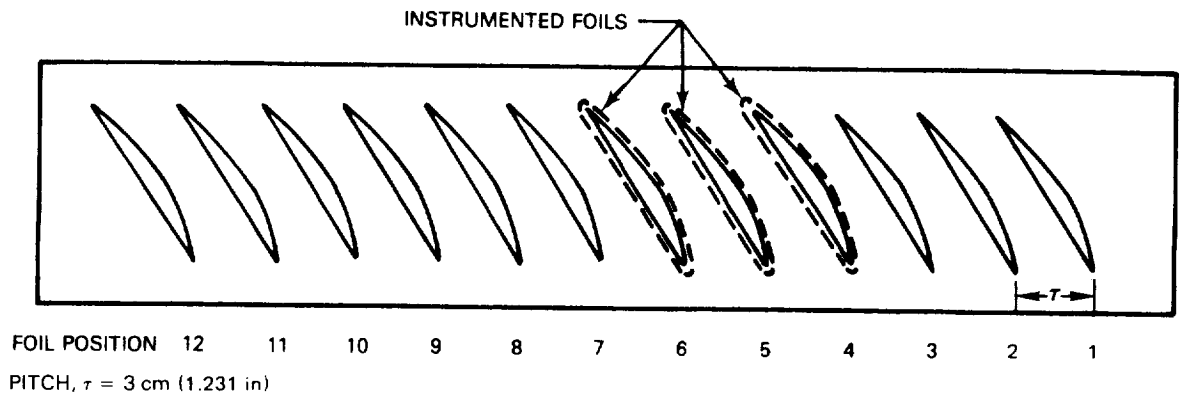
Figure 5-1 Cascade Test Facility

TABLE 5-I

TEST PROGRAM INSTRUMENTATION

<u>Location</u>	<u>Measurement</u>	<u>Type</u>	<u>Quantity</u>
Tunnel Plenum	Total Temperature	Thermocouple	1
	Total Pressure	Kiel Probe	1
Approach Duct	Static Pressure	Static Taps	3
Discharge Cell	Barometric Pressure	Barometer	1
Survey Plane Downstream of Cascade	Total Pressure	Cone Probe (1)	1
	Static Pressure	Cobra Probe (2)	1
	Yaw Angle Pitch Angle		
Airfoil Surfaces (Each Cascade)	Static Pressure	Static Taps	25

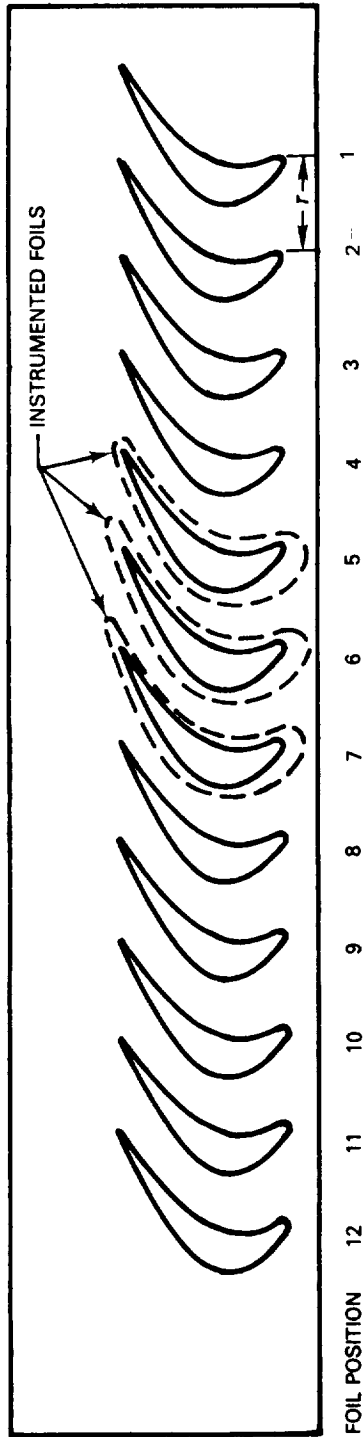
- (1) The cone probe is a five-port combination probe used to obtain measurements of total pressure, static pressure, and pitch and yaw angles over most of the traverse plane. This probe has a stem diameter of 3.97 mm (5/32 in.) and a conical tip with a 70-degree included angle.
- (2) The cobra probe consists of three capillary tubes brazed in parallel. It was used to measure flow conditions close to the endwalls (i.e., within the boundary layer).



*THREE AIRFOILS ARE INSTRUMENTED:
 1 AIRFOIL: SUCTION SURFACE
 1 AIRFOIL: PRESSURE SURFACE
 1 AIRFOIL: SUCTION AND PRESSURE SURFACES
 ARRANGED TO PROVIDE TWO (2) INSTRUMENTED PASSAGES

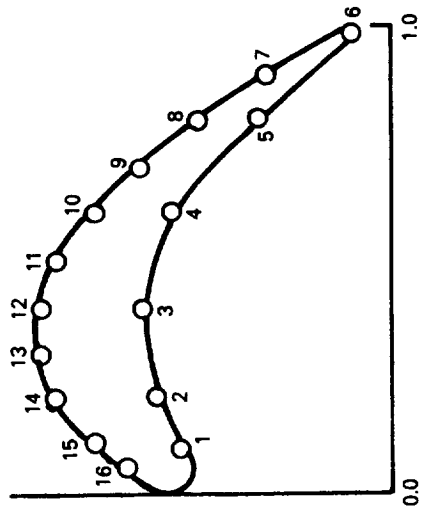
Figure 5-2 Low Camber Vane Cascade Nominal Static Pressure Tap Locations

TOP VIEW



NUMBER OF FOILS = 12
 PITCH, $r = 2.326 \text{ cm (0.916 in)}$

STATIC PRESSURE TAPS (TYPICAL)



PRESSURE SIDE		SUCTION SIDE	
NO.	X/B _x	NO.	X/B _x
1	0.10	7	0.90
2	0.20	8	0.80
3	0.40	9	0.70
4	0.60	10	0.60
5	0.80	11	0.50
6	TE	12	0.40
		14	0.20
		15	0.10
		16	0.05

X/B_x LOCATION

*THREE AIRFOILS ARE INSTRUMENTED:

- 1 AIRFOIL: SUCTION SURFACE
- 1 AIRFOIL: PRESSURE SURFACE
- 1 AIRFOIL: SUCTION AND PRESSURE SURFACES
 ARRANGED TO PROVIDE TWO (2) INSTRUMENTED PASSAGES

Figure 5-3 Blade Cascade Typical Static Pressure Tap Locations

5.3 Test Procedures

5.3.1 Establishing Test Conditions

Test conditions were established to provide exit Mach numbers equal to the Mach numbers required for a particular vane or blade test configuration. These Mach numbers were obtained by setting exit static-to-inlet pressure ratios. The mainstream total temperature was a nominal 150 degrees F. Since the flow exited to atmospheric pressure, the total pressure of the flow approaching the cascade was in the range of 5 to 8 psig. Expansion ratios were calculated to yield a range of Reynolds numbers based on exit flow conditions and on airfoil axial chords. Table 5-II presents the measured test conditions for each cascade.

5.3.2 Shakedown Testing

Shakedown testing consisted of pressure leak checks and calibration of all instrumentation before performance testing was initiated. A preliminary data point was run to verify performance of the instrumentation and data acquisition systems. The performance test program was initiated only after it was determined that all instrumentation and systems were operating properly.

5.3.3 Performance Testing

The subsonic cascade program was structured to permit separate performance evaluations of:

- o low camber vane;
- o alternate loading distribution for fourth stage blade root section;
- o low-pressure turbine airfoil design concepts.

Wake traverse data were used to assess cascade performance in terms of total pressure loss. These traverses were made downstream of the trailing edge. The five-port combination probe was used to obtain measurements of total pressure, static pressure, pitch and yaw angles over most of the traverse plane. This probe was traversed in the pitchwise direction at a constant span height taking measurements at 0.152 cm (0.060 inch) increments. Yaw angles (angles in the plane parallel to endwalls) were obtained by nulling the probe aerodynamically to within one degree and then applying calibration curves. The probe drive axis of rotation passed through the tip of the probe. Pitch angles were obtained for the five-port combination probe through the calibration curves.

Data for the low camber vane and alternate loading distribution test were obtained for an inlet turbulence level of 0.5 percent. Mid-span loss and surface static pressure data for the low-pressure turbine design concept test were also obtained at 2.5 percent turbulence level. This level was achieved by installing a turbulence generating grid at the inlet section. Comparison of data obtained with and without the turbulence grid showed that the grid had little effect on the magnitude of losses and the static pressure distributions (see Section 6.3.2). Therefore, the remainder of the data was obtained without the grid.

TABLE 5-II

VANE AND BLADE CASCADE TEST CONDITIONS

	Low Camber Vane	Alternate Loading Distribution		Low-Pressure Turbine Airfoil Design Concept Evaluation		
		Transonic 'Aft-Loaded'	Subsonic Squared-Off	Aft-Loaded	Heavyweight	Lightweight
Isentropic Exit Mach No.	0.62 - 0.65	0.77 - 0.93	0.77 - 0.89	0.63 - 0.89	0.63 - 0.94	0.63 - 0.92
Upstream Air Angles (Degrees)	128.1 - 150.4	39.5 - 59.5	41.5 - 61.5	39.5 - 64.5	39.5 - 64.5	39.5 - 64.5
Reynolds No. ($U_{exit} b_x$)	1.69×10^5 - 1.93×10^5	4.54×10^5 - 5.85×10^5	4.07×10^5 - 5.02×10^5	3.27×10^5 - 5.34×10^5	3.35×10^5 - 5.62×10^5	3.34×10^5 - 5.41×10^5
Upstream Total Pressure (P_T) - PSI	19.61 - 19.74	22.5 - 28.22	22.5 - 25.29	19.51 - 26.48	19.52 - 26.2	19.2 - 26.2
Total Temperature (T_{OR})	569 - 625	594 - 628	594 - 650	568 - 644	562 - 629	583 - 634

5.3.4 Performance Test Plan

The test plans for the low-pressure turbine cascade tests are shown in Tables 5-III, 5-IV, and 5-V. These plans were developed to achieve the following test objectives.

- o Establish the performance of low camber vane in terms of profile loss and exit angles at design point Mach number for a range of incidences. Also establish secondary loss behavior at design conditions.
- o Evaluate the relative performance of the alternate loading distribution for the fourth stage blade root section in terms of profile loss for a range of incidences and Mach numbers. Evaluate the secondary loss behavior at design conditions.
- o Evaluate low-pressure turbine airfoil design concepts in terms of profile loss for a range of incidence and Mach numbers. Evaluate the secondary loss behavior at design Mach number and three incidences.

TABLE 5-III

LOW CAMBER VANE CASCADE TEST PLAN

Test Sequence	Inlet Angle	Exit Mach No	Expansion Ratio	Data Scan
1 (DP)	141.7	0.649	0.75	Airfoil surface static pressure and exit plane (mid-span) loss survey
2	145.3	0.639	0.7575	"
3	148.5	0.623	0.765	"
4	150.4	0.615	0.77	"
5	135.0	0.655	0.73	"
6	131.5	0.644	0.75	"
7	128.1	0.654	0.73	"
8	141.7	0.65	0.75	Airfoil surface static pressure and exit plane (half-span) loss survey.

(DP) - Design Point

TABLE 5-IV
ALTERNATE LOADING DISTRIBUTION EVALUATION

TRANSONIC AFT-LOADED AIRFOIL CASCADE TEST PLAN

<u>Test Sequence</u>	<u>Inlet Angle</u>	<u>Exit Mach No</u>	<u>Expansion Ratio</u>	<u>Data Scan</u>
1 (DP)	49.5	0.784	0.66	Airfoil surface static pressure and exit plane (mid-span) loss survey
2	49.5	0.852	0.615	"
3	49.5	0.881	0.595	"
4	49.5	0.937	0.56	"
5	49.5	0.969	0.54	"
6	44.5	0.776	0.665	"
7	39.5	0.77	0.665	"
8	54.5	0.778	0.665	"
9	59.5	0.777	0.665	"
10	49.5	0.784	0.66	Airfoil surface static pressure and exit plane (half-span) loss survey.

SUBSONIC SQUARED-OFF AIRFOIL CASCADE TEST PLAN

<u>Test Sequence</u>	<u>Inlet Angle</u>	<u>Exit Mach No</u>	<u>Expansion Ratio</u>	<u>Data Scan</u>
1 (DP)	49.5	0.779	0.665	Airfoil surface static pressure and exit plane (mid-span) loss survey
2	49.5	0.845	0.62	"
3	49.5	0.891	0.59	"
4	49.5	0.94	0.56	"
5	44.5	0.777	0.665	"
6	41.5	0.773	0.665	"
7	54.5	0.776	0.665	"
8	56.5	0.779	0.665	"
9	61.5	0.776	0.665	"
10	49.5	0.776	0.665	Airfoil surface static pressure and exit plane (half-span) loss survey.

(DP) - Design Point

TABLE 5-V
DESIGN CONCEPTS EVALUATION

BASELINE AFT-LOADED AIRFOIL CASCADE TEST PLAN

<u>Test Sequence</u>	<u>Inlet Angle</u>	<u>Exit Mach No</u>	<u>Expansion Ratio</u>	<u>Data Scan</u>
1	49.5*	0.726	0.7	Airfoil surface static pressure and exit plane (mid-span) loss survey
2 (DP)	49.5	0.725	0.7	"
3	49.5	0.633	0.76	"
4	49.5	0.837	0.625	"
5	49.5	0.887	0.59	"
6	49.5	0.939	0.57	"
7	44.5	0.726	0.7	"
8	39.5	0.71	0.7	"
9	54.5	0.729	0.7	"
10	59.5	0.731	0.7	"
11	64.5	0.728	0.7	"
12	44.5	0.726	0.7	Airfoil surface static pressure and exit plane (half-span) loss survey.
13	49.5	0.71	0.7	"
14	54.5	0.729	0.7	"

HEAVYWEIGHT AIRFOIL CASCADE TEST PLAN

<u>Test Sequence</u>	<u>Inlet Angle</u>	<u>Exit Mach No</u>	<u>Expansion Ratio</u>	<u>Data Scan</u>
1	49.5*	0.726	0.705	Airfoil surface static pressure and exit plane (mid-span) loss survey
2 (DP)	49.5	0.721	0.705	"
3	49.5	0.631	0.76	"
4	49.5	0.82	0.64	"
5	49.5	0.87	0.608	"
6	49.5	0.92	0.59	"
7	44.5	0.715	0.705	"
8	39.5	0.716	0.705	"
9	54.5	0.723	0.70	"
10	59.5	0.723	0.70	"
11	64.5	0.727	0.70	"

LIGHTWEIGHT AIRFOIL CASCADE TEST PLAN

<u>Test Sequence</u>	<u>Inlet Angle</u>	<u>Exit Mach No</u>	<u>Expansion Ratio</u>	<u>Data Scan</u>
1	49.5*	0.726	0.7	Airfoil surface static pressure and exit plane (mid-span) loss survey
2 (DP)	49.5	0.723	0.7	"
3	49.5	0.632	0.755	"
4	49.5	0.836	0.635	"
5	49.5	0.883	0.615	"
6	49.5	0.92	0.59	"
7	44.5	0.72	0.7	"
8	39.5	0.712	0.7	"
9	54.5	0.726	0.7	"
10	59.5	0.726	0.7	"
11	64.5	0.729	0.7	"
12	44.5	0.72	0.7	Airfoil surface static pressure and exit plane (half-span) loss survey.
13	49.5	0.723	0.7	"
14	54.5	0.726	0.7	"

(DP) - Design Point

* - Turbulence grid installed at inlet

5.4 Data Reduction and Analysis

The data acquisition sequence for the low-pressure turbine vane and blade cascade tests is presented in Table 5-VI while the data analysis methods employed for the cascade tests are shown in Table 5-VII.

TABLE 5-VI
CASCADE TEST DATA ACQUISITION SEQUENCE

<u>Sequence</u>	<u>Data Obtained</u>
1. Apply known pressures to transducers.	Transducer calibration.
2. Set cascade expansion ratio.	None
3. Program probe controller and start data acquisition sequence.	Flow field exit traverse local total pressure, static pressure, pitch angle, and yaw angle.
4. Check cascade expansion ratio to be repeated periodically during data acquisition sequence.	Check for drift of test conditions; test ended if significant drift occurs.
5. After test is completed, repeat (1).	Check of transducer calibration; repeat test if calibration has drifted.

TABLE 5-VII
CASCADE TEST DATA ANALYSIS METHODS

1. Comparison of measured airfoil surface static pressures with analytical predictions.
2. Comparison of mid-span total pressure loss with analytical predictions.
3. Comparison of secondary loss data with empirical correlations.

Profile Loss Data Reduction

In keeping with the common practice of presenting measured airfoil section (two-dimensional) performance, the current cascade results are presented on a "mixed out state" basis. This approach not only defines the experimental results on an unambiguous basis but also is the flow state corresponding to most airfoil section performance computation schemes. Figure 5.4 presents the control volume which is employed to analytically mix out the measured wake traverse data (total pressure, static pressure and air angle measurements) to a uniform state through the application of the equations for conservation of mass, energy and X and Y momentum and the equation of state. It should be pointed out that no empiricism is required for this method. It is also worth mentioning that for all the test results being reported, the mixed out loss in total pressure was found to be less than 10 percent higher than the mass weighed measurement plane value.

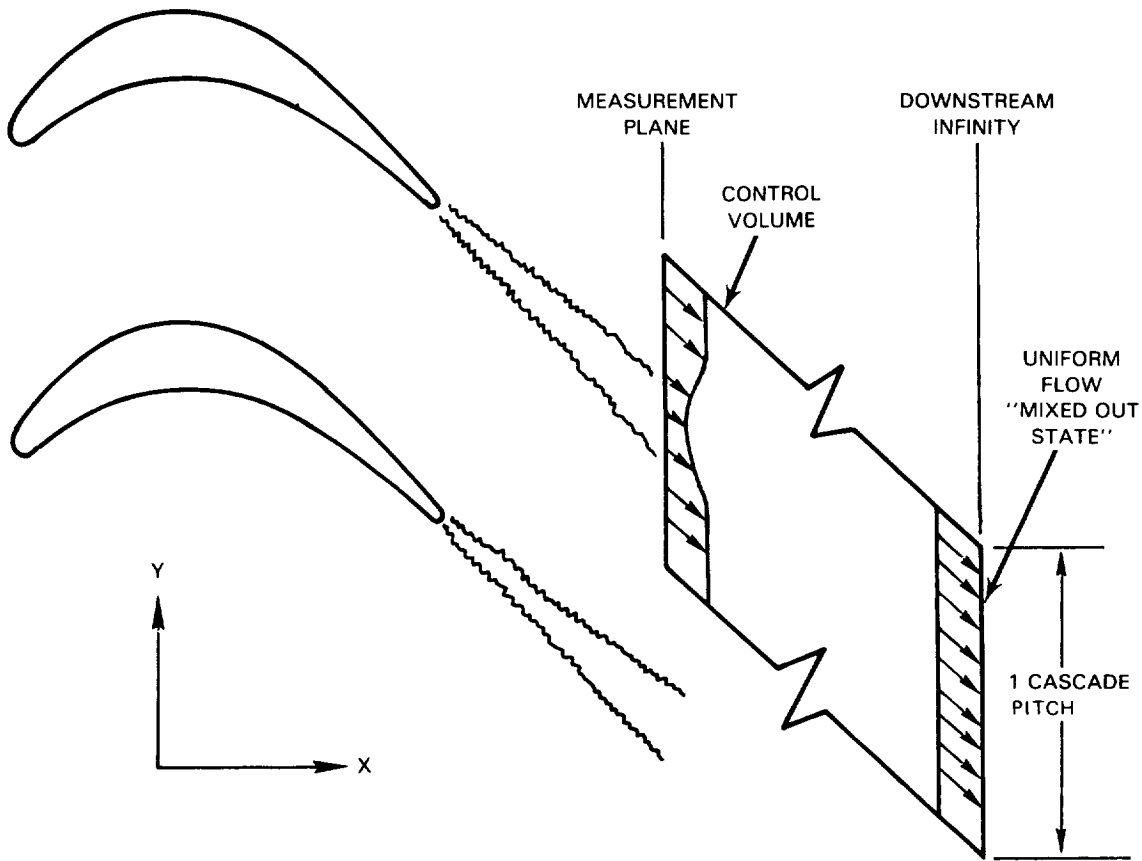


Figure 5.4 Wake Mixing Control Volume

SECTION 6.0 RESULTS

The data obtained from the low-pressure turbine subsonic cascade technology program were reduced and analyzed. The results of this program are presented in the following order: (1) low camber first vane performance, (2) testing of an alternate aerodynamic loading distribution on the fourth stage blade root section, and (3) verification of low-pressure turbine design concepts.

6.1 Low Camber Vane Cascade Performance

Results of the low camber vane testing included (1) surface flow visualizations (conducted prior to performance testing) to assess the behavior of limiting streamlines and establish if any flow separation problems existed and (2) performance testing to assess the following:

- o the impact of incidence angle changes on predicted and measured airfoil pressure distributions;
- o cascade design point half span loss characteristics;
- o cascade profile loss at off-design incidence.

Results of these assessments are described in the following sections.

6.1.1 Flow Visualization

Flow visualizations were made by applying a mixture of lampblack and oil to the airfoil and endwall surfaces. The cascade tunnel was then operated at the test point conditions for approximately one minute. Figure 6-1 depicts a typical flow visualization.

Flow visualizations were conducted at three incidence settings: -13 degrees, -4.3 degrees (near the aerodynamic design point), and +9.3 degrees. Evidence of flow separation was observed near the leading edge at off-design incidence angles. The separation bubble is shown schematically in the inset of Figure 6-1. This figure also shows the flow separation and reattachment locations on the airfoil surface. Separation bubbles such as that shown are characteristic of the flow near airfoil leading edges at off-design incidence angles.

The flow visualizations were also used to assess the secondary flow regions at the vane endwalls. These regions are caused by flow interactions at the vane airfoil-cascade endwall interface and the penetration of this three-dimensional flow into the cascade two-dimensional flow region increases from the airfoil leading edge to its trailing edge, as depicted in Figure 6-2. The height of this penetration is approximately the size of the secondary flow passage vortex. For each of the flow visualization incidence settings, the suction surface separation line at the trailing edge was measured. These measurements are summarized in Table 6-I. Based on a 7.620 cm (3.0 in) vane span, this secondary flow region is seen to represent a very small portion of the total passage flow area.

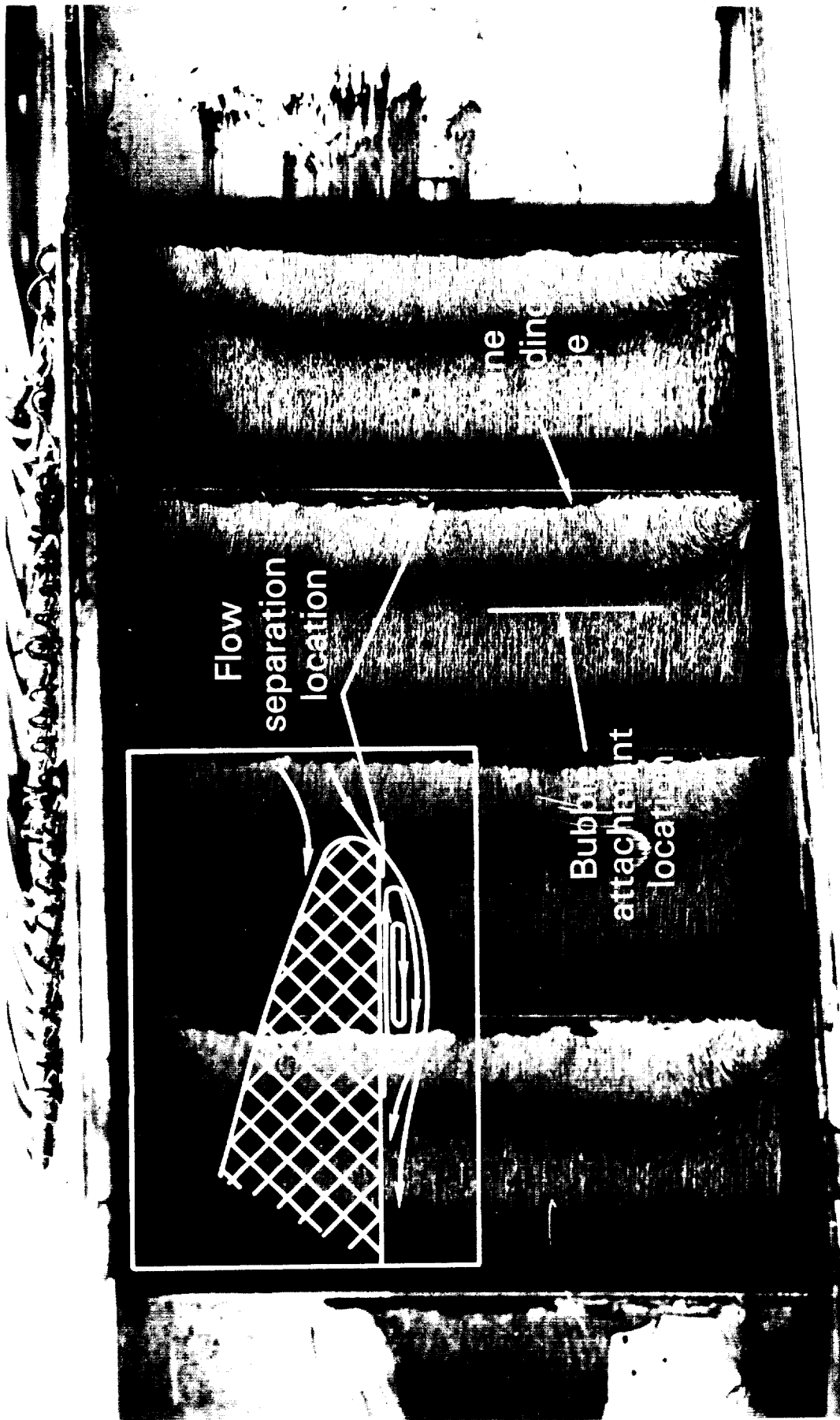


Figure 6-1 Flow Visualization at -13.0 Degrees Incidence Showing Pressure Surface Separation Bubble

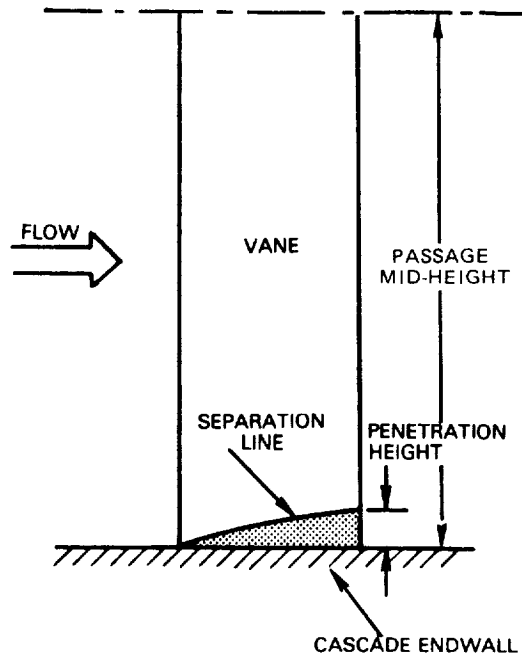


Figure 6-2 Endwall Flow Schematic

TABLE 6-1

TRAILING EDGE SUCTION SURFACE SEPARATION LINE MEASUREMENTS

<u>Incidence(deg)</u>	<u>Penetration Height of Separation Line On the Airfoil Suction Surface - cm (inches)</u>
-13	0.177 (0.07)
-4.3	0.279 (0.11)
+9.3	0.381 (0.15)

6.1.2 Performance Results

6.1.2.1 Airfoil Pressure Distributions

Illustrated in Figure 6-3 are the results of the Pratt & Whitney Aircraft Potential Flow Model prediction versus measured data. A good match was obtained except for the extremes of positive and negative incidence settings where the Pratt & Whitney Aircraft Potential Flow Model did not accurately predict the leading edge separation bubble region. This is most noticeable in Figures 6-3 (c), (d), (f), and (g) for the range of X/BX from 0.00 to 0.25.

The improved data match illustrated in Figure 6-4 was obtained with a first-pass attempt at modeling the separation bubble. The bubble length was estimated with the aid of flow visualization and airfoil static pressure data. The bubble displacement surface was approximated by a circular arc with a length/maximum height ratio of 10.

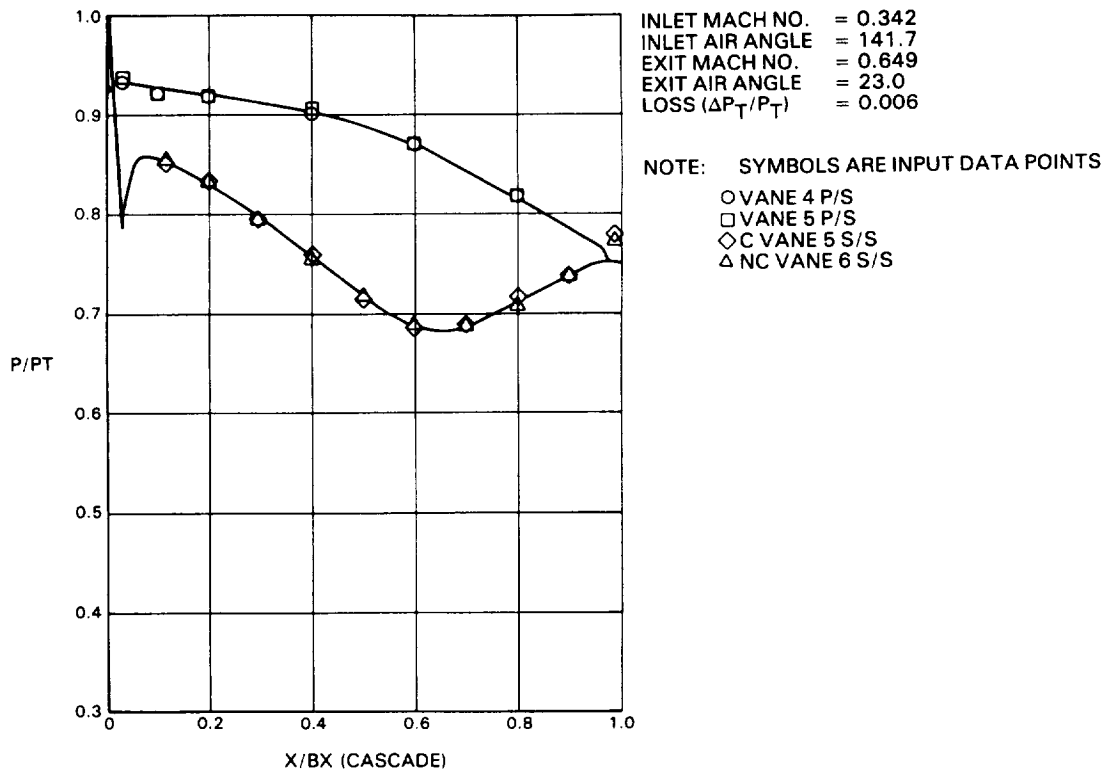


Figure 6-3 (a) Predicted Versus Measured Airfoil Surface Static Pressure Distribution at -4.3 Degrees Incidence

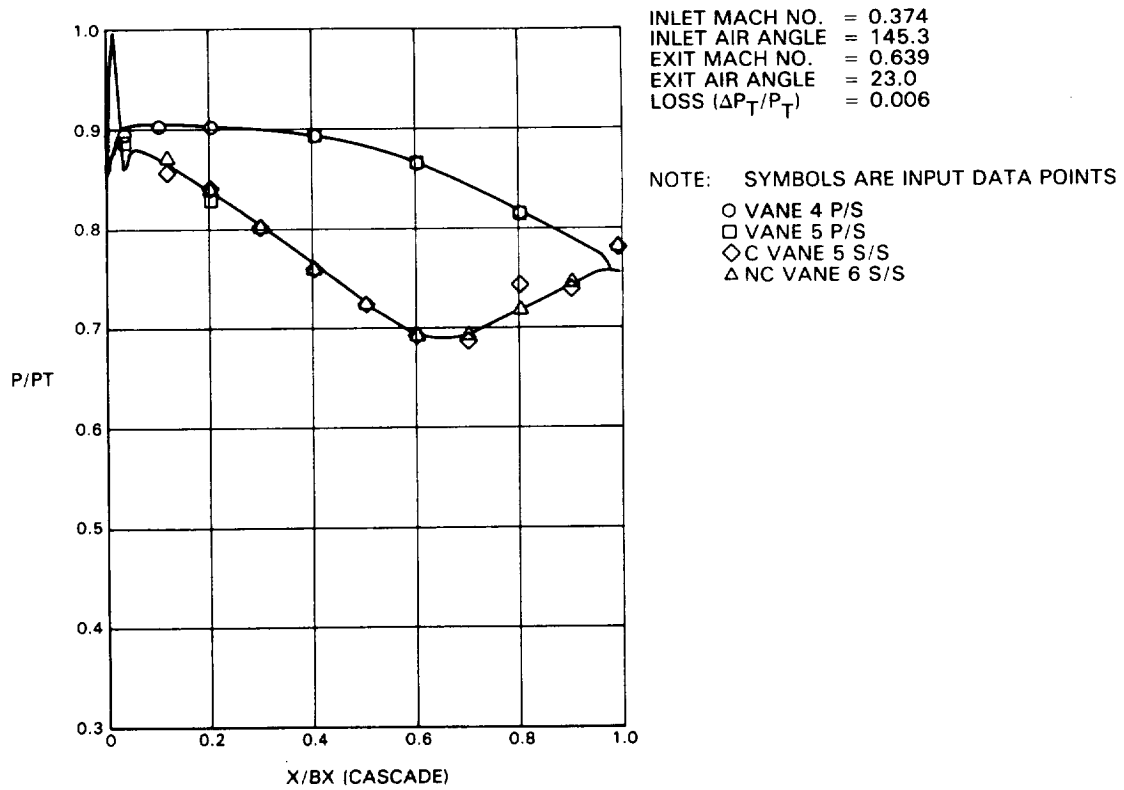


Figure 6-3 (b) Predicted Versus Measured Airfoil Surface Static Pressure Distribution at -7.9 Degrees Incidence

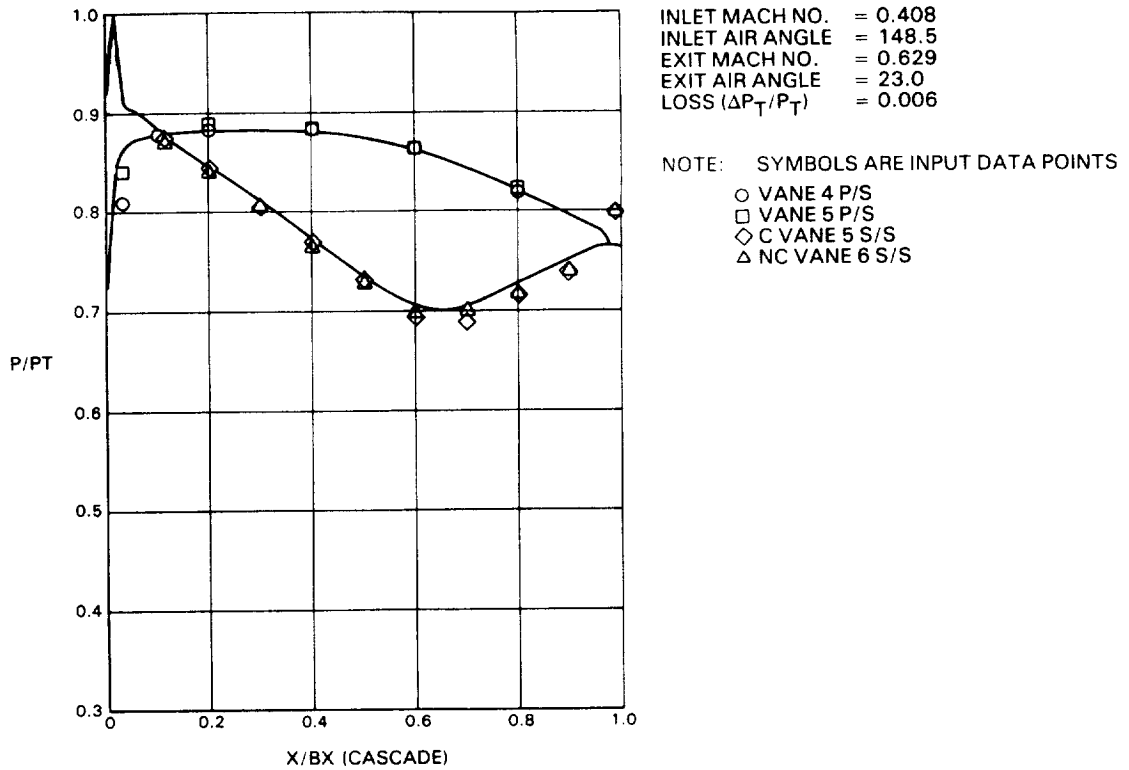


Figure 6-3 (c) Predicted Versus Measured Airfoil Surface Static Pressure Distribution at -11.1 Degrees Incidence

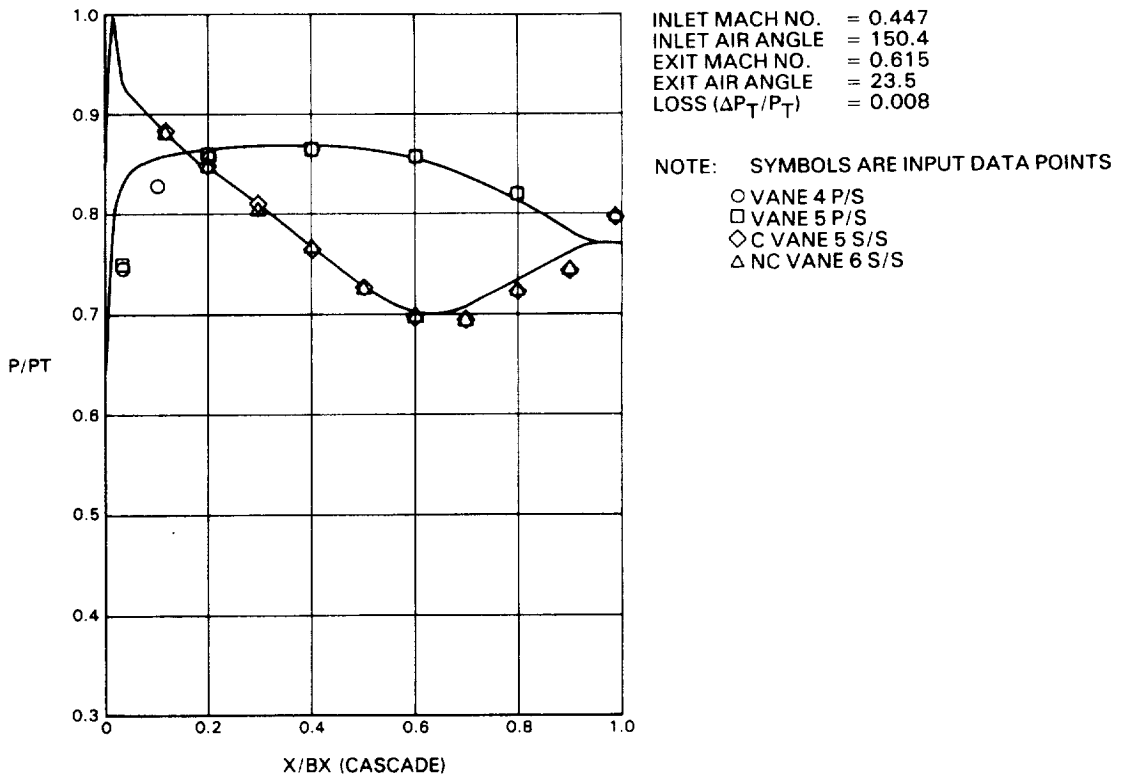


Figure 6-3 (d) Predicted Versus Measured Airfoil Surface Static Pressure Distribution at -13.0 Degrees Incidence

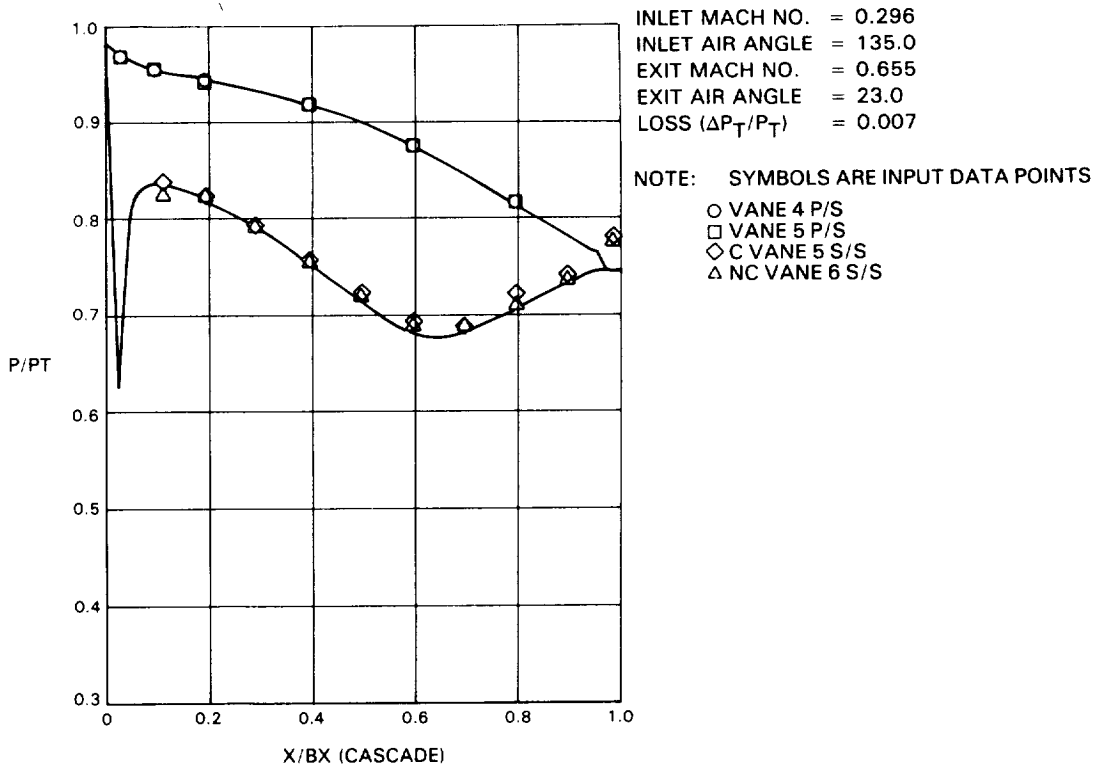


Figure 6-3 (e) Predicted Versus Measured Airfoil Surface Static Pressure Distribution at +2.4 Degrees Incidence

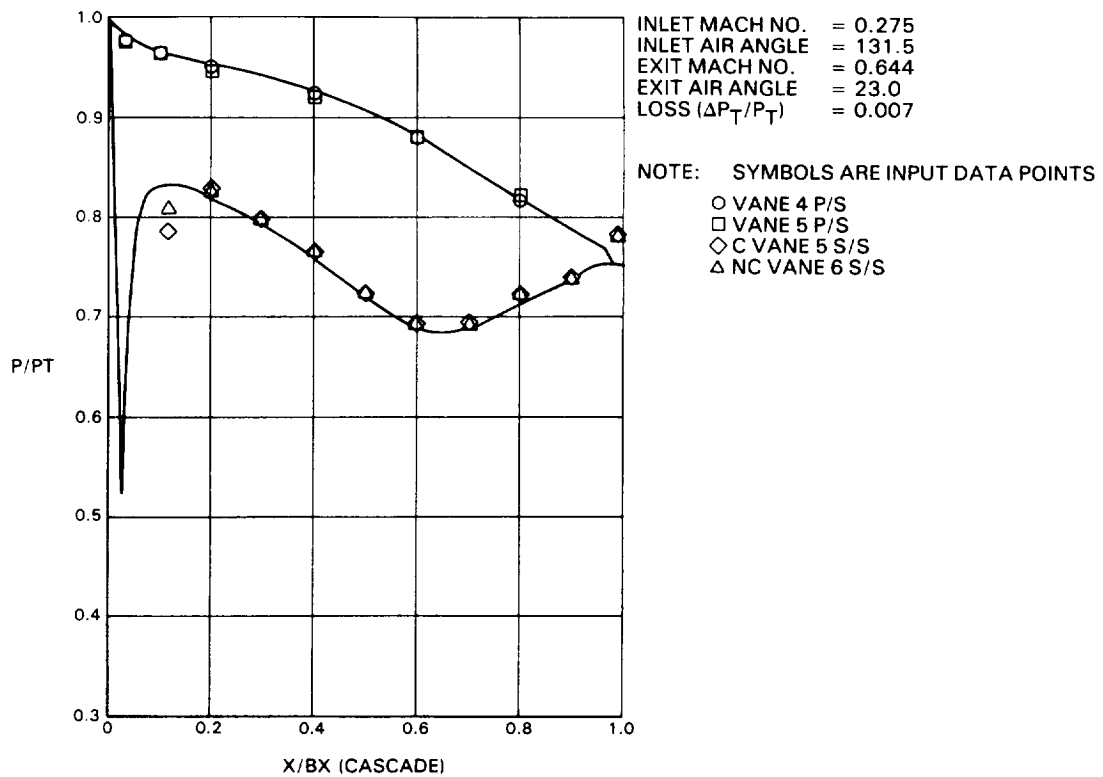


Figure 6-3 (f) Predicted Versus Measured Airfoil Surface Static Pressure Distribution at +5.9 Degrees Incidence

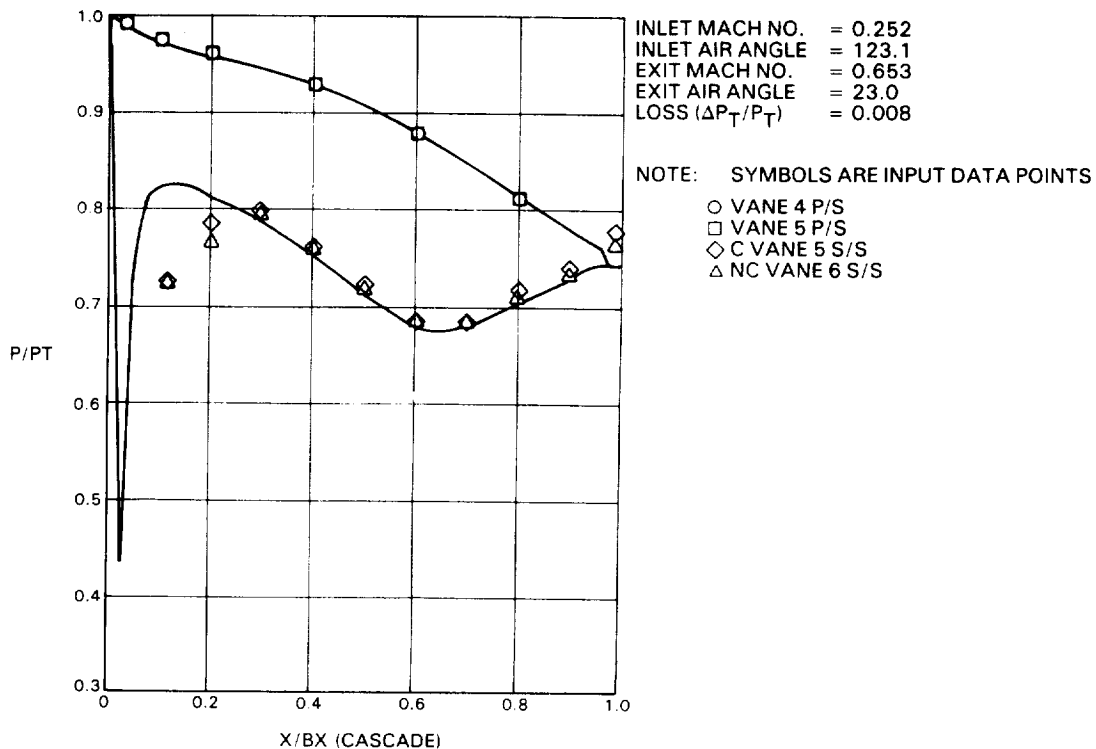


Figure 6-3 (g) Predicted Versus Measured Airfoil Surface Static Pressure Distribution at +9.3 Degrees Incidence

6.1.2.2 Design Point Loss

Cascade total pressure loss data were generated through the use of loss contour plots such as that shown in Figure 6-5. Loss contour plots were generated from the traverse data used to determine total loss. Sets of cone probe data and boundary layer probe data make up the plot. Integration of the pressures represented by the isobars yielded the design-point spanwise loss data shown in Figure 6-6. This figure identifies the regions of profile and secondary losses.

Mass-averaged measured secondary losses are compared to predicted secondary losses in Table 6-II. The measured gross secondary loss of 0.56 percent $\Delta P_T/P_T$ at design point conditions was reasonably well predicted by the Pratt & Whitney Aircraft secondary loss correlation. Both the Dunham and Came (Appendix B - Reference 4) and Mukhtarov and Krichakin (Appendix B - Reference 5) loss correlations considerably underestimate the secondary losses.

TABLE 6-II

SECONDARY LOSS DATA VERSUS PREDICTIONS FROM VARIOUS CORRELATIONS
LOSSES $\Delta P_T/P_T$ (Percent)

<u>Cascade</u>	<u>Data</u>	<u>P&WA Cascade Correlation</u>	<u>Dunham & Came</u>	<u>Mukhtarov & Krichakin</u>
Low Camber Vane	0.56	0.59	0.39	0.12

Note: SYMBOLS ARE INPUT DATA POINTS

- VANE 4 P/S
- ◇ VANE 5 S/S
- VANE 5 P/S
- ▲ VANE 6 S/S

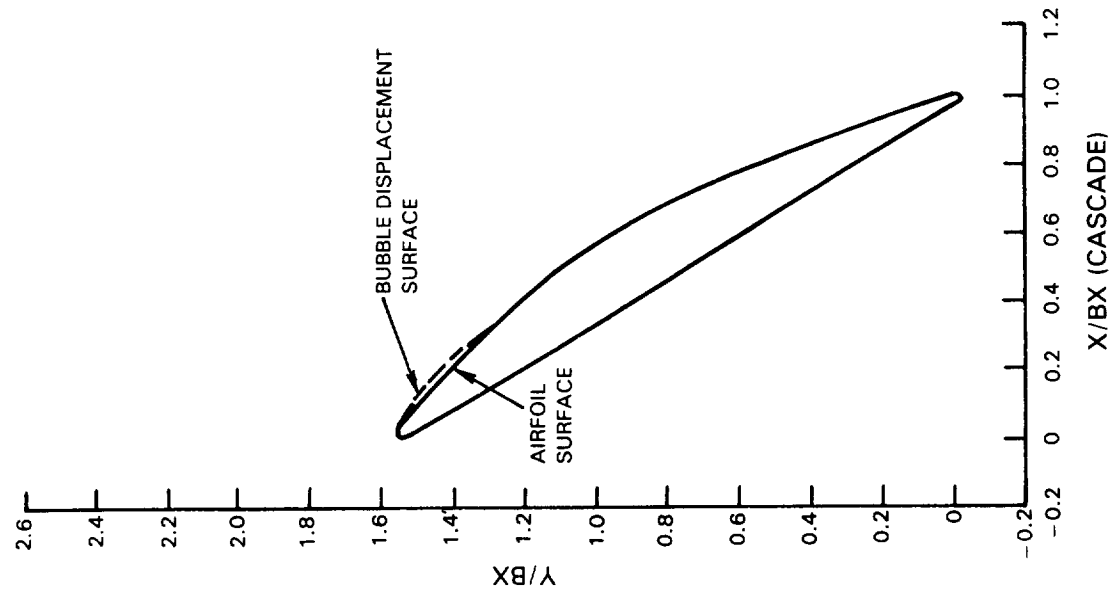
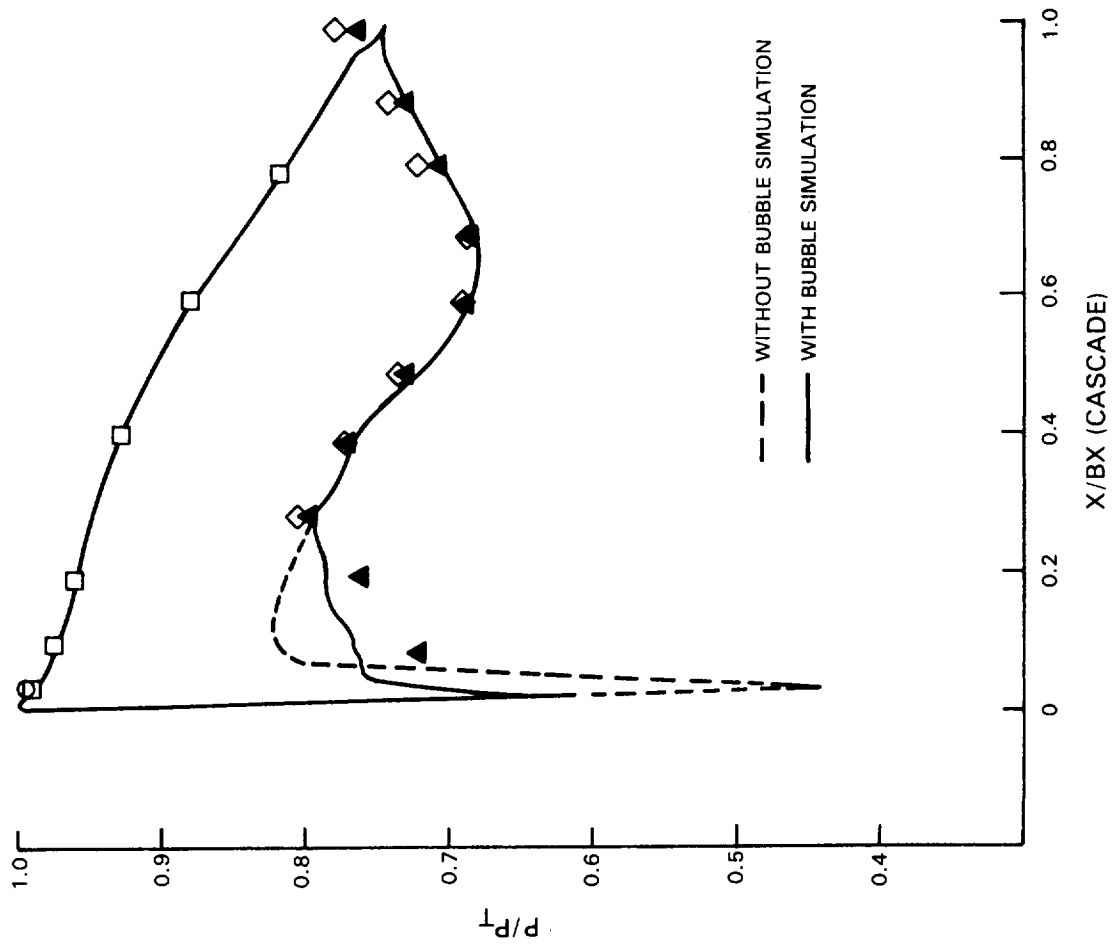


Figure 6-4 Bubble Simulation at +9.3 Degrees Incidence

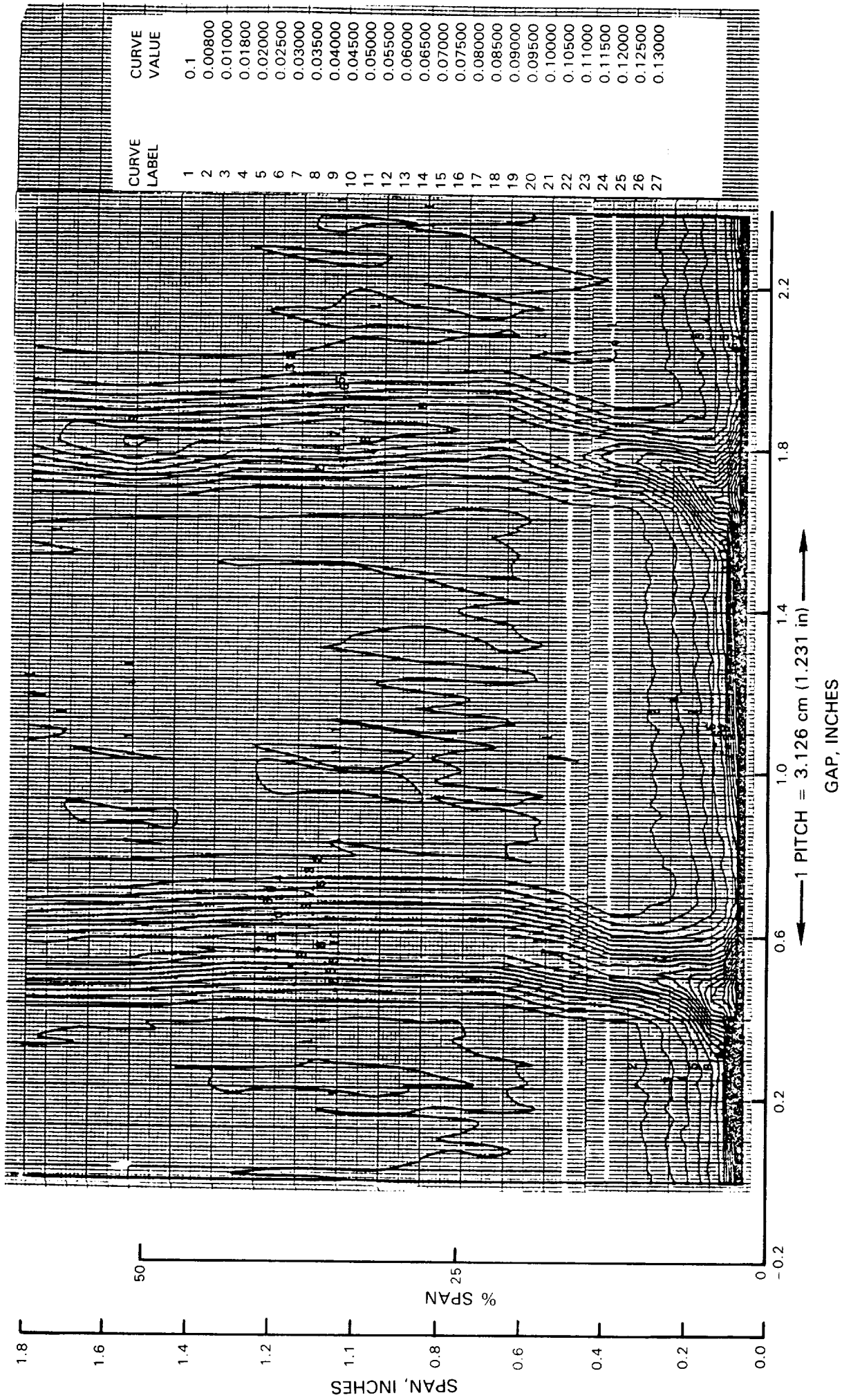


Figure 6-5 Loss Contours for -4.3 Degrees Incidence Data Point

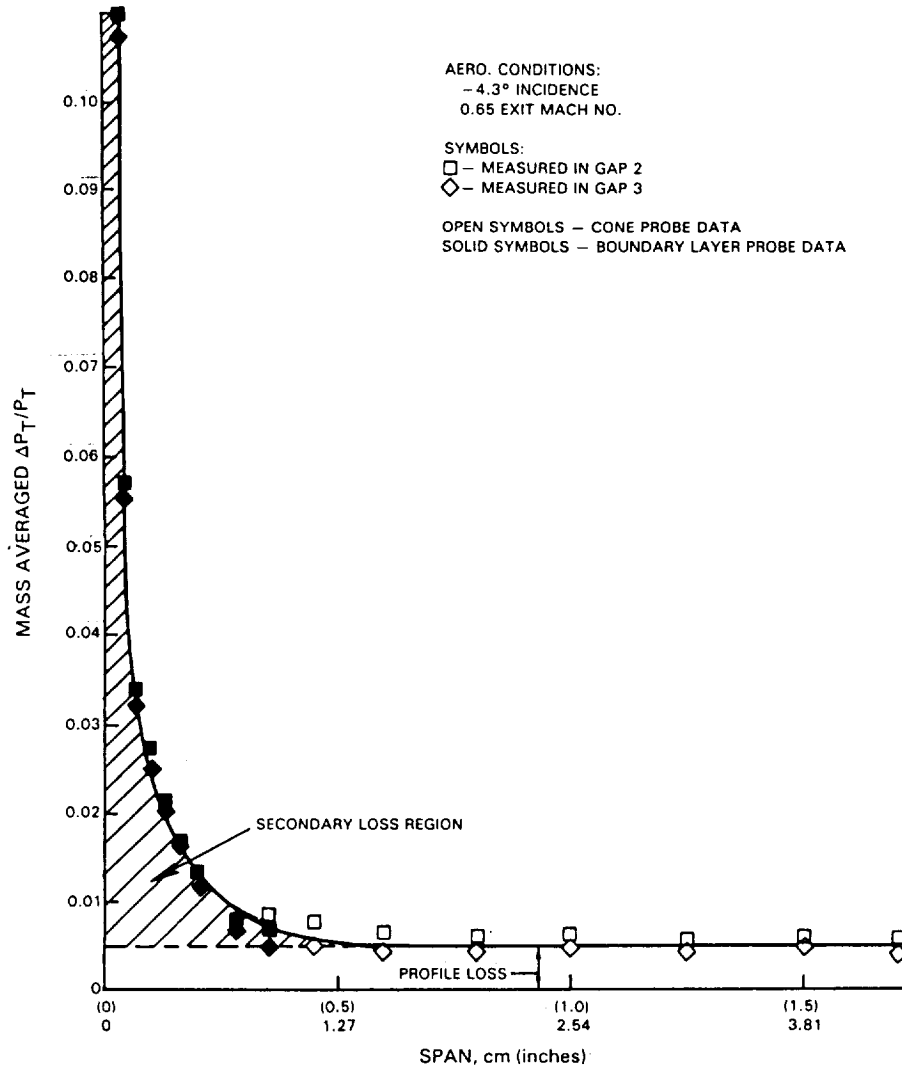


Figure 6-6 Design Point Spanwise Loss Profile

Measured mixed out profile losses at the design point were 0.535 ± 0.065 percent $\Delta P_T/P_T$ and were in good agreement with predictions, as shown in Figure 6-7.

6.1.2.3 Off-Design Profile Loss

Mixed out total pressure profile losses, as a function of incidence for fixed exit Mach number, are shown in Figure 6-7. The dotted line in this figure indicates variation of the average loss as a function of incidence. This line drawn through the data indicates that the minimum losses occur at -8° incidence and the losses become 150 percent of the minimum losses at -12.4° and $+7^\circ$ giving an overall incidence range of 19.4° . With respect to the present design incidence of -4.3° , the line drawn through the data indicates that this vane has a negative incidence range of 8.1° and a positive incidence range of 11.3° . In order to improve upon the negative incidence range, it was recommended that the -4.3° design incidence in the low pressure turbine preliminary design be changed to -2.7° in the final detail design.

The solid line in the above figure show theoretical predictions obtained by Pratt & Whitney Aircraft profile loss prediction system and is in good agreement with the measured data over the entire range of incidence angles.

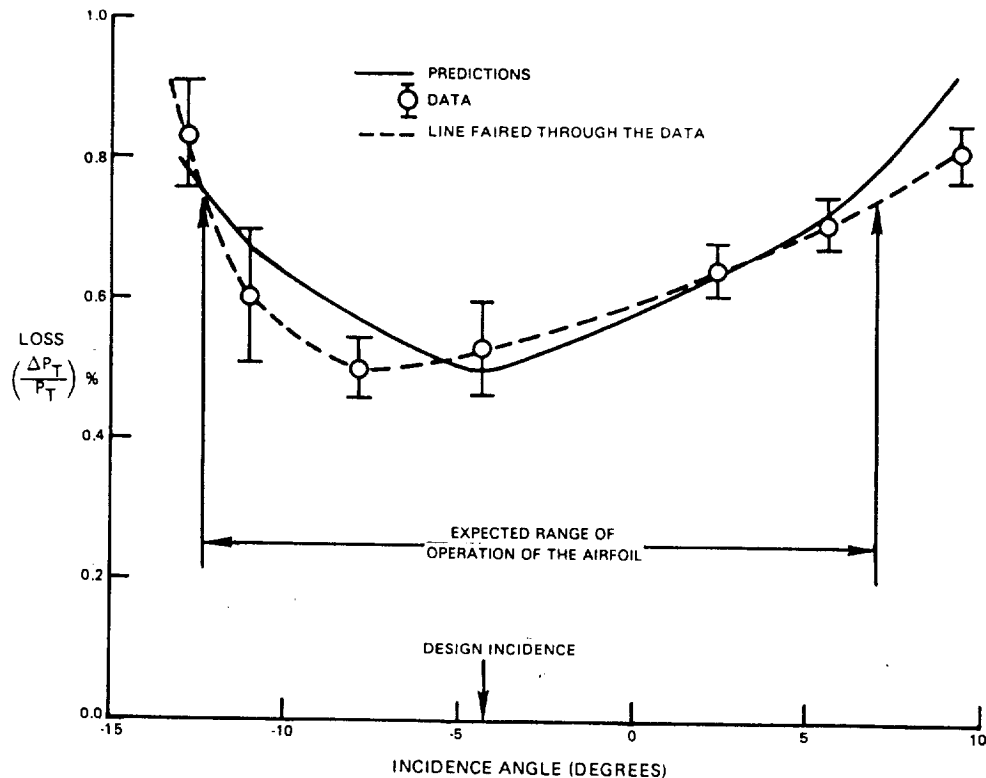


Figure 6-7 Profile Loss Versus Incidence for the Low Camber Vane

6.2 Fourth Stage Blade Cascade Performance

Fourth stage blade cascade testing results compare the performance of the base 'aft-loaded' airfoil and the alternate 'squared-off' airfoil over a range of Mach numbers and incidence angles. Specifically, these results include: (1) surface flow visualizations (conducted prior to performance testing) to assess the behavior of limiting streamline and to identify whether any separation problem existed, (2) assessing the impact of incidence angle and Mach number variation on predicted and measured airfoil pressure distributions, (3) assessing cascade loss with Mach number variations at design point incidence, and (4) assessing cascade loss with fixed Mach number and off-design incidence angle variations. Results of these assessments are discussed in the following sections.

6.2.1 Flow Visualization

Surface flow visualizations were obtained by applying a mixture of lampblack and oil to the airfoil and endwall surfaces. The cascade tunnel was then operated at the test point condition for approximately one minute. Figures 6-8 and 6-9 depict a typical flow visualization for the subsonic 'squared-off' airfoil and the transonic 'aft-loaded' airfoil, respectively. These flow visualizations were obtained at the design point for both airfoils. Figures 6-8 and 6-9 show the flow patterns on the airfoil suction surfaces. The flow patterns in the endwall and pressure surfaces for these two airfoils were found to be similar to the flow patterns described in the studies performed by Langston, Nice, and Hooper (Appendix B - Reference 2) and Kopper, Milano, and Vanco (Appendix B - Reference 3). Therefore, no permanent record of these regions was retained.



Figure 6-8 Subsonic 'Squared-Off' Suction Surface Flow Visualization



Figure 6-9 Transonic 'Aft-Loaded' Suction Surface Flow Visualization

Figures 6-8 and 6-9 show that, at the intersection between the suction surface and the endwalls, both airfoils exhibit a separation line formed due to the presence of a secondary flow vortex. The penetration height of the separation line at the trailing edge of the airfoil, an indicator of the size of the passage vortex in the channel, was found to be 14.2 percent of the span for the subsonic 'squared-off' airfoil and 13.2 percent for the transonic 'aft-loaded' airfoil. The low camber vane showed, at design incidence, the penetration height of the separation line at the trailing edge to be about 0.037 percent of the span (a much lower percentage than that obtained in the present test). This information indicates that the present two airfoil suction surfaces have much larger regions influenced by the endwall passage vortex than the low camber airfoil. Further information regarding the relative magnitudes of the penetration height of the separation line for the present two airfoils is contained in section 6.2.4.

In the middle region of the airfoil suction surface the transonic 'aft-loaded' airfoil showed lampblack collected near the throat of the airfoil. The subsonic 'squared-off' airfoil showed no such phenomenon. Collection of lampblack at a particular location on the airfoil has usually been attributed to separation of the flow. However, separation of the flow also influences the airfoil surface static pressure distributions. In the present case, airfoil surface static pressure distributions (as shown in Figure 6-14) showed no systematic deviation from potential flow calculations. Thus it may be summarized that either the bubble for the transonic 'aft-loaded' airfoil was too small to influence the pressure distributions or the region where the lampblack had collected had very low wall shear stress (usually associated to the earlier part of transition in boundary layers).

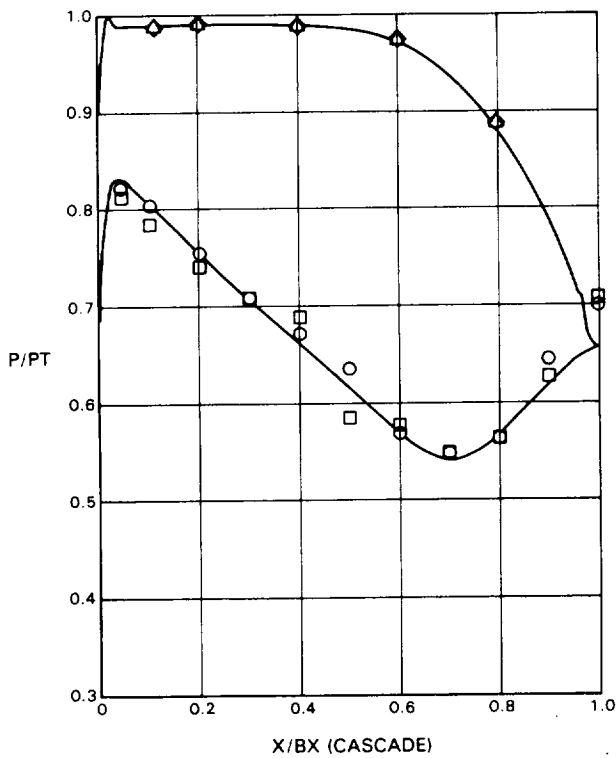
6.2.2 Airfoil Pressure Distributions

Figures 6-10 and 6-11 compare the measured airfoil surface static pressure data for the 'aft-loaded' airfoil and the 'squared-off' airfoil to theoretical predictions obtained by the Pratt & Whitney Aircraft Potential Flow Model. In general, predictions for both airfoils are in good agreement with test data at negative incidence angles over the range of Mach numbers tested. However, at positive incidence angles, the theoretical predictions indicate more diffusion near the airfoil leading edge than is shown by the test data (see Figures 6-10 (f), (g) and 6-11 (e), (f)). This suggests the presence of a separation bubble near the leading edge at positive incidence angles. Accurately predicting the viscous-inviscid interaction effects of this phenomenon requires more sophisticated calculation procedures than are in general use.

6.2.3 Design Point Loss

Mixed-out* mid-span loss data for transonic 'aft-loaded' and subsonic 'squared-off' airfoils are compared to predictions in Figure 6-12 at design point incidence over the range of Mach numbers tested. Agreement between predictions and data is good over the entire range and the data indicate that the losses for the 'aft-loaded' airfoil are about 18 percent lower than those for the 'squared-off' airfoil.

* Mixed-out refers to an analytical mixing of the two-dimensional element of the total flow composition to a homogeneous state. It is a technique commonly used to calculate total cascade loss and it is discussed in section 5-4.

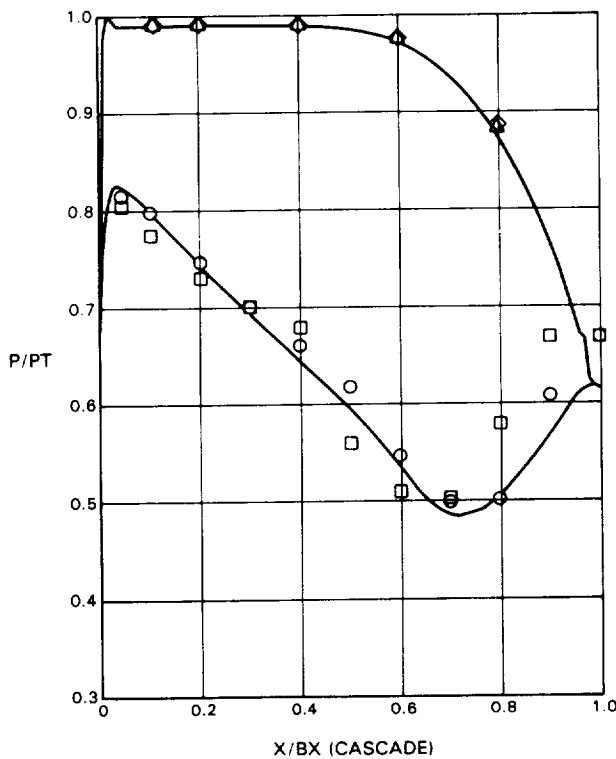


INLET MACH NO. = 0.3415
 INLET AIR ANGLE = 49.5
 EXIT MACH NO. = 0.784
 EXIT AIR ANGLE = 26.2
 LOSS ($\Delta P_T/P_T$) = 0.0078
 INCIDENCE = -4.72

NOTE: SYMBOLS ARE INPUT DATA POINTS

- BLADE 5 S/S
- BLADE 6 S/S
- ◇ BLADE 6 P/S
- △ BLADE 7 P/S

Figure 6-10 (a) 'Aft-Loaded' Airfoil - Predicted Versus Measured Pressure Distribution at -4.72 Degrees Incidence, Mach Number 0.784



INLET MACH NO. = 0.351
 INLET AIR ANGLE = 49.5
 EXIT MACH NO. = 0.852
 EXIT AIR ANGLE = 26.2
 LOSS ($\Delta P_T/P_T$) = 0.0082
 INCIDENCE = -4.72

NOTE: SYMBOLS ARE INPUT DATA POINTS

- BLADE 5 S/S
- BLADE 6 S/S
- ◇ BLADE 6 P/S
- △ BLADE 7 P/S

Figure 6-10 (b) 'Aft-Loaded' Airfoil - Predicted Versus Measured Pressure Distribution at -4.72 Degrees Incidence, Mach Number 0.852

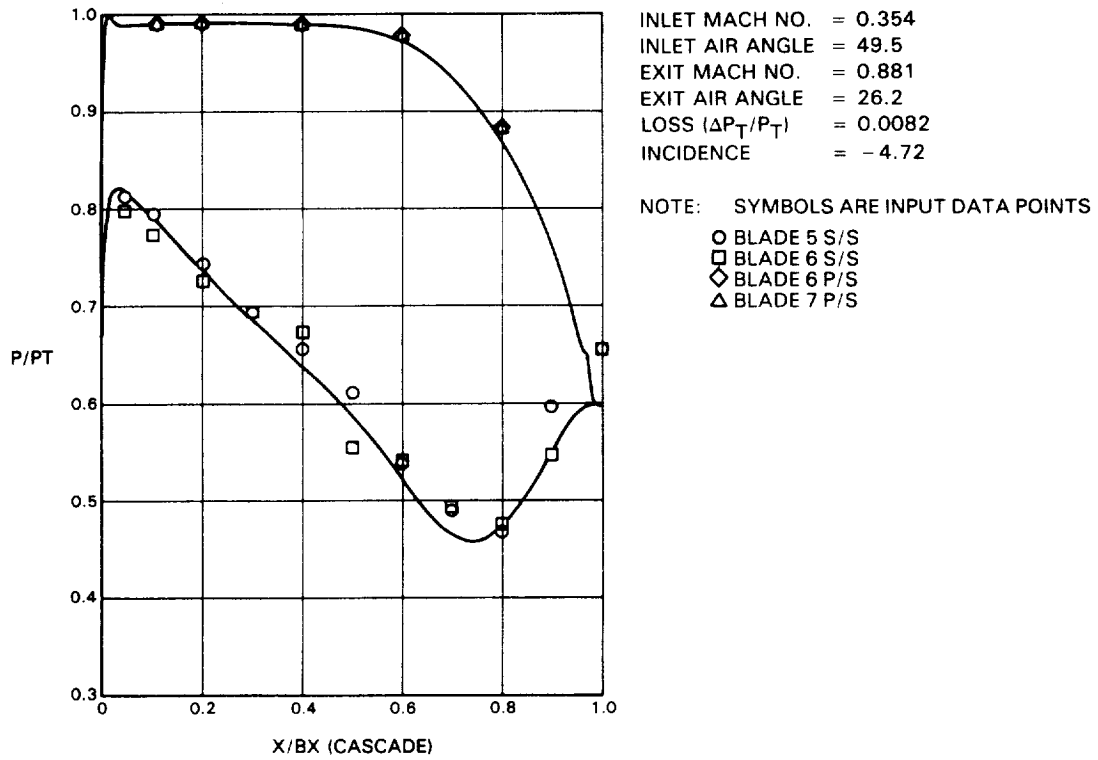


Figure 6-10 (c) 'Aft-Loaded' Airfoil - Predicted Versus Measured Pressure Distribution at -4.72 Degrees Incidence, Mach Number 0.881

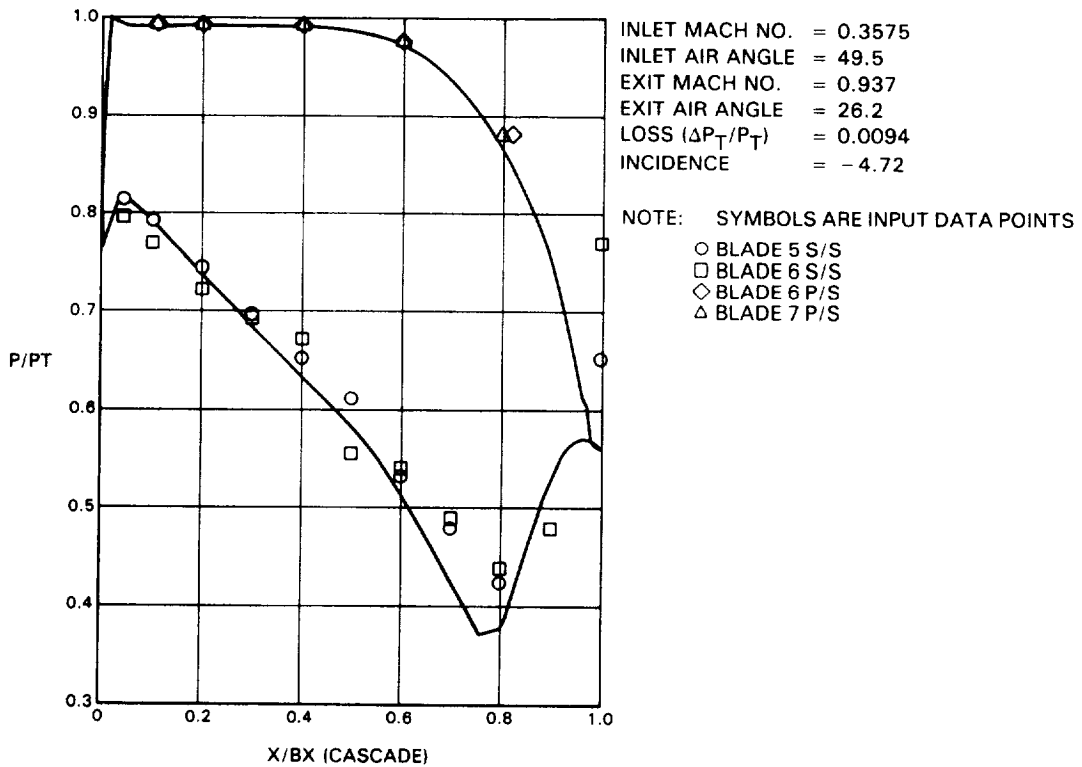


Figure 6-10 (d) 'Aft-Loaded' Airfoil - Predicted Versus Measured Pressure Distribution at -4.72 Degrees Incidence, Mach Number 0.937

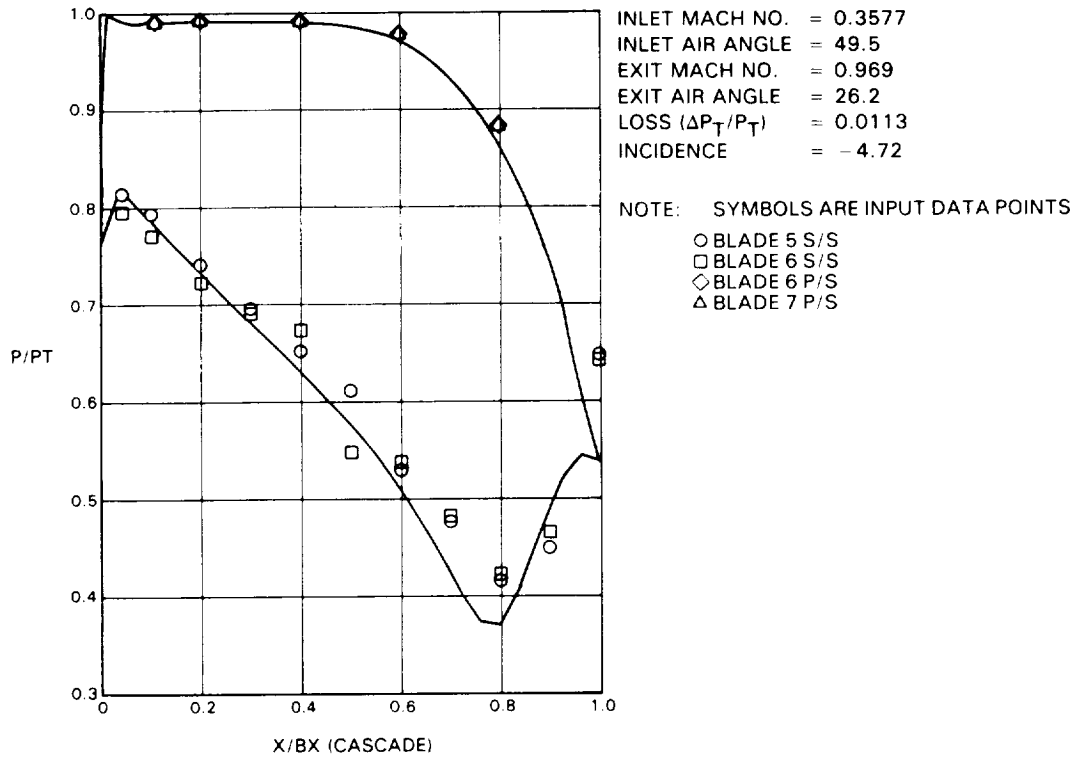


Figure 6-10 (e) 'Aft-Loaded' Airfoil - Predicted Versus Measured Pressure Distribution at -4.72 Degrees Incidence, Mach Number 0.969

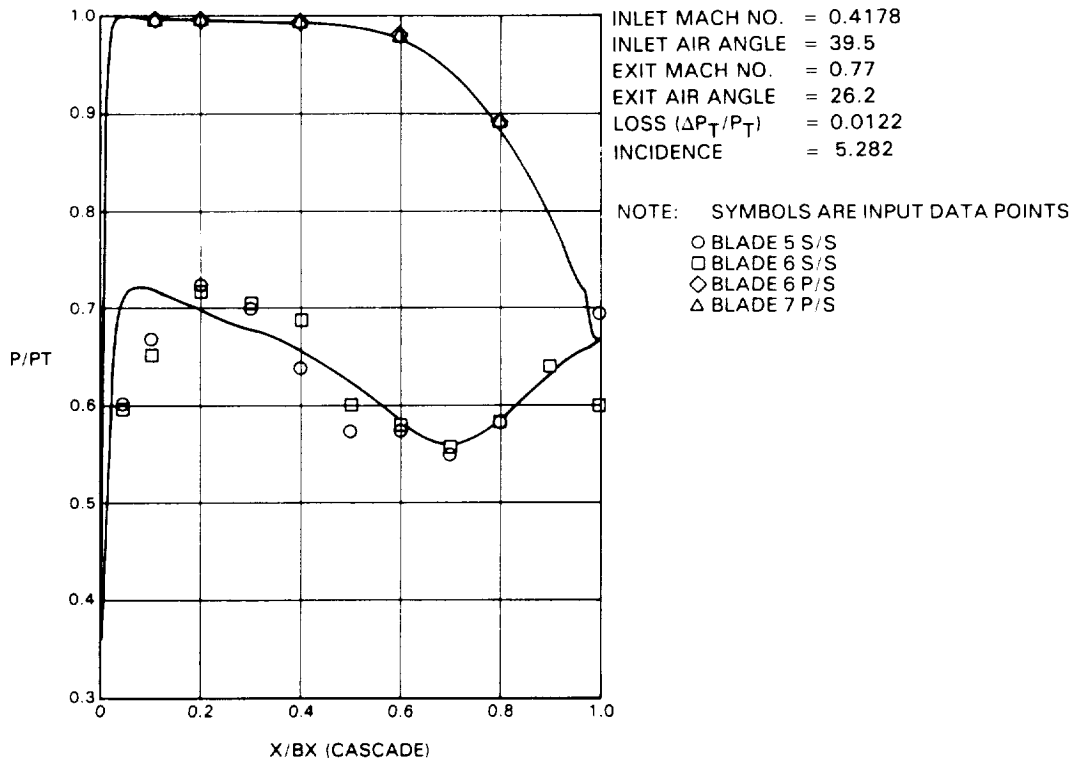


Figure 6-10 (f) 'Aft-Loaded' Airfoil - Predicted Versus Measured Pressure Distribution at +5.28 Degrees Incidence, Mach Number 0.770

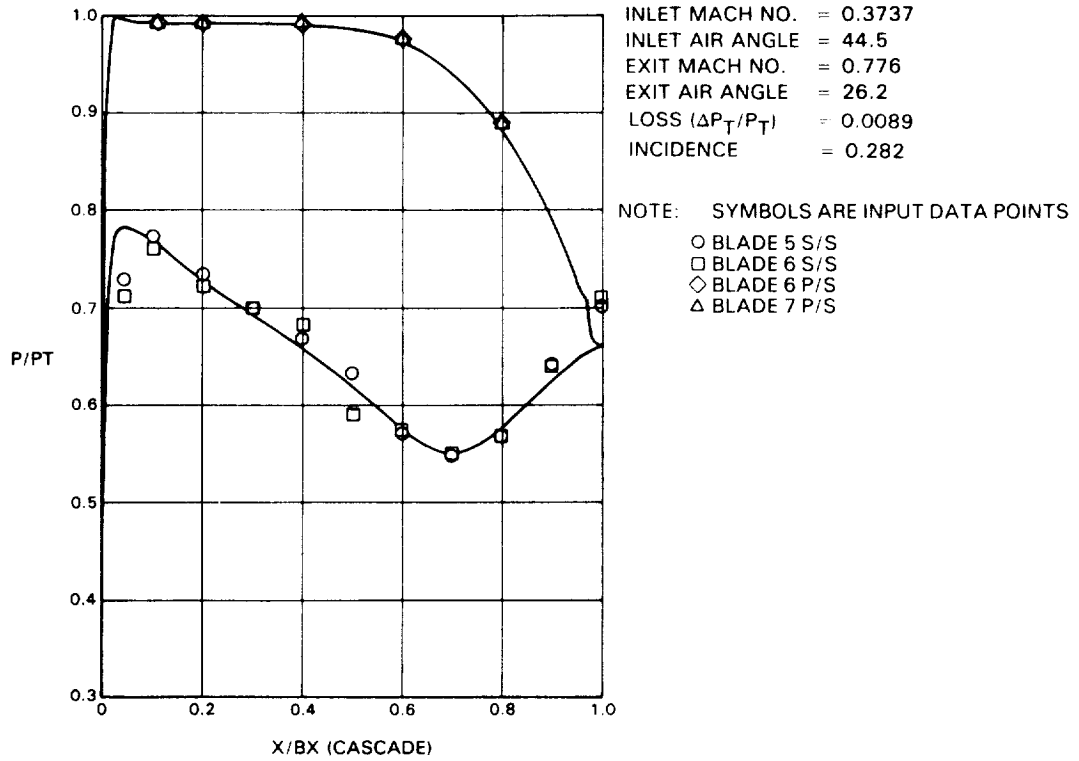


Figure 6-10 (g) 'Aft-Loaded' Airfoil - Predicted Versus Measured Pressure Distribution at +0.28 Degrees Incidence, Mach Number 0.776

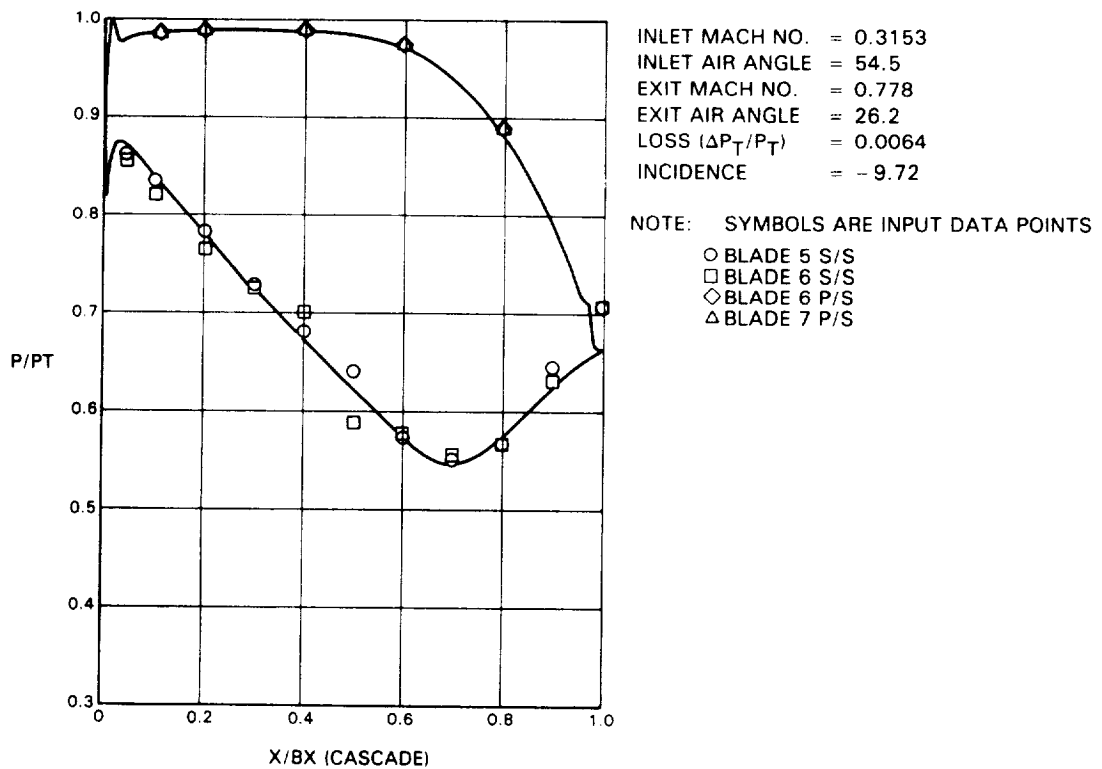


Figure 6-10 (h) 'Aft-Loaded' Airfoil - Predicted Versus Measured Pressure Distribution at -9.72 Degrees Incidence, Mach Number 0.778

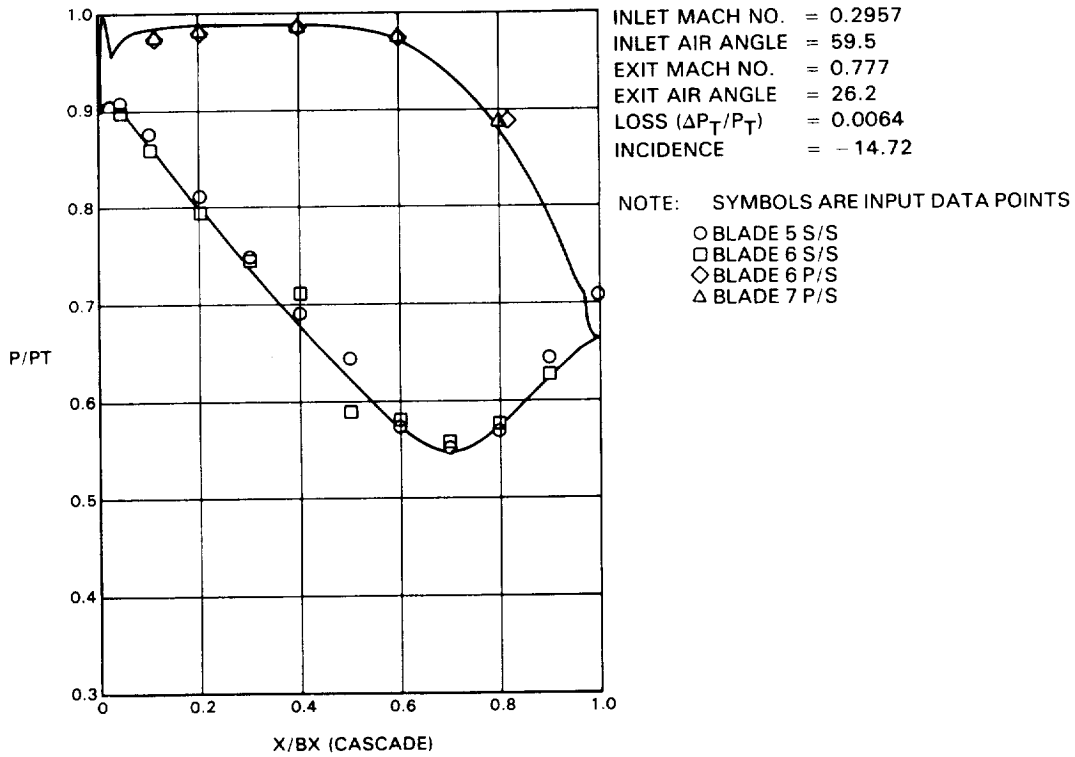


Figure 6-10 (i) 'Aft-Loaded' Airfoil - Predicted Versus Measured Pressure Distribution at -14.72 Degrees Incidence, Mach Number 0.777

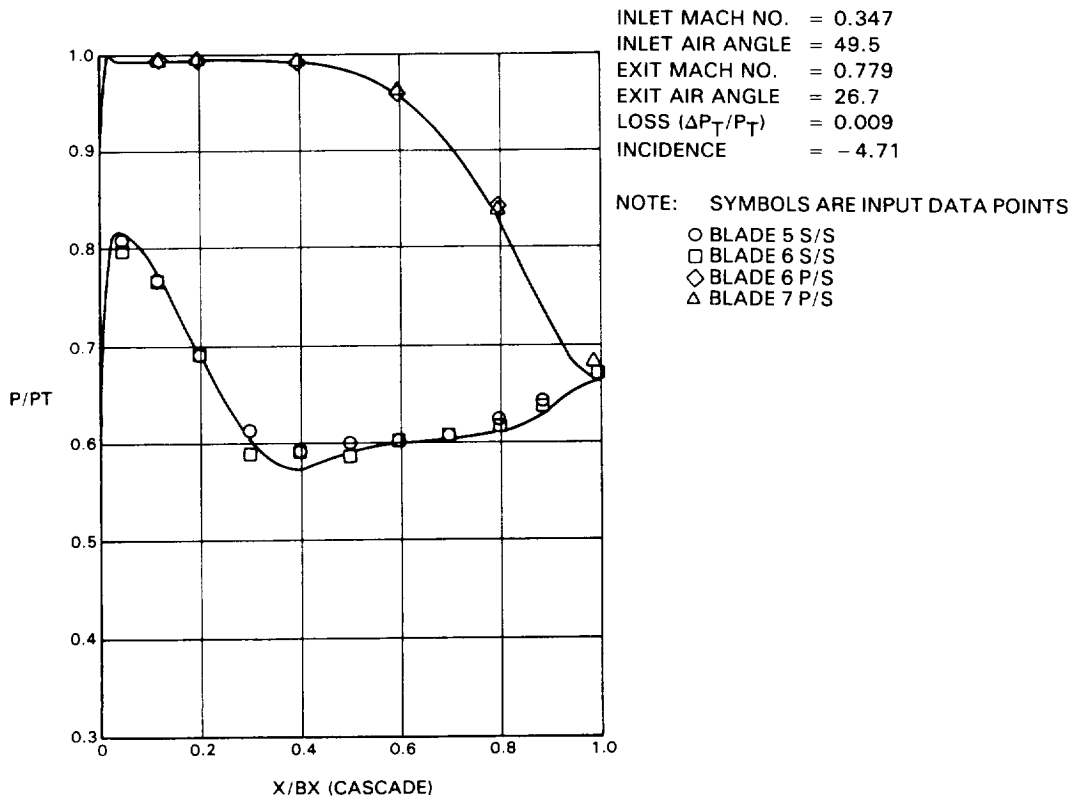


Figure 6-11 (a) 'Squared-Off' Airfoil - Predicted Versus Measured Pressure Distribution at -4.71 Degrees Incidence, Mach Number 0.779

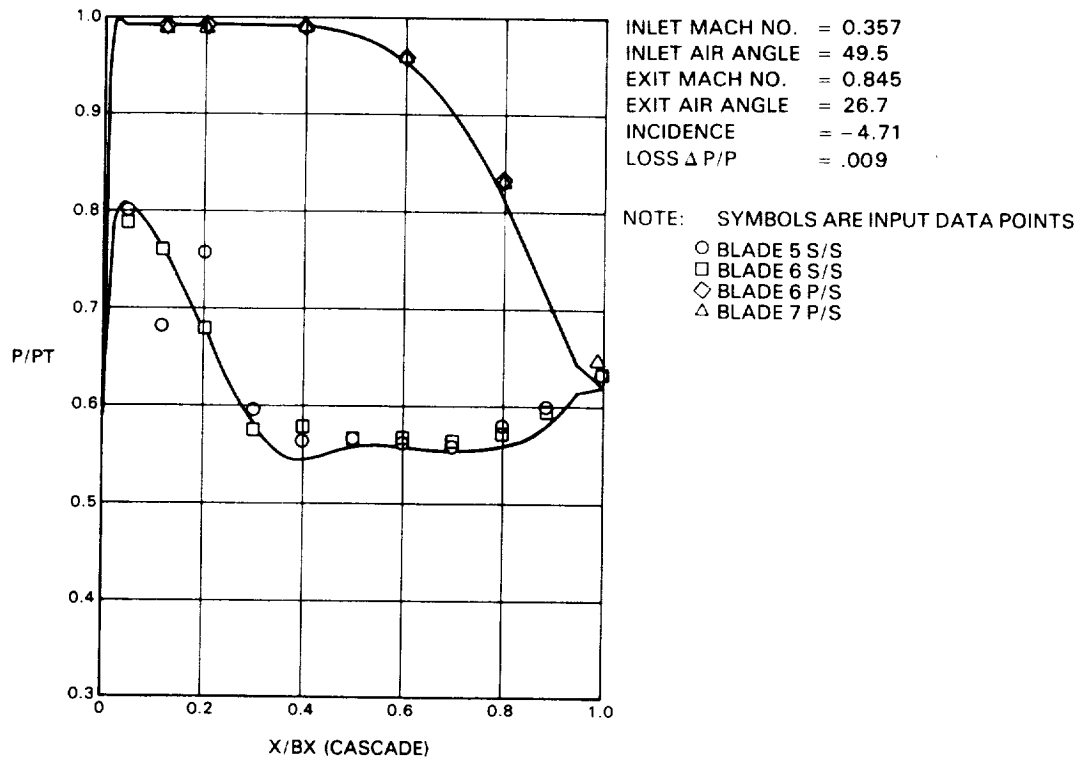


Figure 6-11 (b) 'Squared-Off' Airfoil - Predicted Versus Measured Pressure Distribution at -4.71 Degrees Incidence, Mach Number 0.845

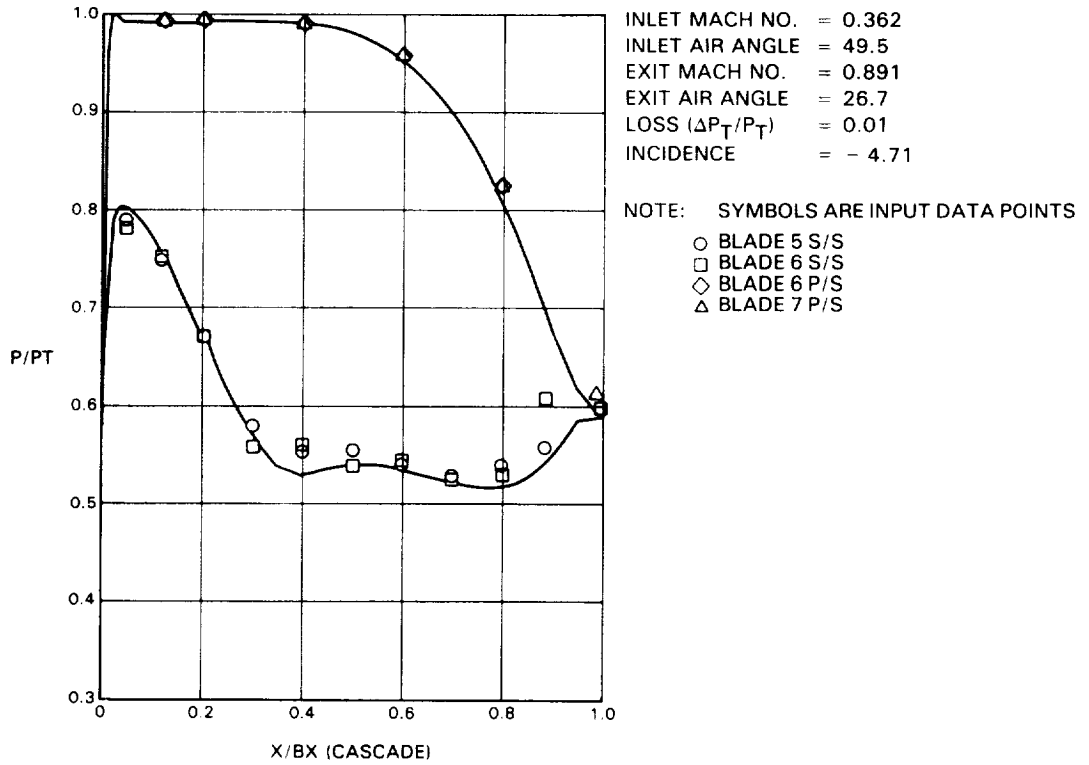


Figure 6-11 (c) 'Squared-Off' Airfoil - Predicted Versus Measured Pressure Distribution at -4.71 Degrees Incidence, Mach Number 0.891

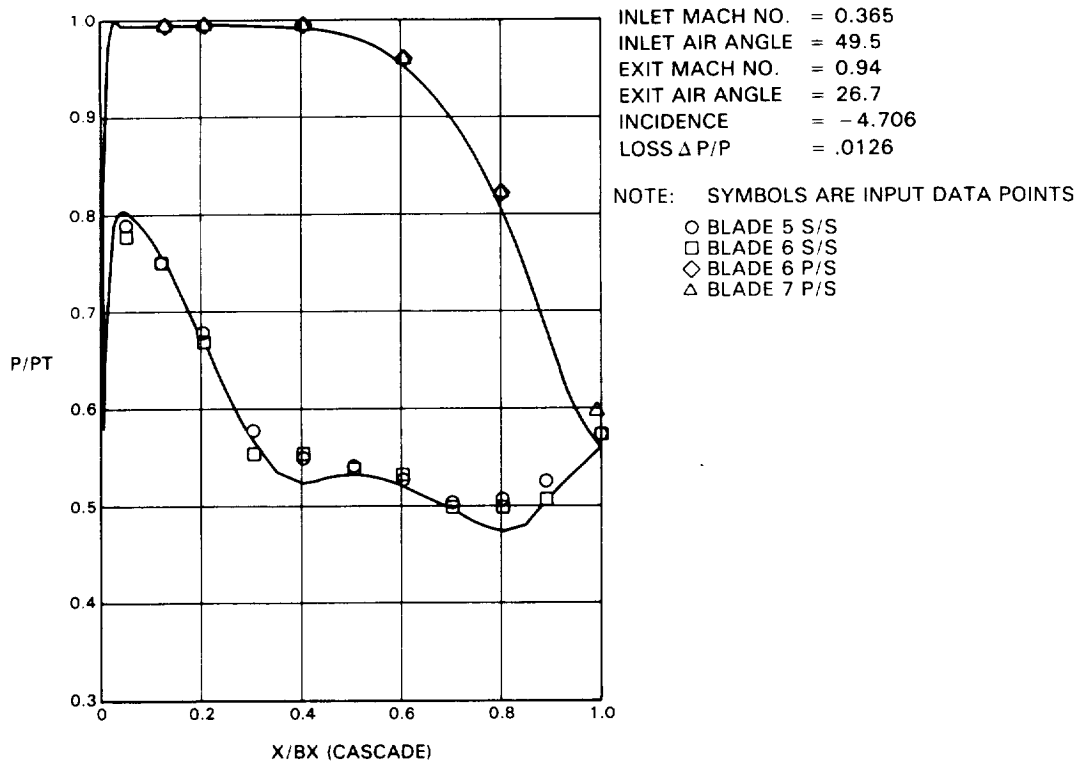


Figure 6-11 (d) 'Squared-Off' Airfoil - Predicted Versus Measured Pressure Distribution at -4.71 Degrees Incidence, Mach Number 0.940

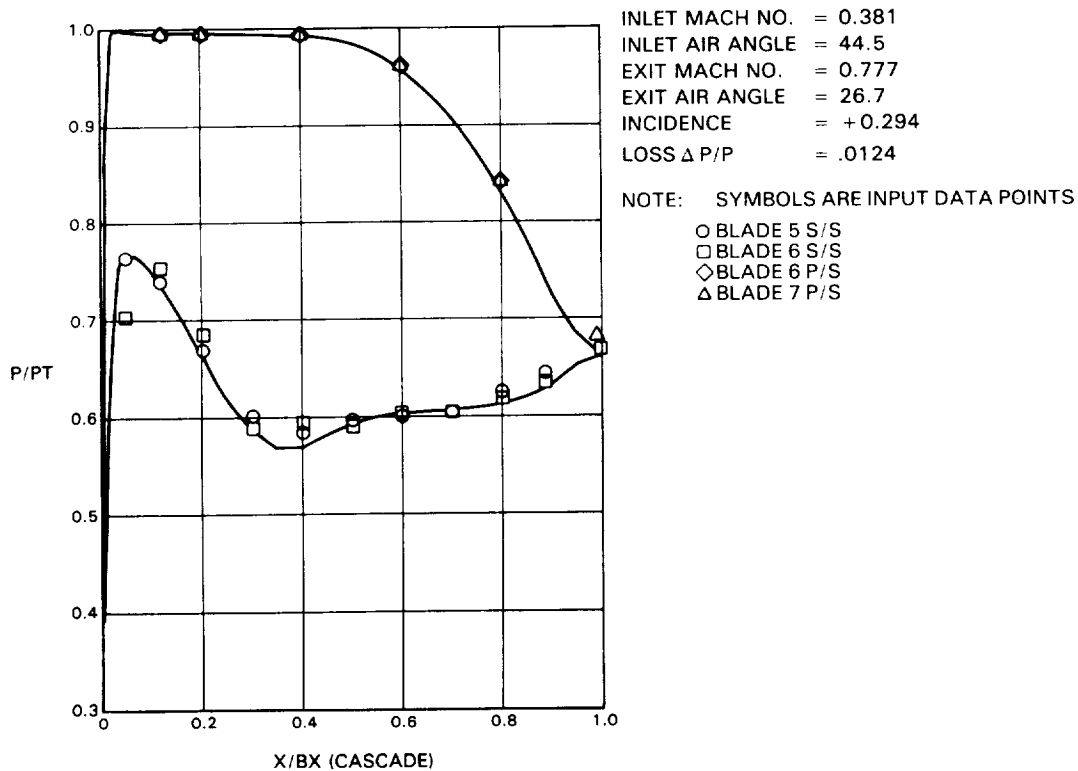


Figure 6-11 (e) 'Squared-Off' Airfoil - Predicted Versus Measured Pressure Distribution at +0.29 Degrees Incidence, Mach Number 0.777

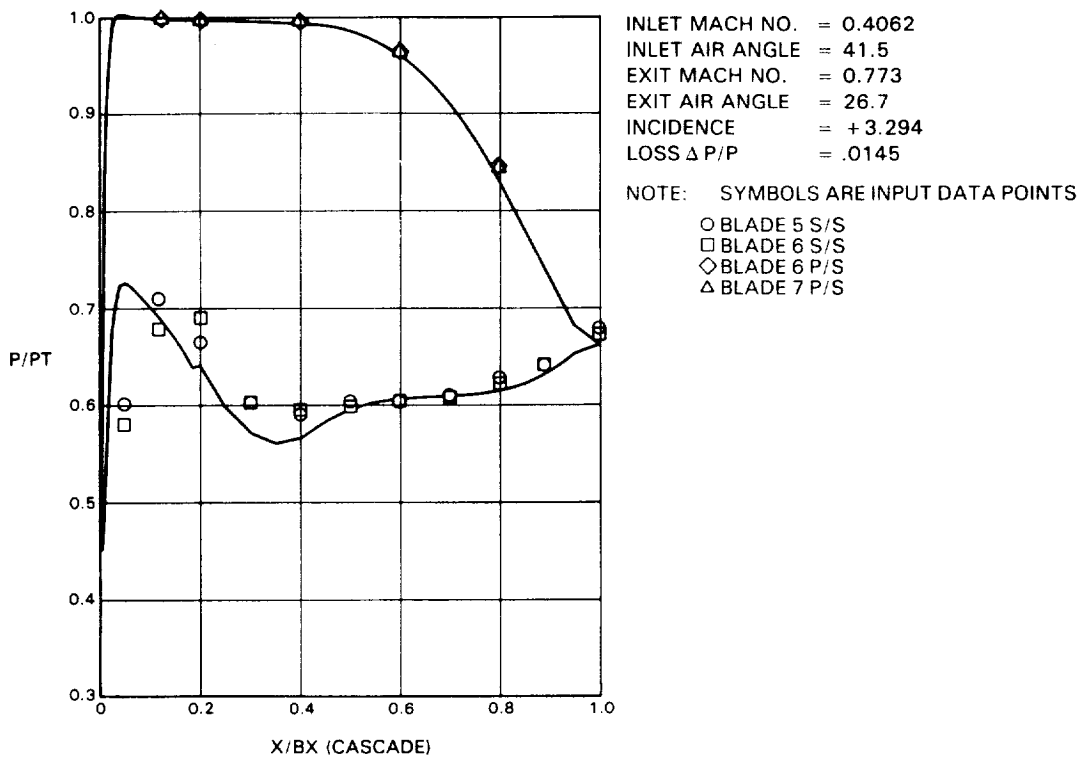


Figure 6-11 (f) 'Squared-Off' Airfoil - Predicted Versus Measured Pressure Distribution at +3.3 Degrees Incidence, Mach Number 0.773

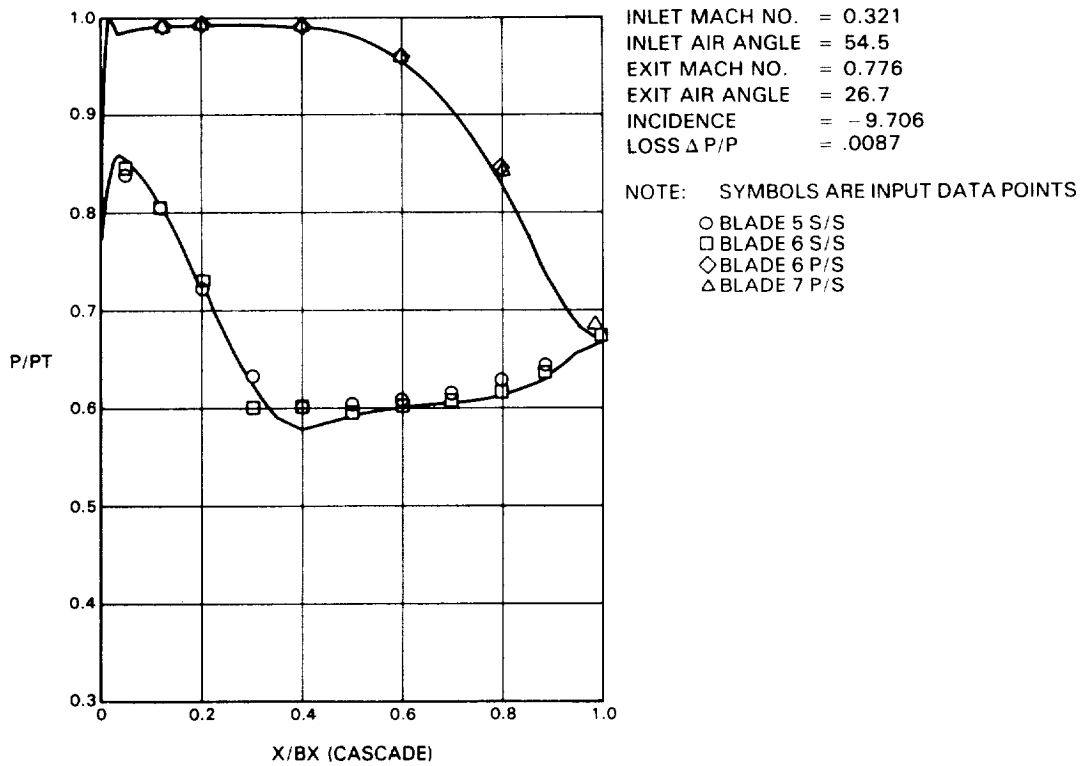


Figure 6-11 (g) 'Squared-Off' Airfoil - Predicted Versus Measured Pressure Distribution at -9.71 Degrees Incidence, Mach Number 0.776

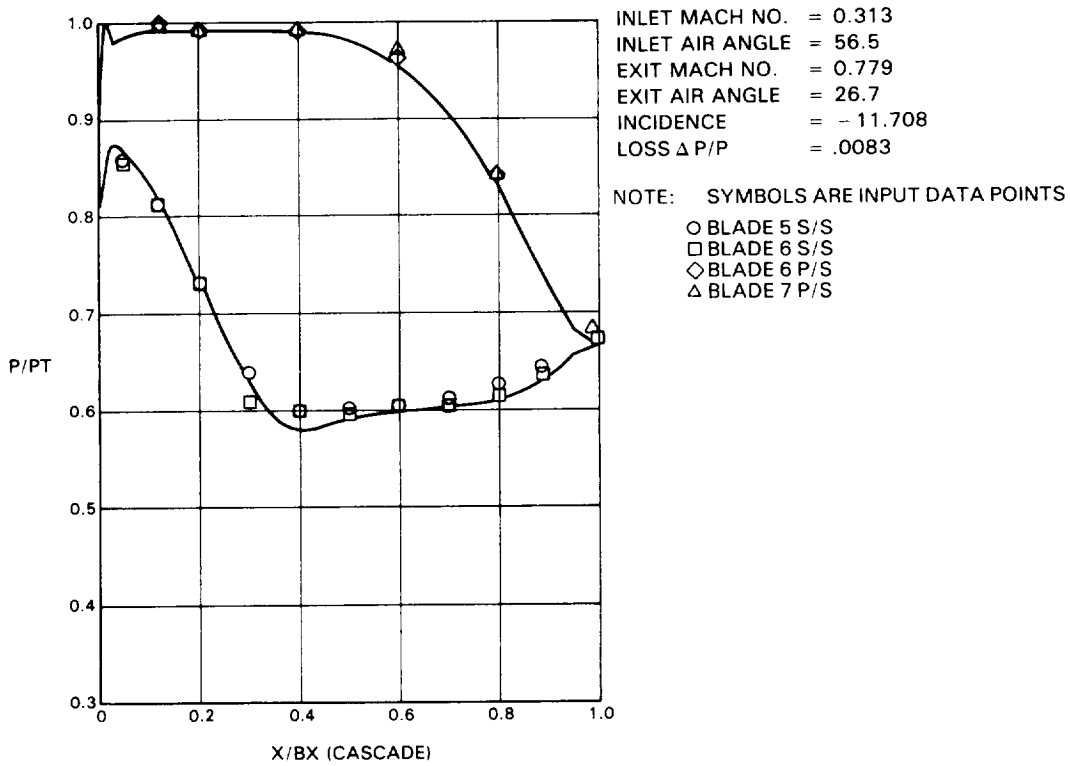


Figure 6-11 (h) 'Squared-Off' Airfoil - Predicted Versus Measured Pressure Distribution at -11.71 Degrees Incidence, Mach Number 0.779

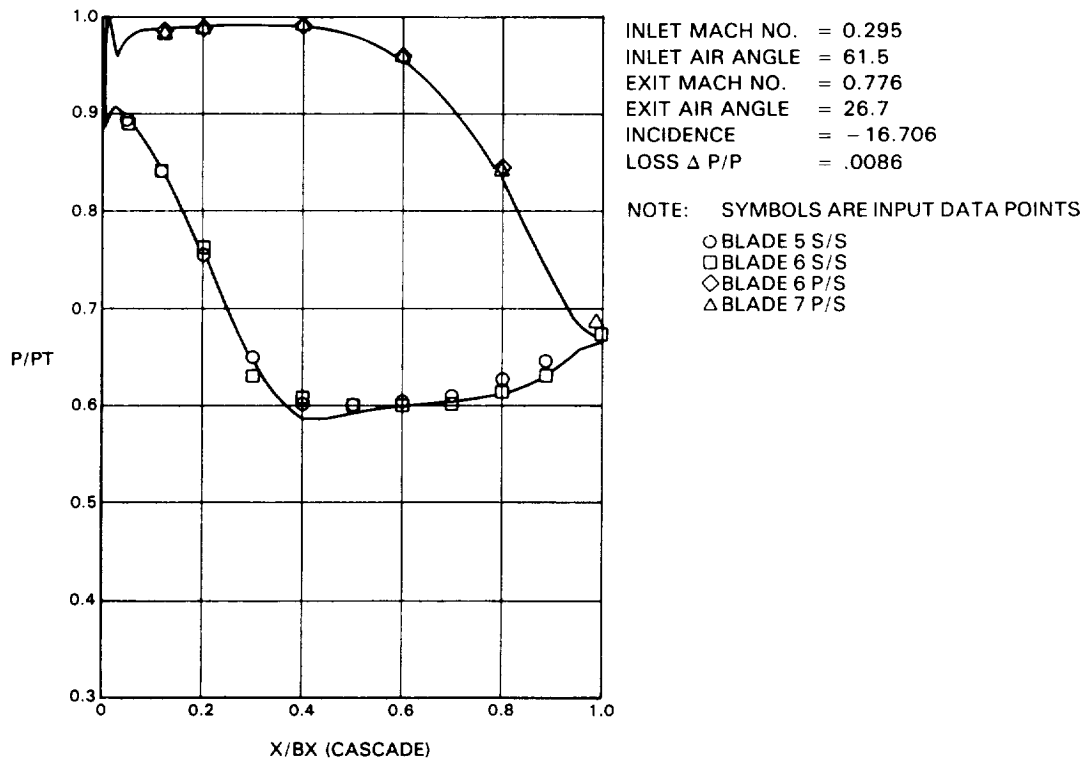


Figure 6-11 (i) 'Squared-Off' Airfoil - Predicted Versus Measured Pressure Distribution at -16.71 Degrees Incidence, Mach Number 0.776

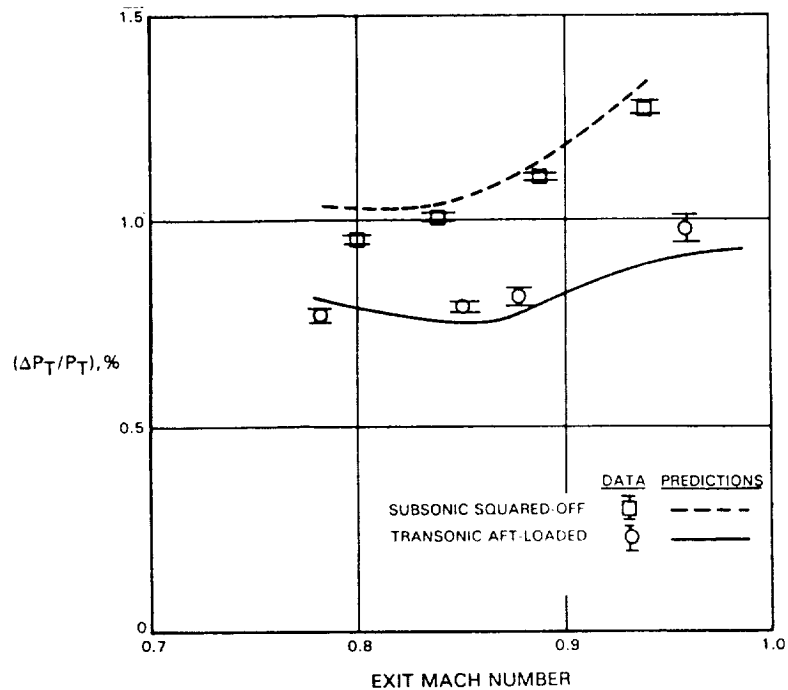


Figure 6-12 'Squared-Off' and 'Aft-Loaded' Airfoils Predicted Versus Measured Mixed-Out, Mid-Span Losses

The gap averaged secondary losses for the transonic 'aft-loaded' and the subsonic 'squared-off' airfoils at the design point are shown in Figure 6-13. An interesting observation made from Figure 6-13 shows maxima in the loss curve closer to the endwall for the transonic 'aft-loaded' airfoil than the subsonic 'squared-off' airfoil. This is consistent with lower penetration height of the separation line for the transonic 'aft-loaded' airfoil when compared to the subsonic 'squared-off' airfoil as discussed in section 6.2.1.

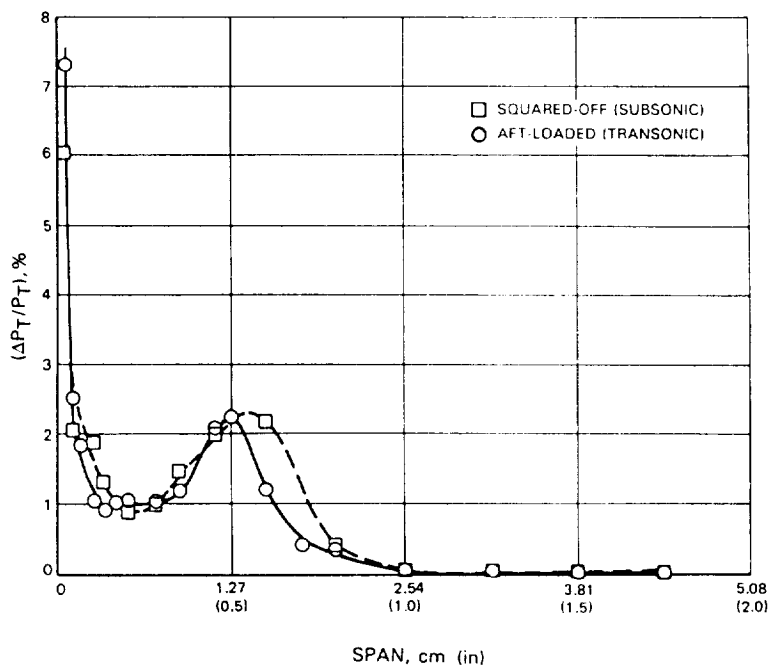


Figure 6-13 'Squared-Off' and 'Aft-Loaded' Airfoils Measured Gap-Averaged Secondary Losses

Gap-averaged secondary losses for the 'aft-loaded' and 'squared-off' airfoils are compared to predictions in Table 6-III, items 2 and 3 at the design point. As shown in Table 6-III, the Pratt & Whitney Aircraft cascade correlation is in good agreement with the data although it does not predict an advantage for either type of airfoil. The prediction of Dunham And Came (Appendix B - Reference 4) considerably overestimates the secondary losses of both airfoils while the Mukhtarov and Krichakin (Appendix B - Reference 5) prediction considerably underestimates them.

TABLE 6-III

SECONDARY LOSS DATA VERSUS PREDICTIONS FROM VARIOUS CORRELATIONS
LOSSES $\Delta P_T/P_T$ (Percent)

<u>Cascade</u>	<u>Data</u>	<u>P&WA Cascade Correlation</u>	<u>Dunham & Came</u>	<u>Mukhtarov & Krichakin</u>
Transonic Aft-Loaded	0.79	0.90	1.89	0.67
Subsonic Squared-Off	0.9	0.89	1.89	0.67

6.2.4 Off-Design Loss

Mixed-out mid-span profile loss data for the transonic 'aft-loaded' and the subsonic 'squared-off' airfoils are compared to predictions in Figure 6-14 over a range of inlet gas angles with fixed exit Mach number. Agreement between predictions and data is good over the entire range and the data indicate that the profile loss for the 'aft-loaded' airfoil is lower than or equal to that of the 'squared-off' airfoil over the incidence range tested.

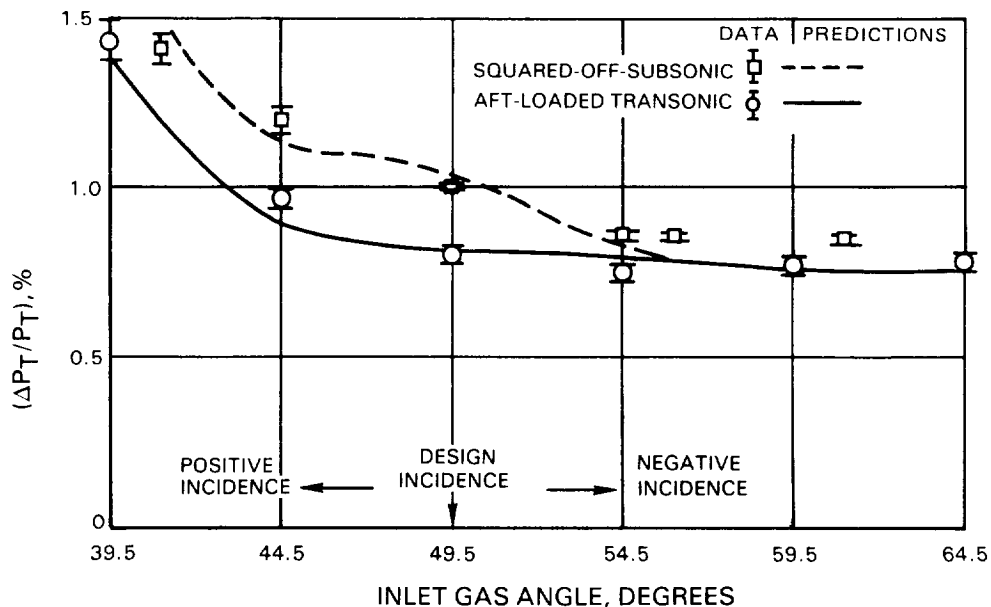


Figure 6-14

Subsonic 'Squared-Off' and Transonic 'Aft-Loaded' Airfoils Predicted Versus Measured Profile Loss Data

6.3 Design Concept Verification

Design concept verification test results compare the performance of the base 'aft-loaded' airfoil design to two 'squared-off' candidates: a 'heavyweight' design and a 'lightweight' design (both described in Section 3.2 of this report). Specifically, these results include (1) assessing the impact of incidence angle and Mach number variation on predicted and measured airfoil pressure distributions, (2) assessing cascade loss with Mach number variations at design point incidence, and (3) assessing cascade loss with fixed Mach number and off-design incidence angle variations. Results of these assessments are discussed in the following sections. Flow visualizations were not included in this effort. However, an attempt was made to determine if higher levels of inlet turbulence, generated by a turbulence grid installed at the inlet to the test section, would influence the outcome of the results.

6.3.1 Airfoil Pressure Distributions

Figures 6-15, 6-16, and 6-17 compare the measured airfoil surface static pressure data for the 'aft-loaded' baseline and the heavyweight and lightweight designs to predictions over a range of incidence angles at fixed exit Mach number and over a range of exit Mach numbers at the design point incidence angle. In general, predictions for all three airfoils are in good agreement with test data at negative incidence angles over the range of Mach numbers tested. However, as was the case with the alternate loading tests, at positive incidence angles the theoretical predictions indicate more diffusion overspeed near the airfoil leading edge than was shown by the test data. Again, this suggests the presence of a separation bubble near the leading edge at positive incidence angles.

As shown in the following figures, the potential flow prediction for the 'aft-loaded' and the 'heavyweight' airfoils show better agreement with the measured data in the leading edge regions (Figures 6-15(a) and 6-16(a)) than it does for the 'lightweight' airfoil (Figure 6-17(a)). The 'aft-loaded' and the 'heavyweight' airfoils were designed for about -4.72 degrees incidence. The 'lightweight' airfoil was designed for about +0.3 degrees incidence which could result in larger overspeeds at the leading edges. Further comments concerning the effect of leading edge overspeed on the performance of the 'lightweight' airfoil are contained in the following subsection of this report.

6.3.2 Design Point Loss

Mixed-out mid-span profile loss data for the three airfoil designs are compared to predictions in Figure 6-18 at design point incidence over the range of Mach numbers tested. Agreement between predictions and data is good over the entire range and the data indicate that profile losses for the 'aft-loaded' baseline airfoil are about 34 percent lower than those for the 'lightweight' design and about 21.3 percent lower than those for the 'heavyweight' design.

Testing with the turbulence grid installed at design point conditions did not result in a significant change in profile losses, as shown in Figure 6-18. Therefore, testing at off-design incidence angles was conducted with the turbulence grid removed.

It should be noted that higher loss magnitudes obtained for the 'lightweight' airfoil at the design point are possibly due to the higher leading edge overspeeds for this airfoil when compared to the 'aft-loaded' and 'heavyweight' airfoils.

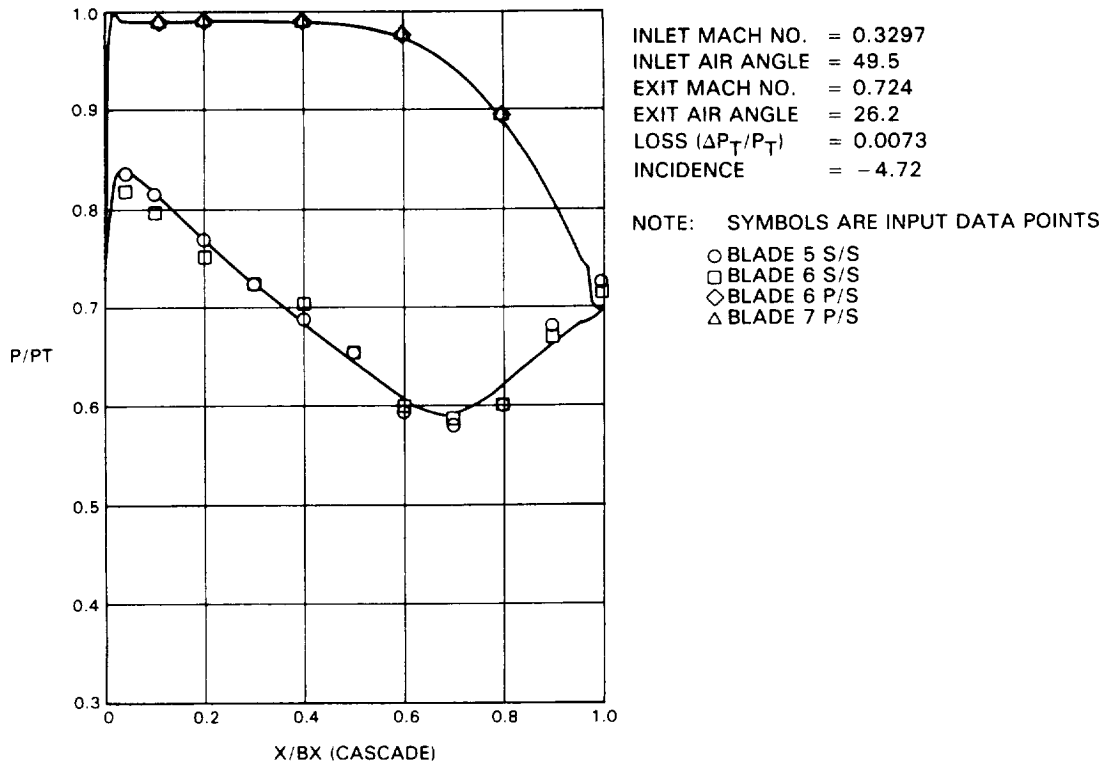


Figure 6-15 (a) 'Aft-Loaded' Baseline - Predicted Versus Measured Pressure Distribution at -4.72 Degrees Incidence, Mach Number 0.724

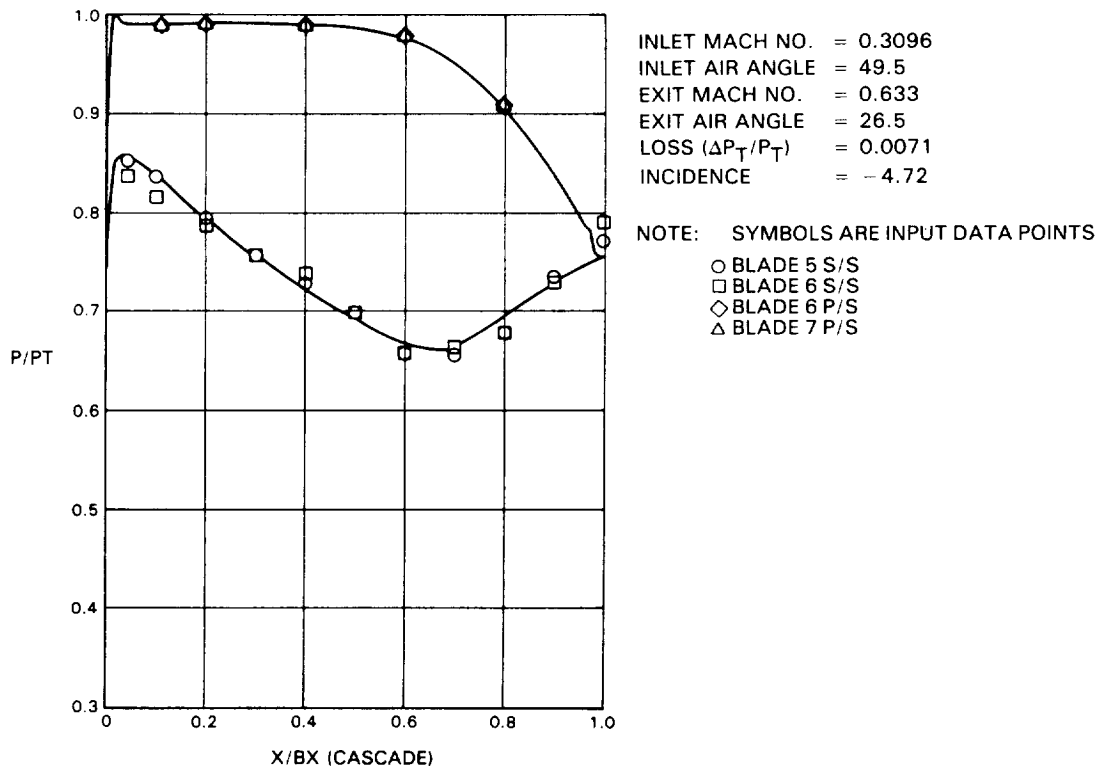


Figure 6-15 (b) 'Aft-Loaded' Baseline - Predicted Versus Measured Pressure Distribution at -4.72 Degrees Incidence, Mach Number 0.633

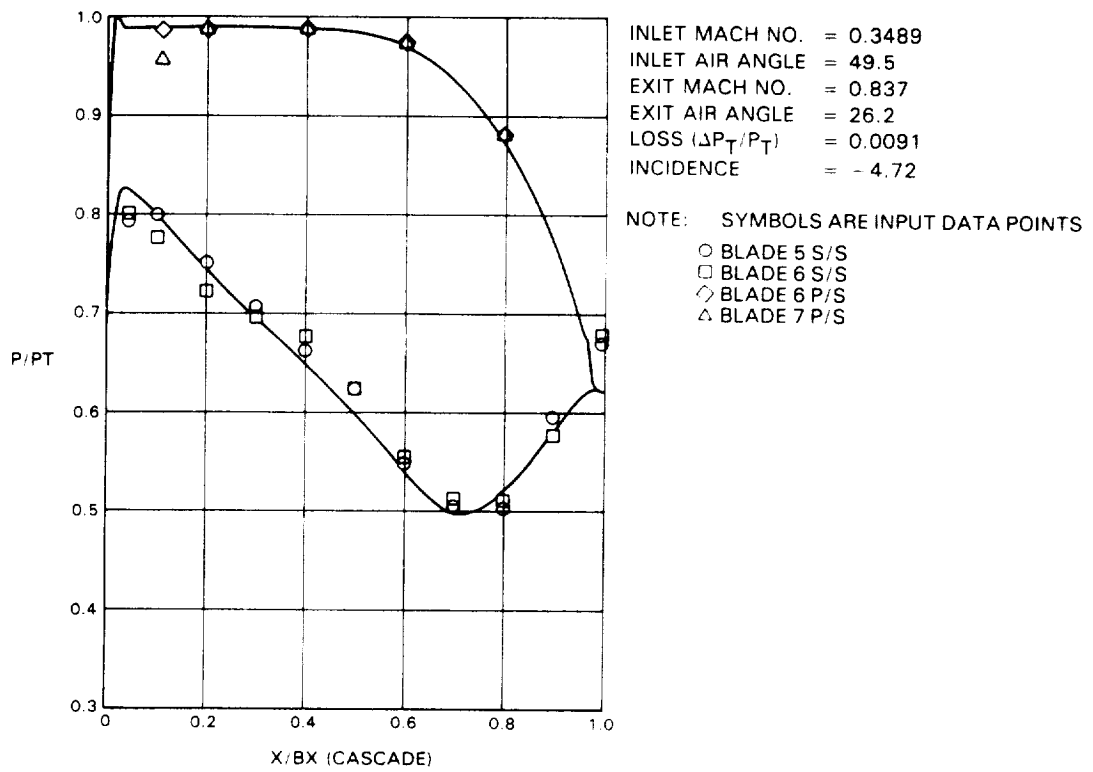


Figure 6-15 (c) 'Aft-Loaded' Baseline - Predicted Versus Measured Pressure Distribution at -4.72 Degrees Incidence, Mach Number 0.837

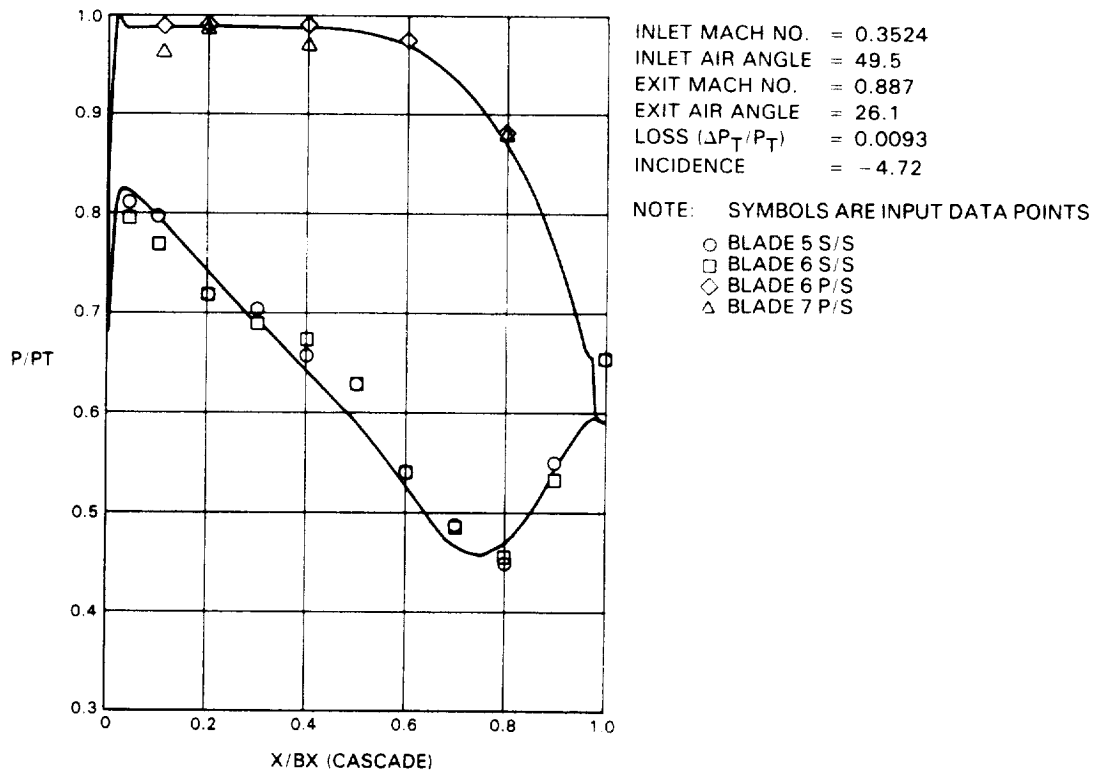


Figure 6-15 (d) 'Aft-Loaded' Baseline - Predicted Versus Measured Pressure Distribution at -4.72 Degrees Incidence, Mach Number 0.887

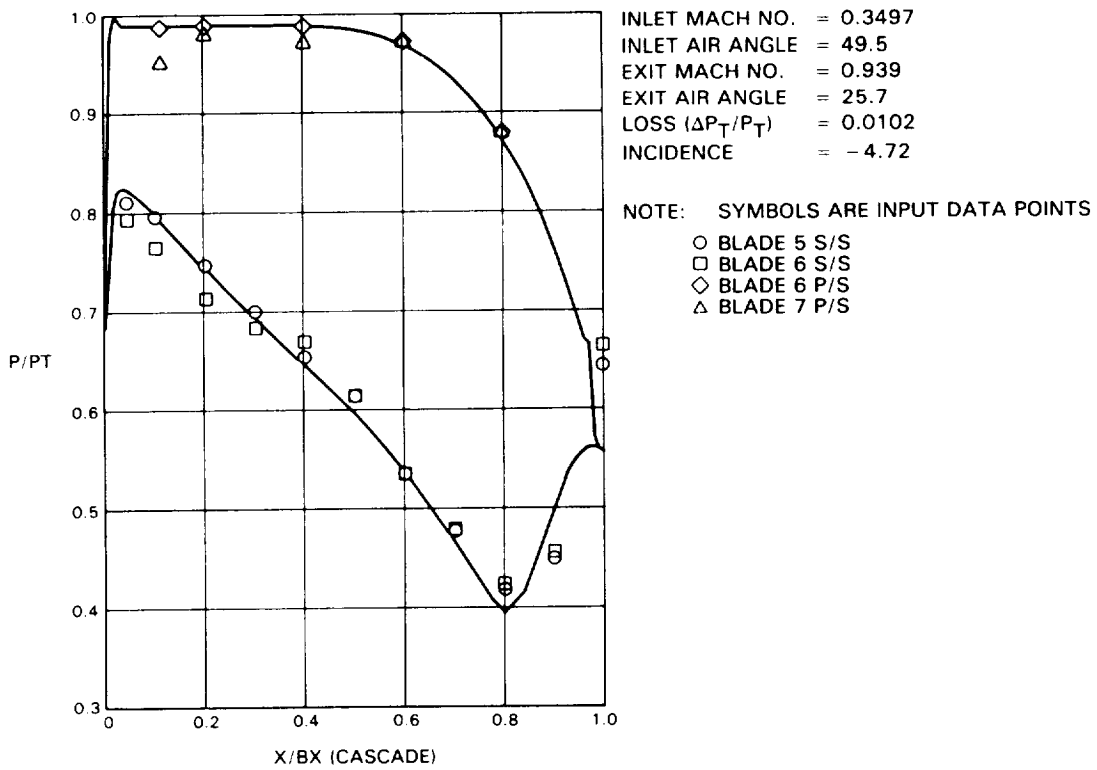


Figure 6-15 (e) 'Aft-Loaded' Baseline - Predicted Versus Measured Pressure Distribution at -4.72 Degrees Incidence, Mach Number 0.939

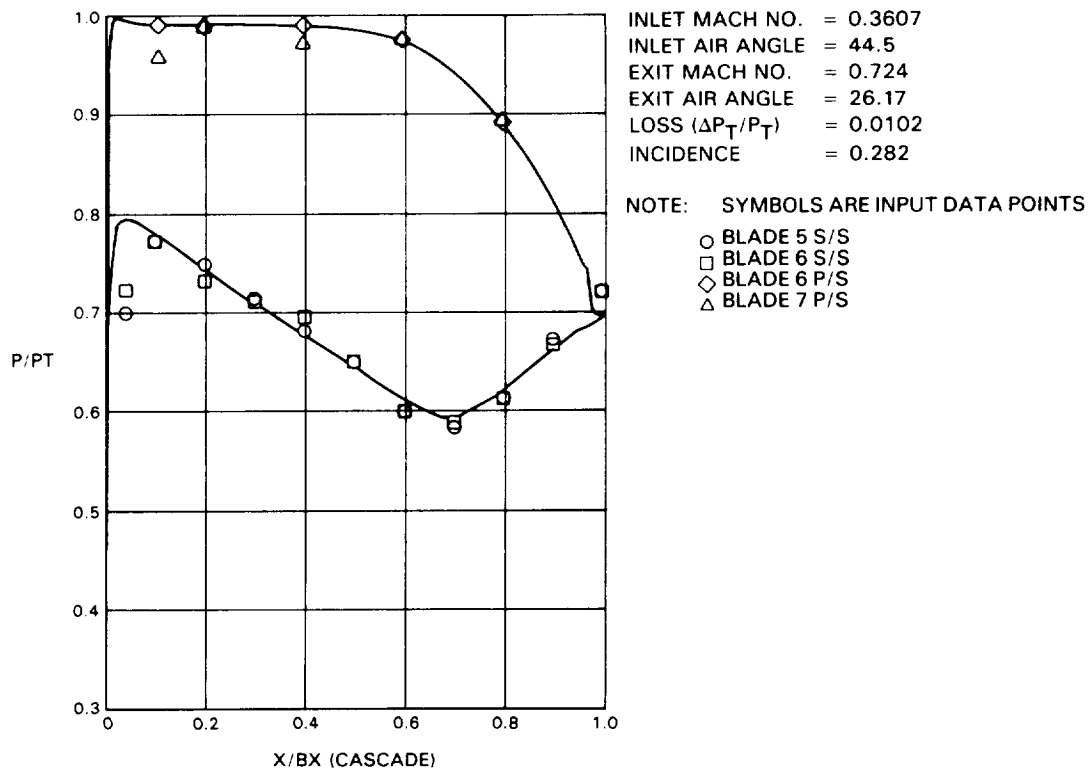


Figure 6-15 (f) 'Aft-Loaded' Baseline - Predicted Versus Measured Pressure Distribution at +0.282 Degrees Incidence, Mach Number 0.724

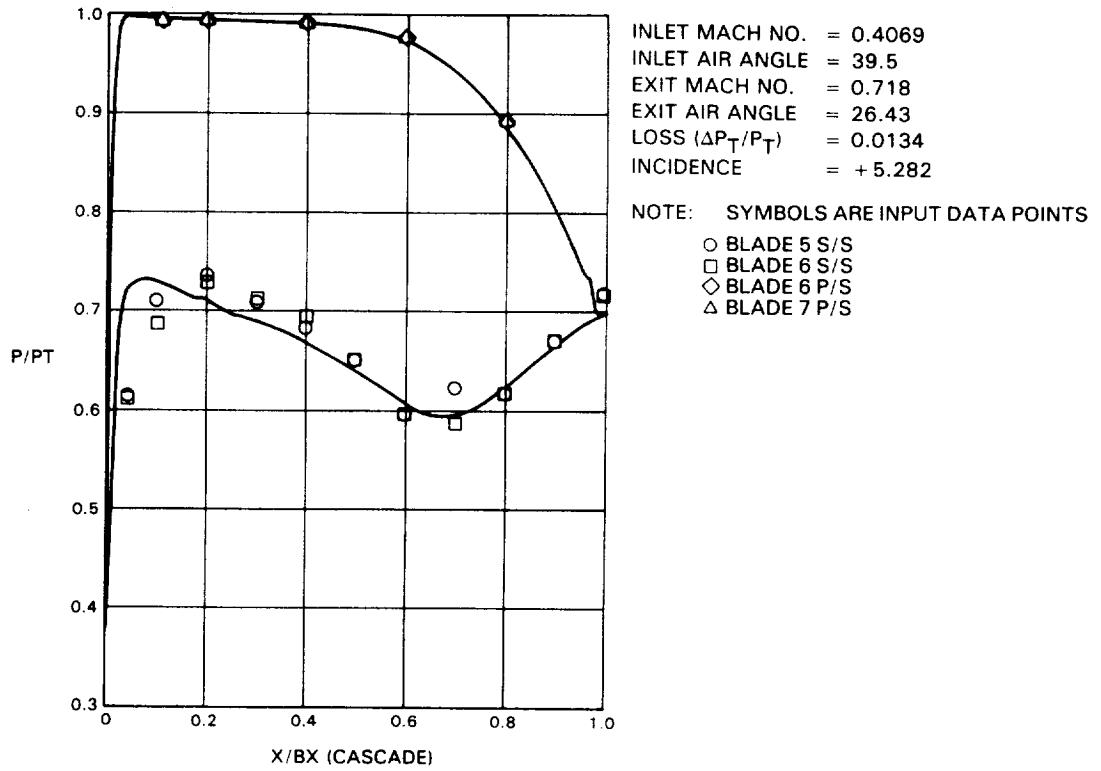


Figure 6-15 (g) 'Aft-Loaded' Baseline - Predicted Versus Measured Pressure Distribution at +5.282 Degrees Incidence, Mach Number 0.718

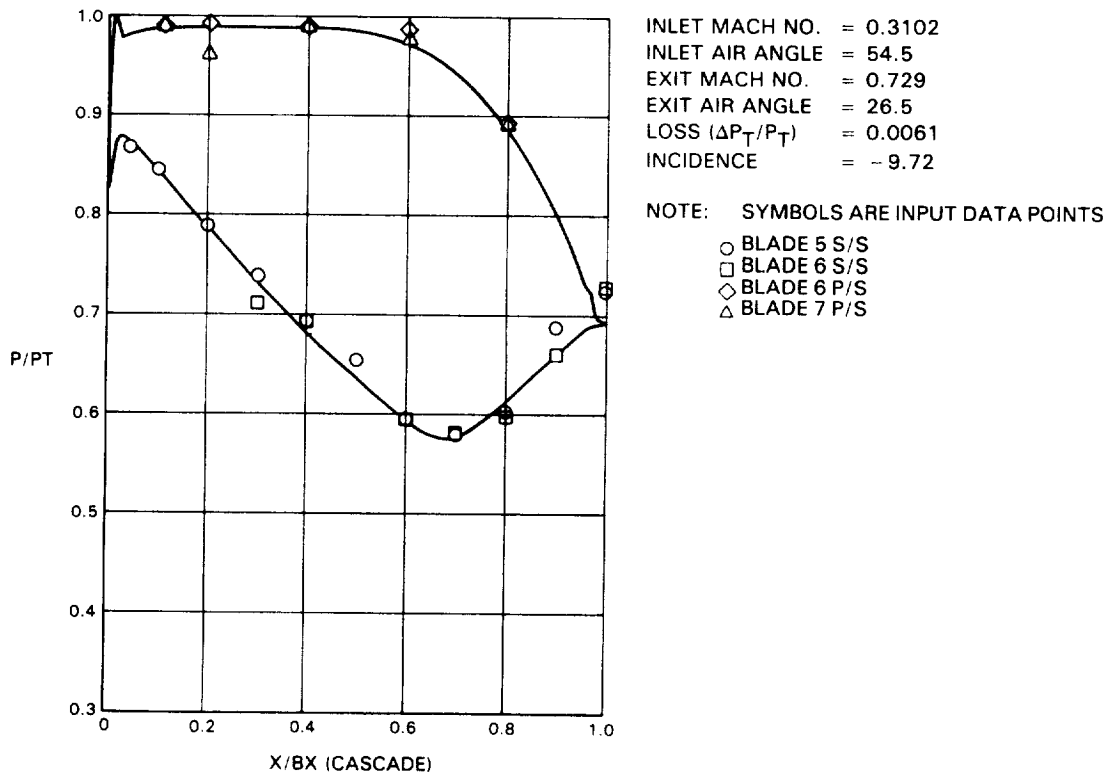


Figure 6-15 (h) 'Aft-Loaded' Baseline - Predicted Versus Measured Pressure Distribution at -9.72 Degrees Incidence, Mach Number 0.729

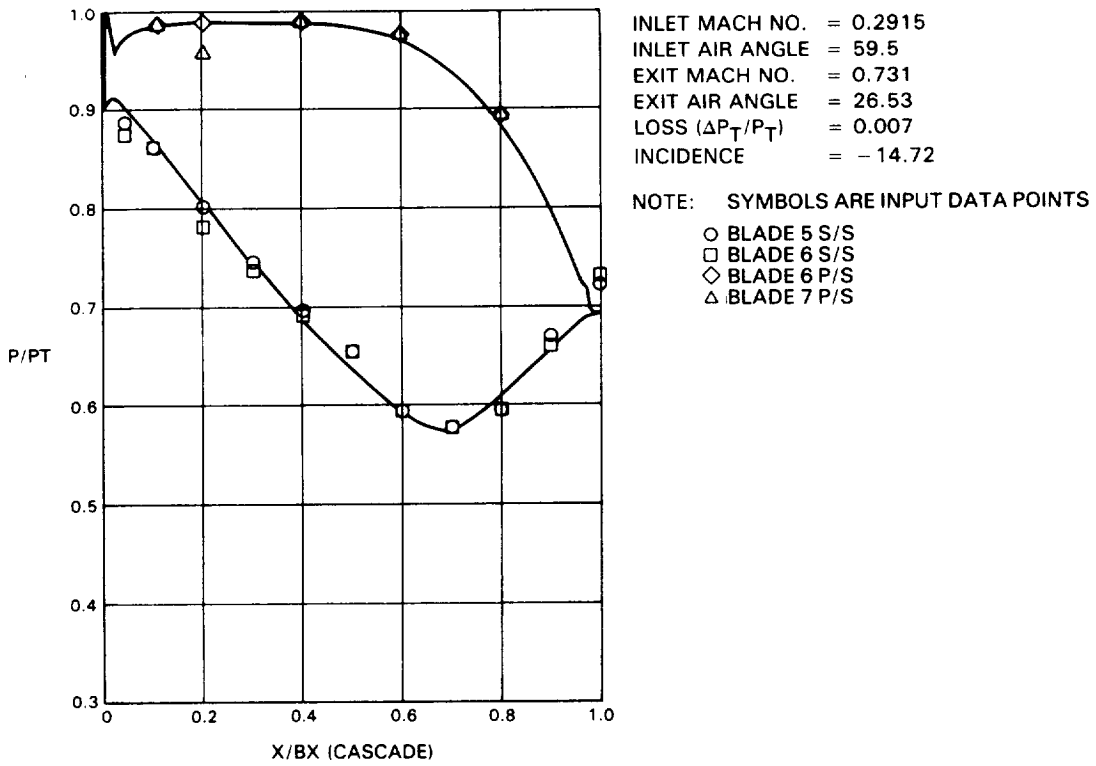


Figure 6-15 (i) 'Aft-Loaded' Baseline - Predicted Versus Measured Pressure Distribution at -14.72 Degrees Incidence, Mach Number 0.731

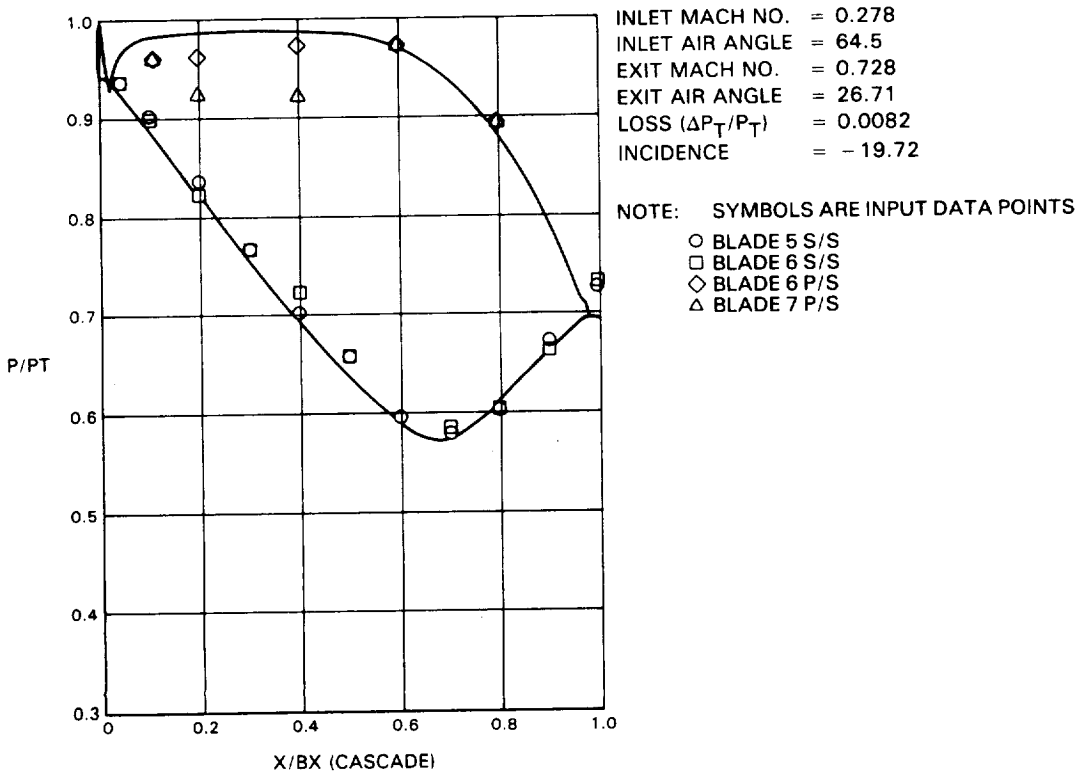


Figure 6-15 (j) 'Aft-Loaded' Baseline - Predicted Versus Measured Pressure Distribution at -19.72 Degrees Incidence, Mach Number 0.728

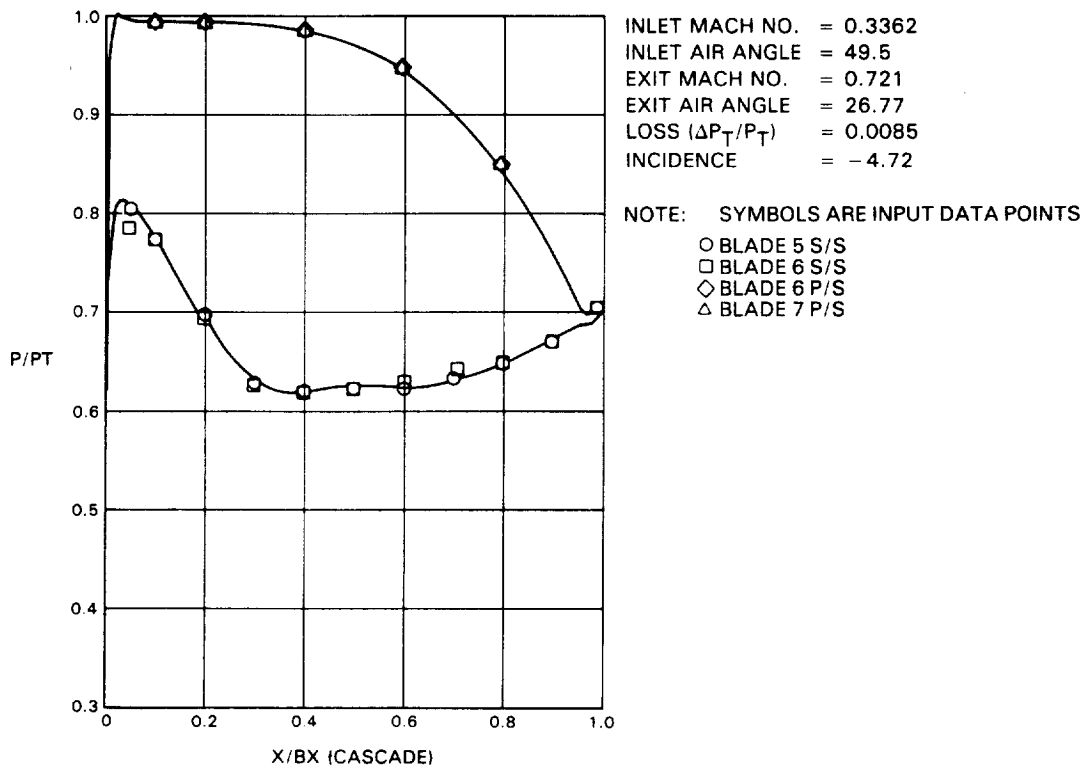


Figure 6-16 (a) 'Heavyweight' - Predicted Versus Measured Pressure Distribution at -4.72 Degrees Incidence, Mach Number 0.721

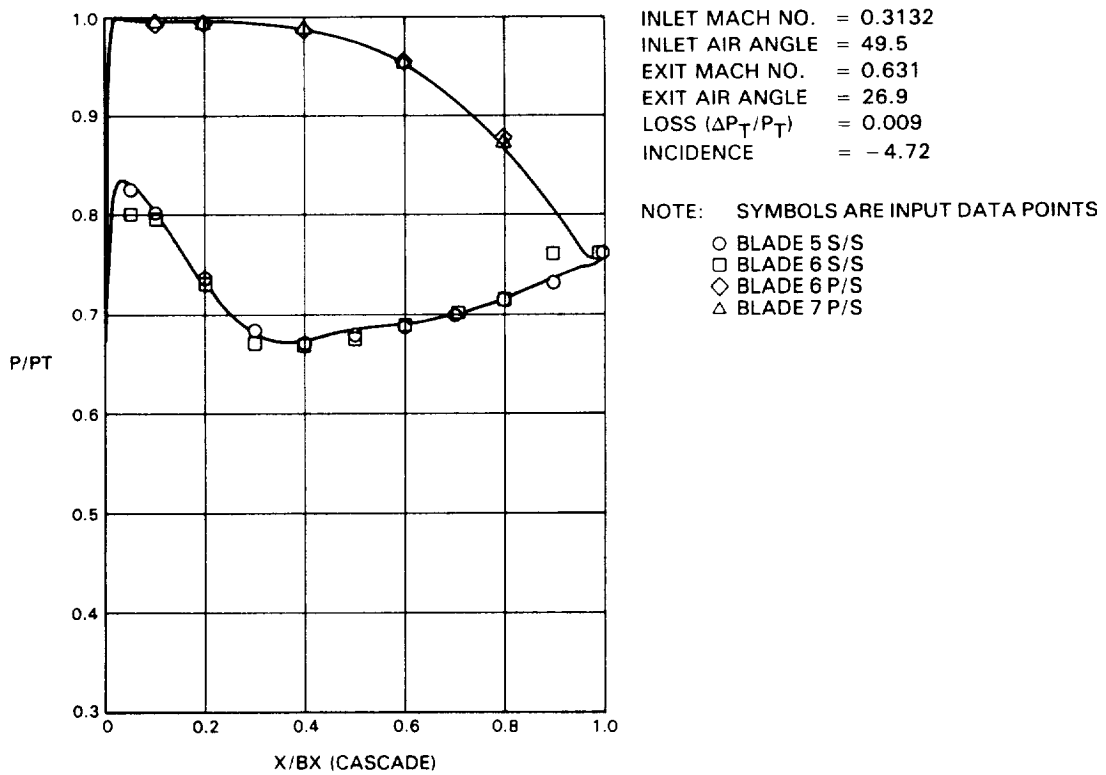


Figure 6-16 (b) 'Heavyweight' - Predicted Versus Measured Pressure Distribution at -4.72 Degrees Incidence, Mach Number 0.631

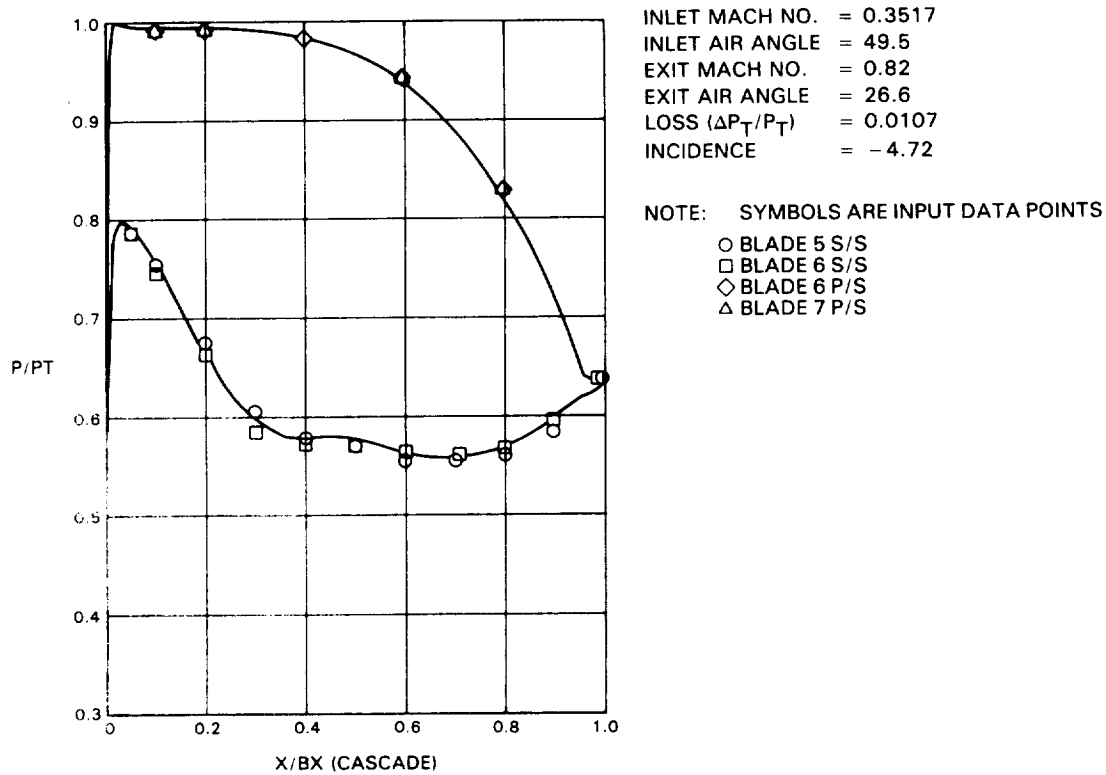


Figure 6-16 (c) 'Heavyweight' - Predicted Versus Measured Pressure Distribution at -4.72 Degrees Incidence, Mach Number 0.82

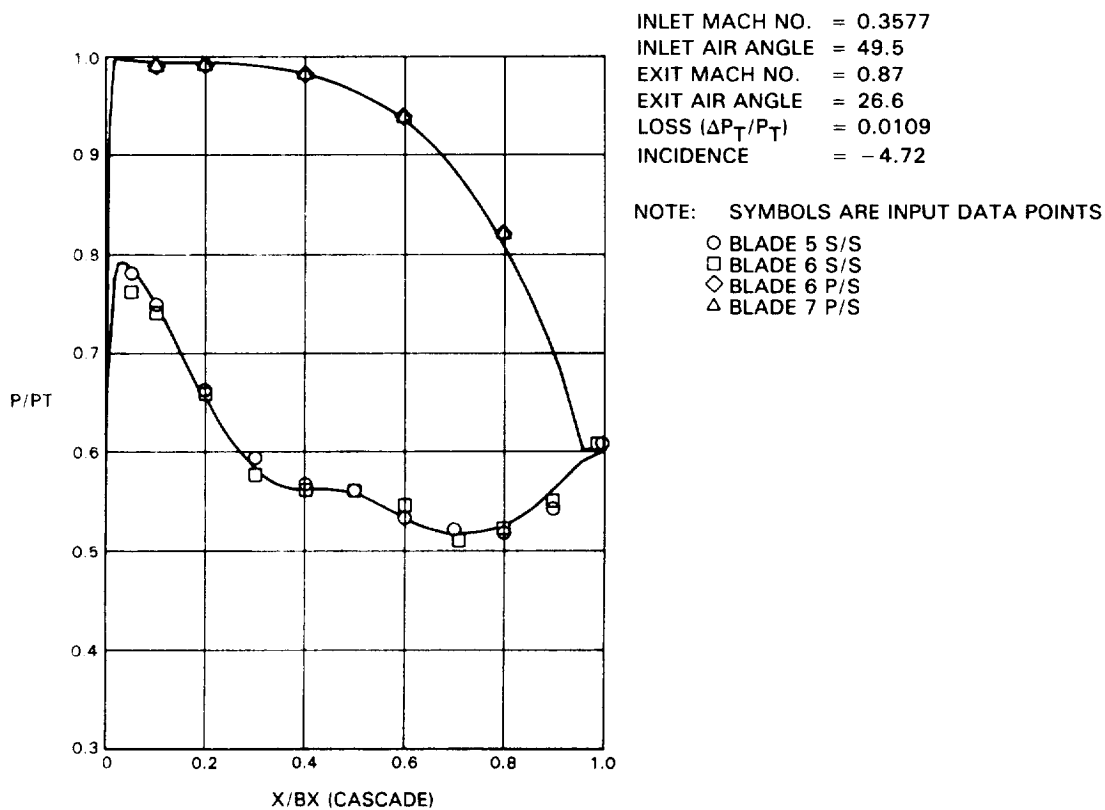


Figure 6-16 (d) 'Heavyweight' - Predicted Versus Measured Pressure Distribution at -4.72 Degrees Incidence, Mach Number 0.87

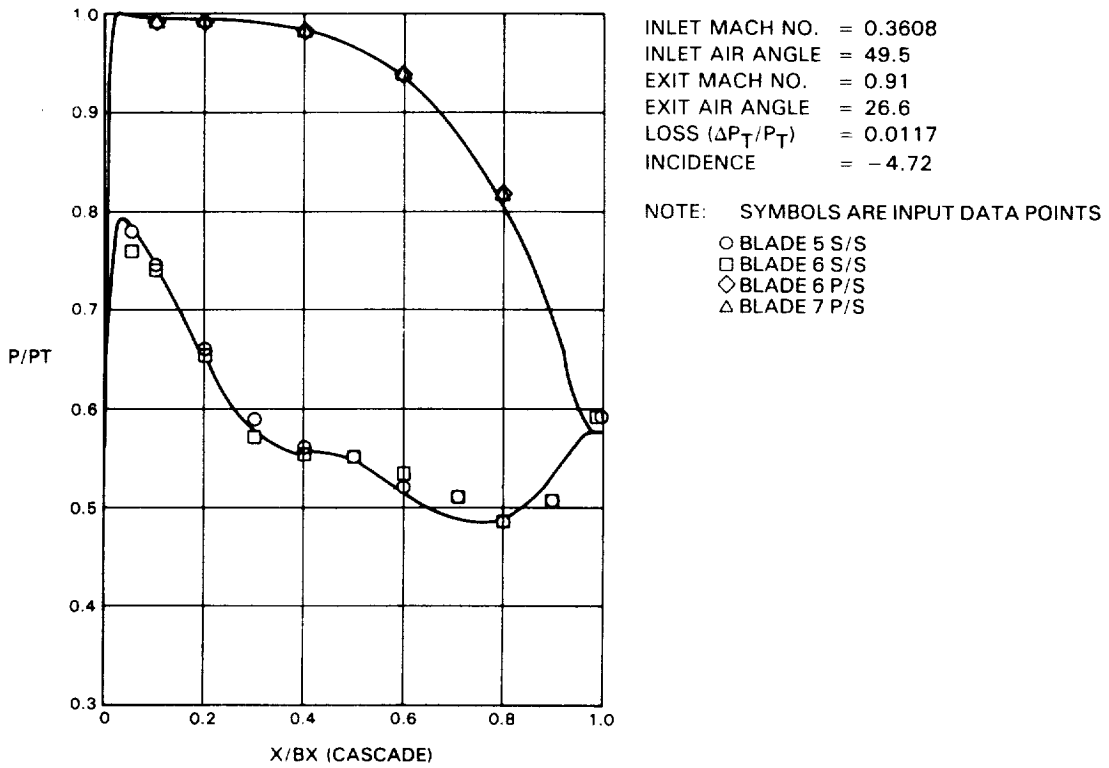


Figure 6-16 (e) 'Heavyweight' - Predicted Versus Measured Pressure Distribution at -4.72 Degrees Incidence, Mach Number 0.91

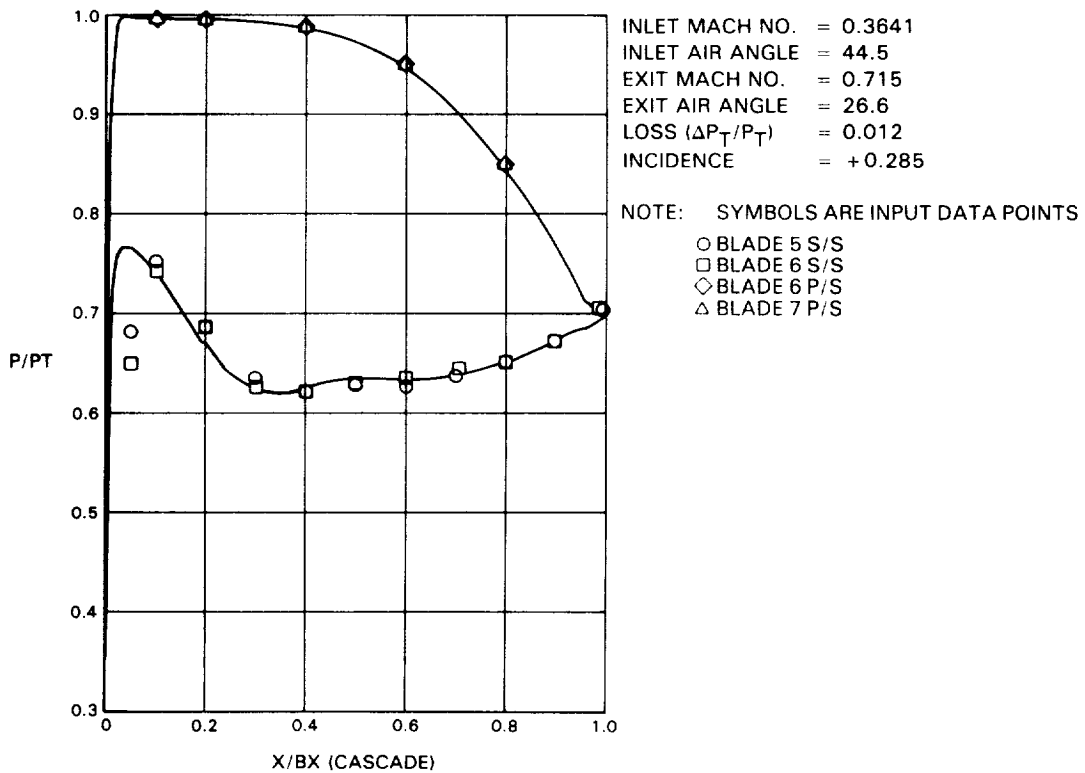


Figure 6-16 (f) 'Heavyweight' - Predicted Versus Measured Pressure Distribution at +0.285 Degrees Incidence, Mach Number 0.715

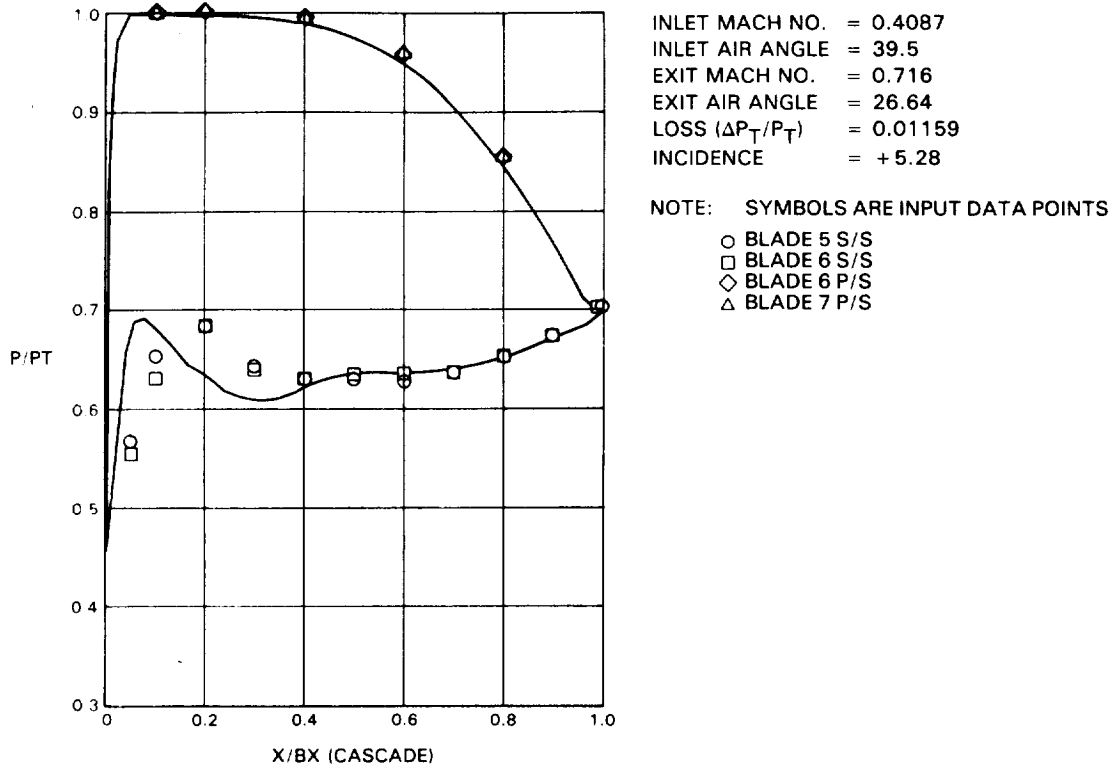


Figure 6-16 (g) 'Heavyweight' - Predicted Versus Measured Pressure Distribution at +5.28 Degrees Incidence, Mach Number 0.716

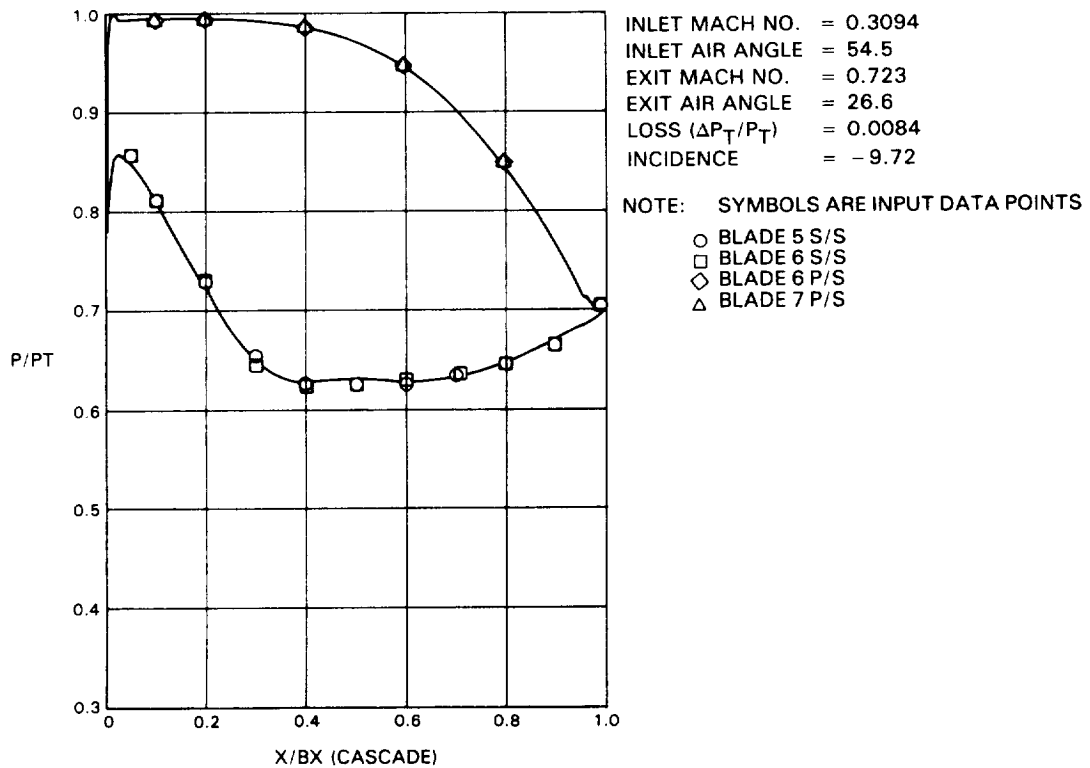


Figure 6-16 (h) 'Heavyweight' - Predicted Versus Measured Pressure Distribution at -9.72 Degrees Incidence, Mach Number 0.723

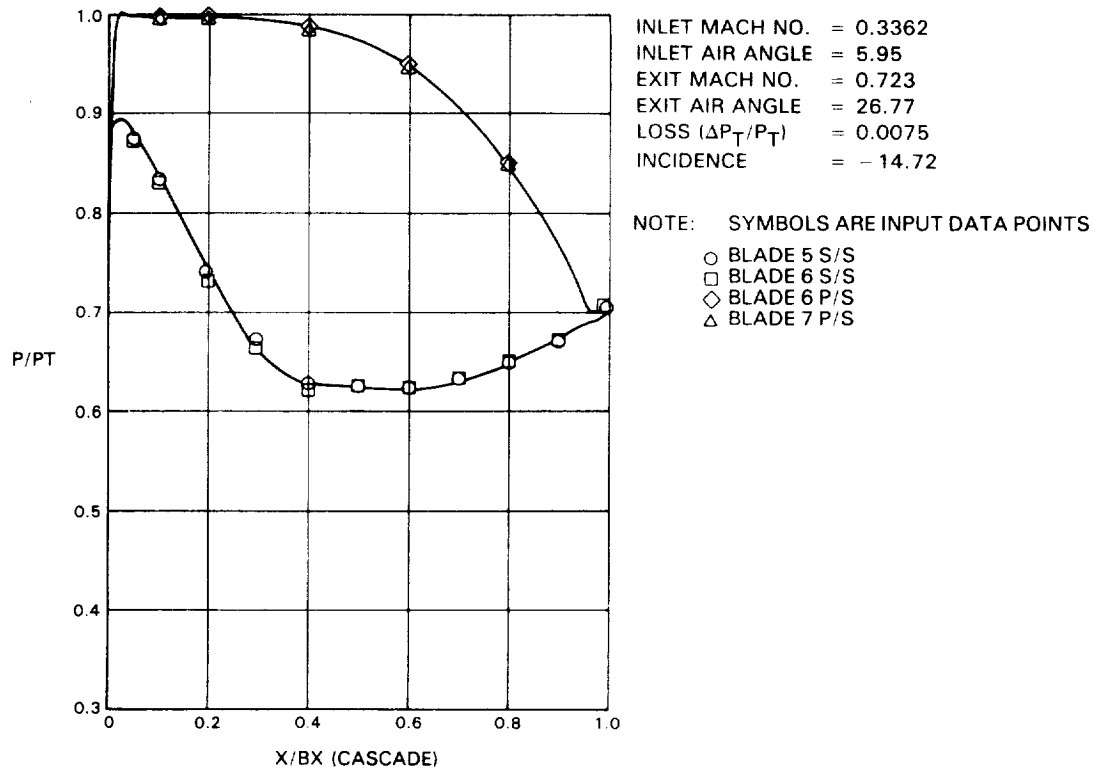


Figure 6-16 (i) 'Heavyweight' - Predicted Versus Measured Pressure Distribution at -14.72 Degrees Incidence, Mach Number 0.723

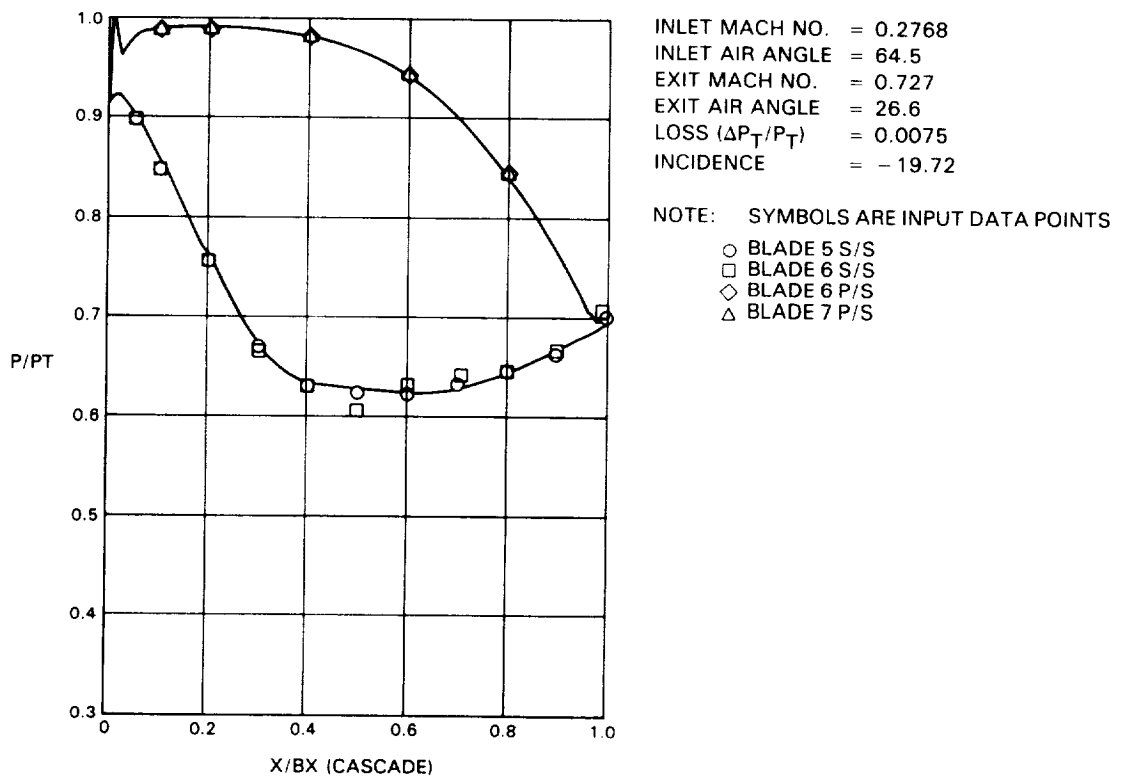


Figure 6-16 (j) 'Heavyweight' - Predicted Versus Measured Pressure Distribution at -19.72 Degrees Incidence, Mach Number 0.727

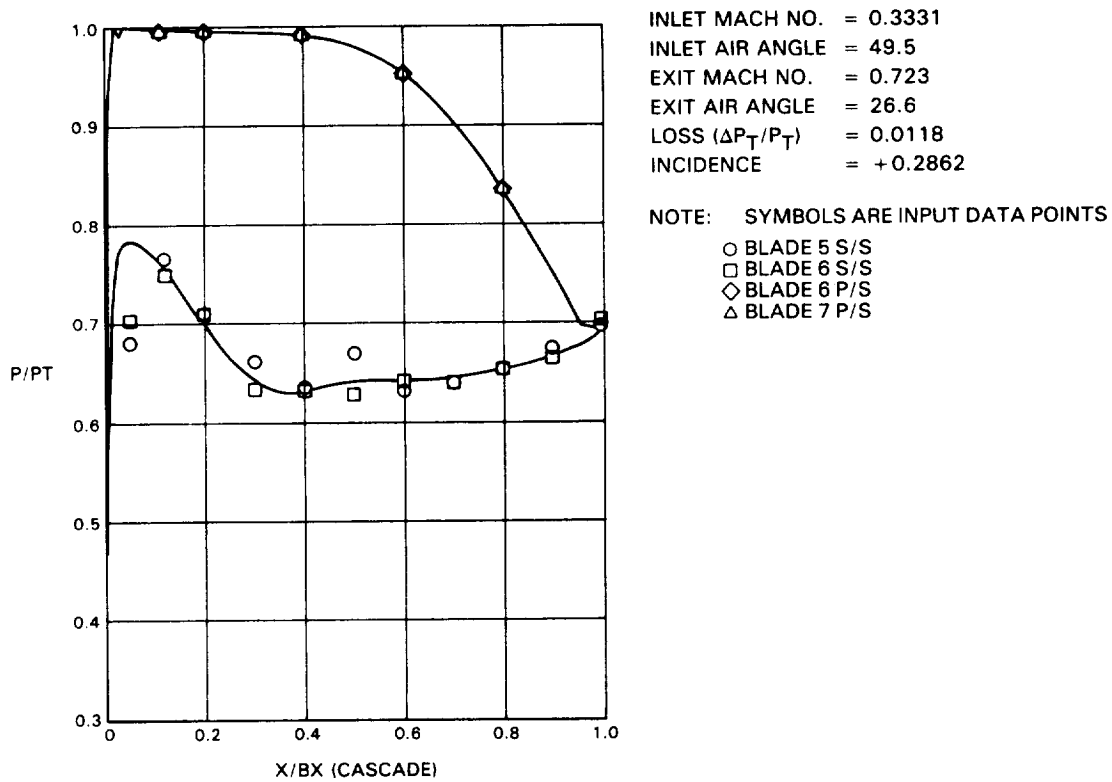


Figure 6-17 (a) 'Lightweight' - Predicted Versus Measured Pressure Distribution at +0.2862 Degrees Incidence, Mach Number 0.723

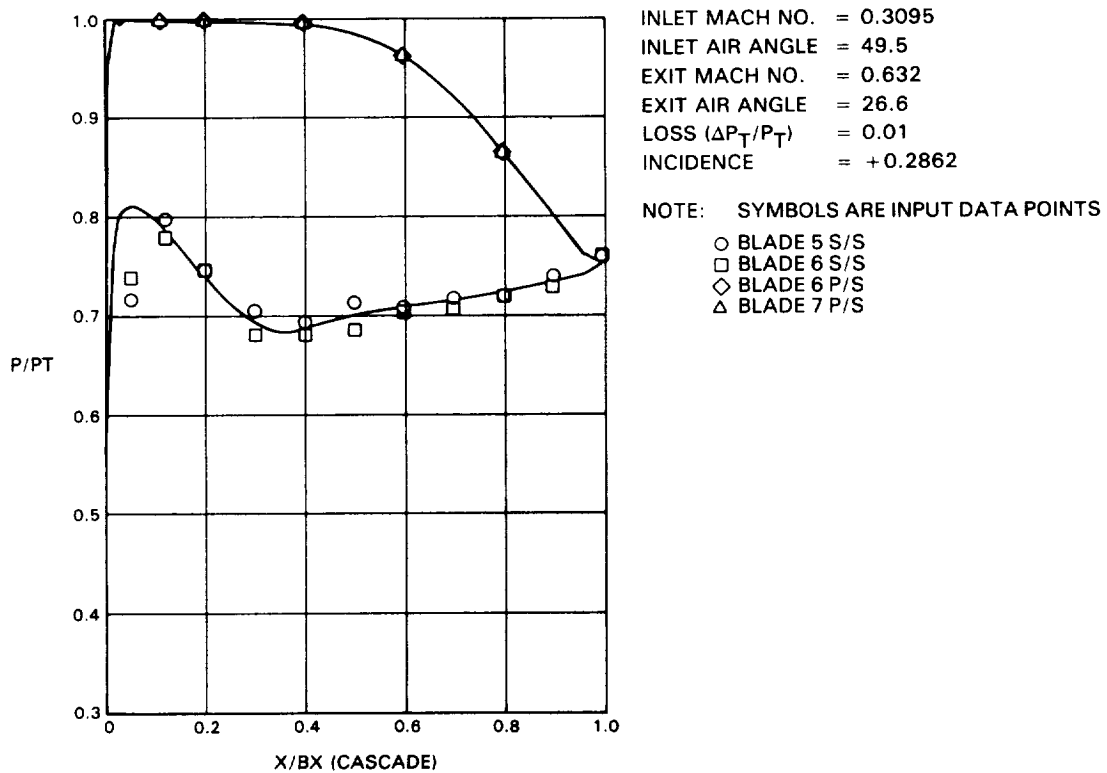


Figure 6-17 (b) 'Lightweight' - Predicted Versus Measured Pressure Distribution at +0.2862 Degrees Incidence, Mach Number 0.632

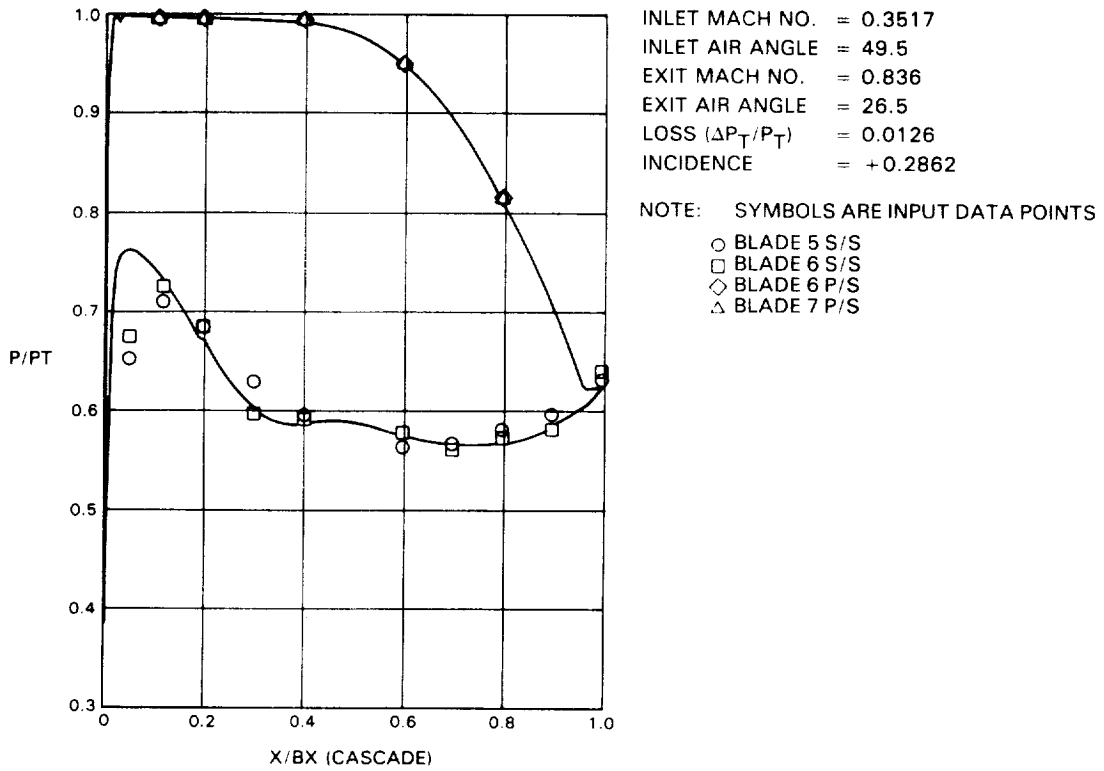


Figure 6-17 (c) 'Lightweight' - Predicted Versus Measured Pressure Distribution at +0.2862 Degrees Incidence, Mach Number 0.836

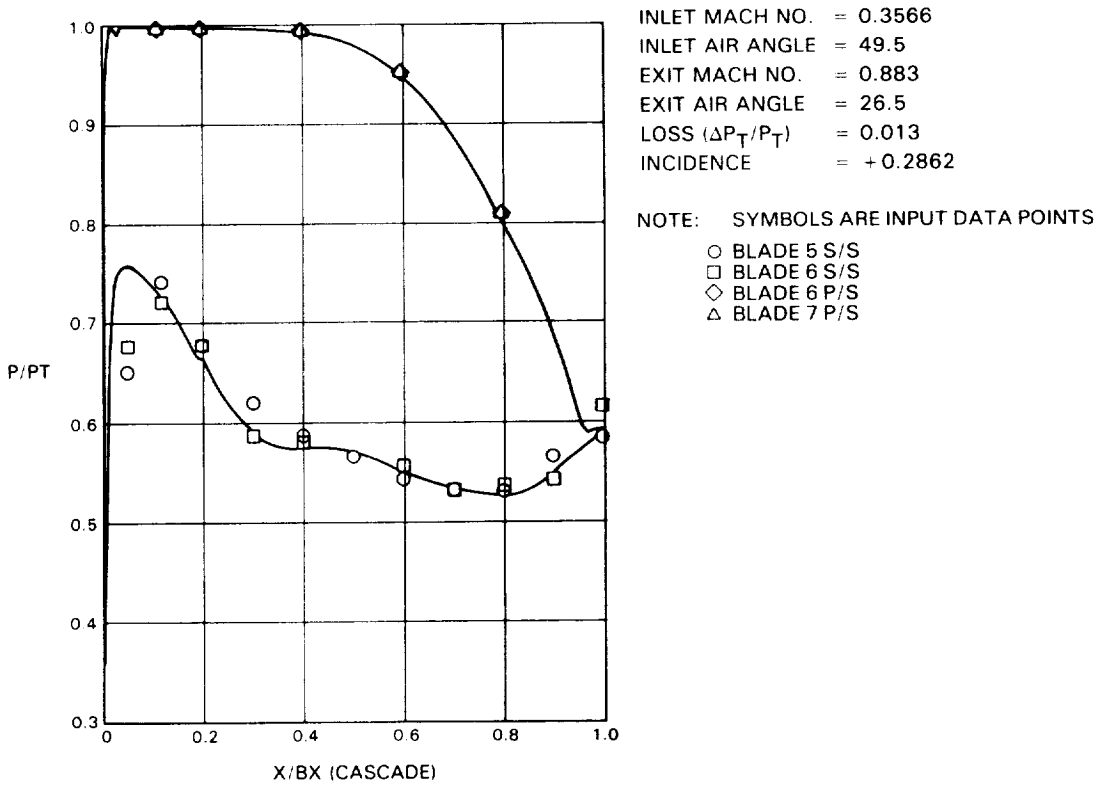


Figure 6-17 (d) 'Lightweight' - Predicted Versus Measured Pressure Distribution at +0.2862 Degrees Incidence, Mach Number 0.883

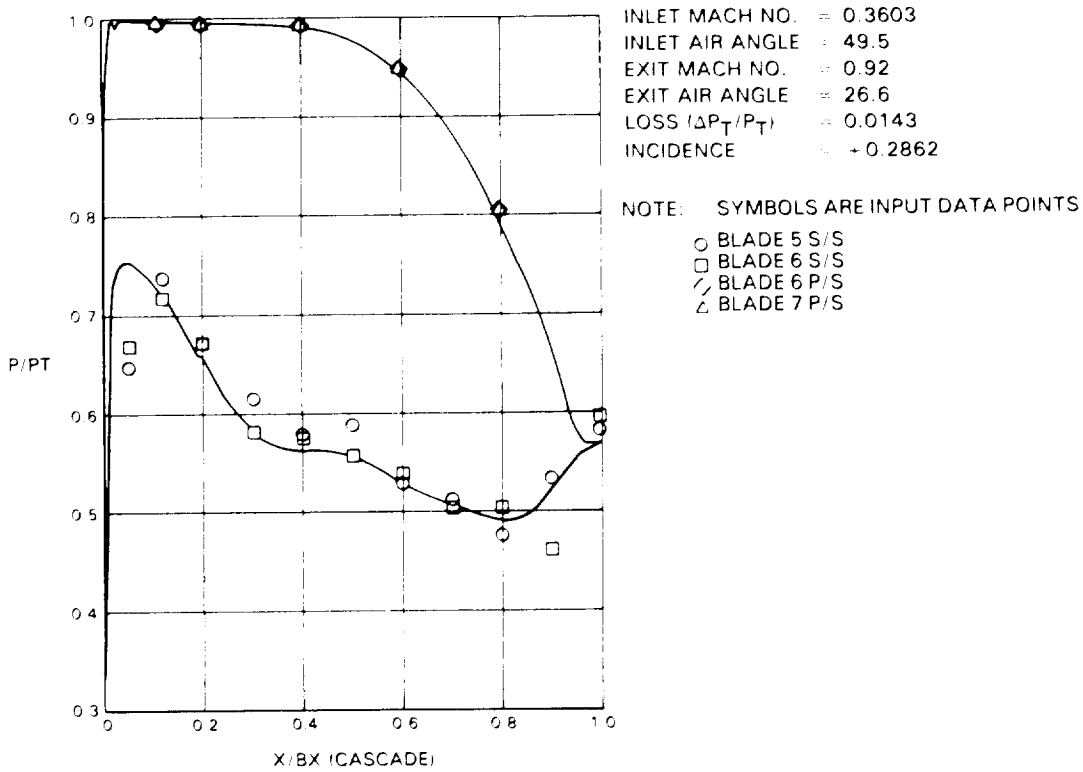


Figure 6-17 (e) 'Lightweight' - Predicted Versus Measured Pressure Distribution at +0.2862 Degrees Incidence, Mach Number 0.92

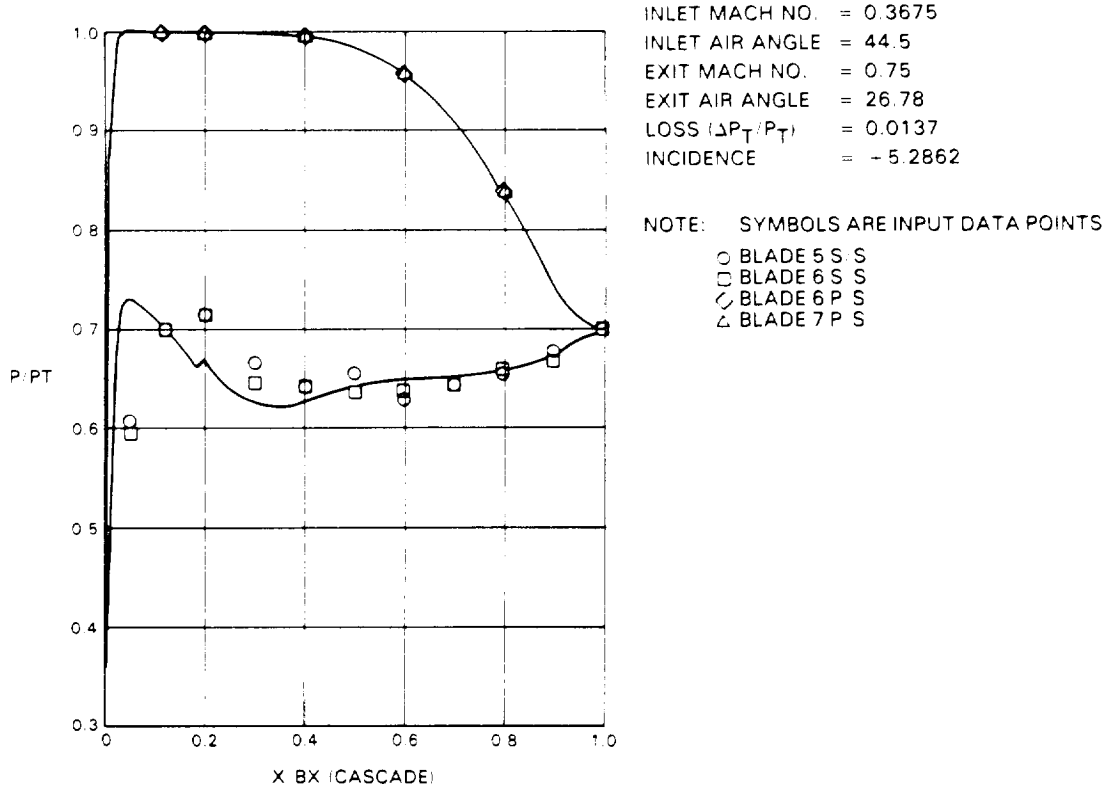


Figure 6-17 (f) 'Lightweight' - Predicted Versus Measured Pressure Distribution at +5.2862 Degrees Incidence, Mach Number 0.75

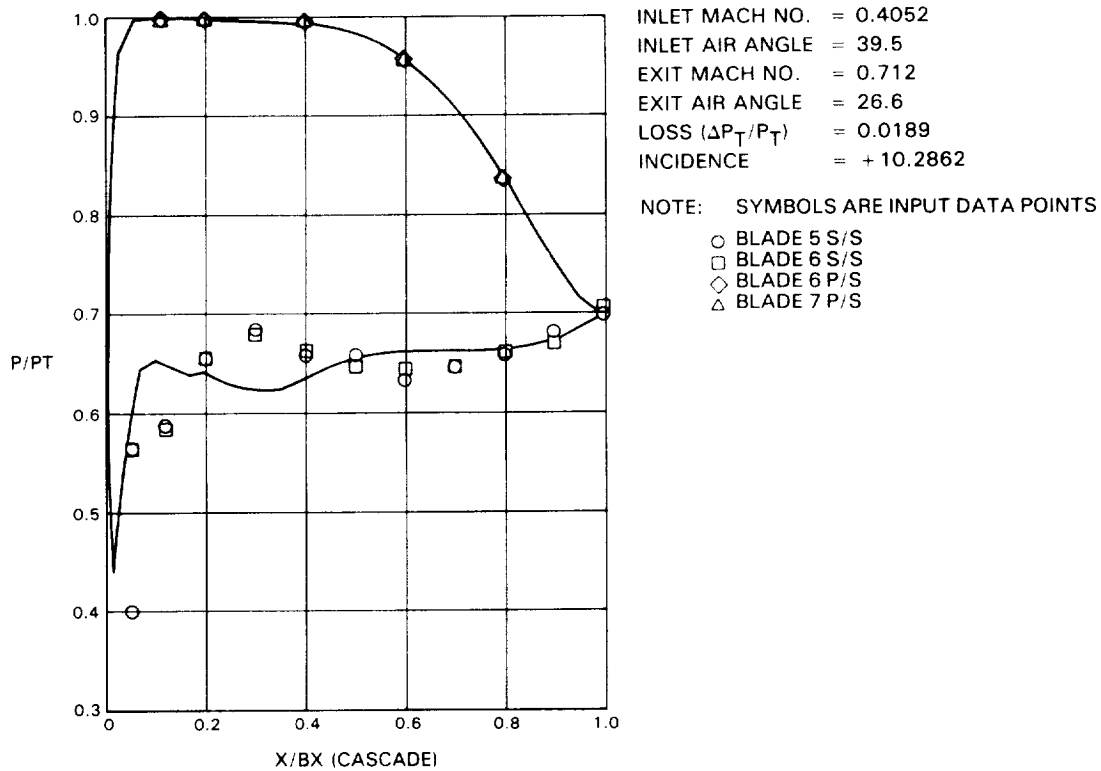


Figure 6-17 (g) 'Lightweight' - Predicted Versus Measured Pressure Distribution at +10.2862 Degrees Incidence, Mach Number 0.712

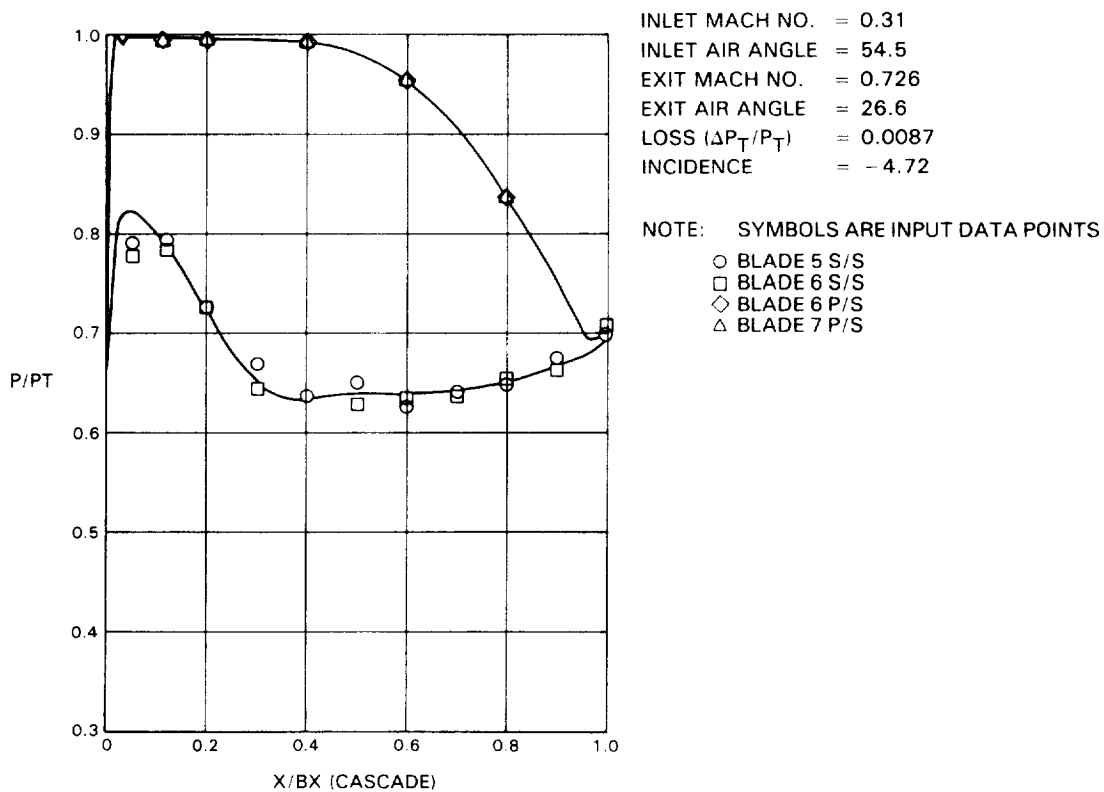


Figure 6-17 (h) 'Lightweight' - Predicted Versus Measured Pressure Distribution at -4.72 Degrees Incidence, Mach Number 0.726

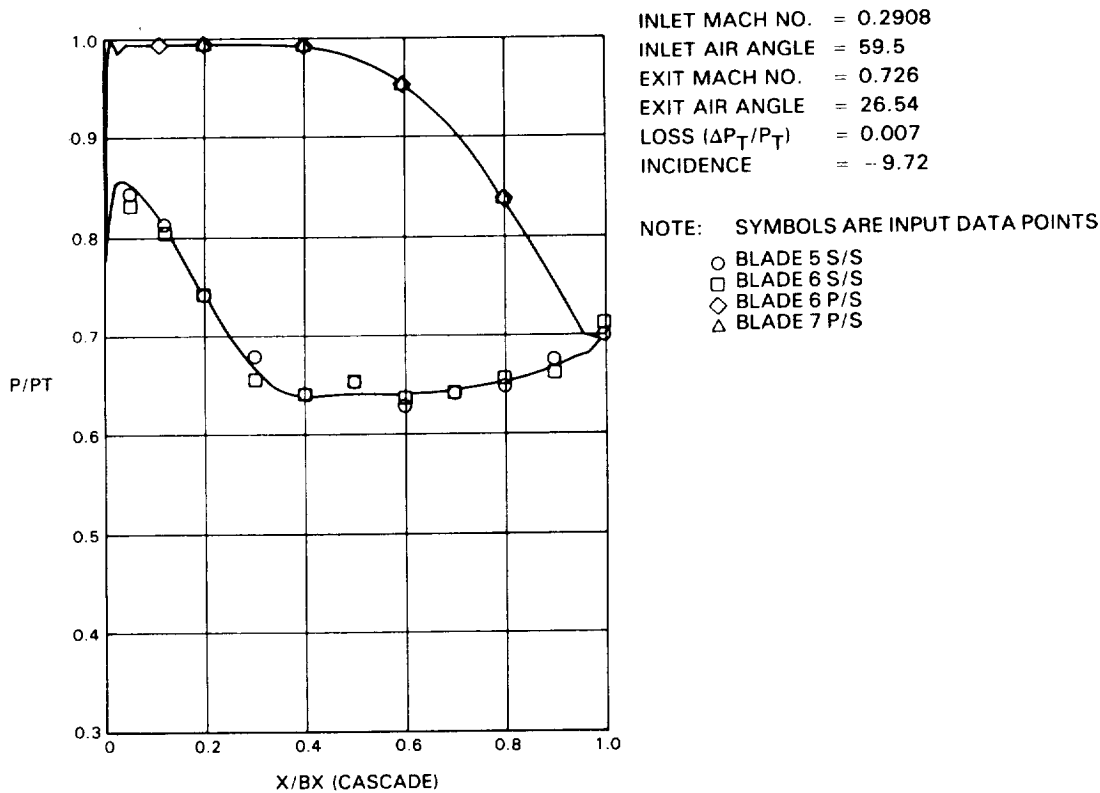


Figure 6-17 (i) 'Lightweight' - Predicted Versus Measured Pressure Distribution at -9.72 Degrees Incidence, Mach Number 0.726

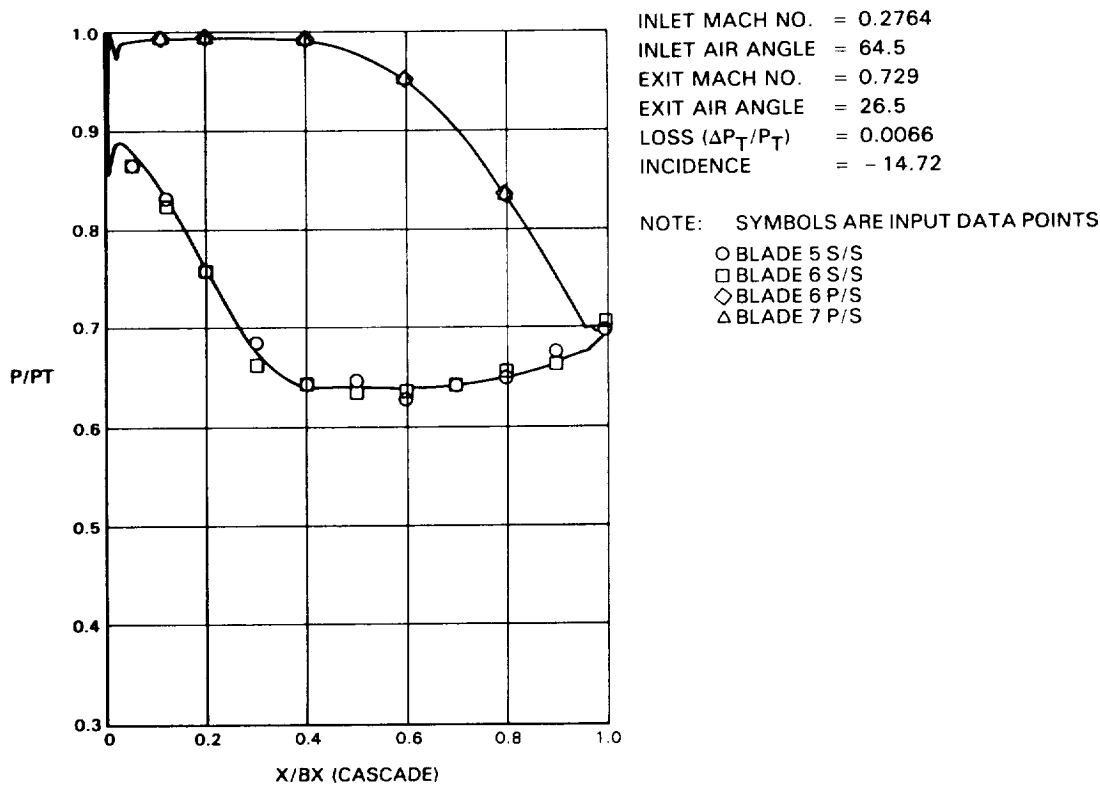


Figure 6-17 (j) 'Lightweight' - Predicted Versus Measured Pressure Distribution at -14.72 Degrees Incidence, Mach Number 0.729

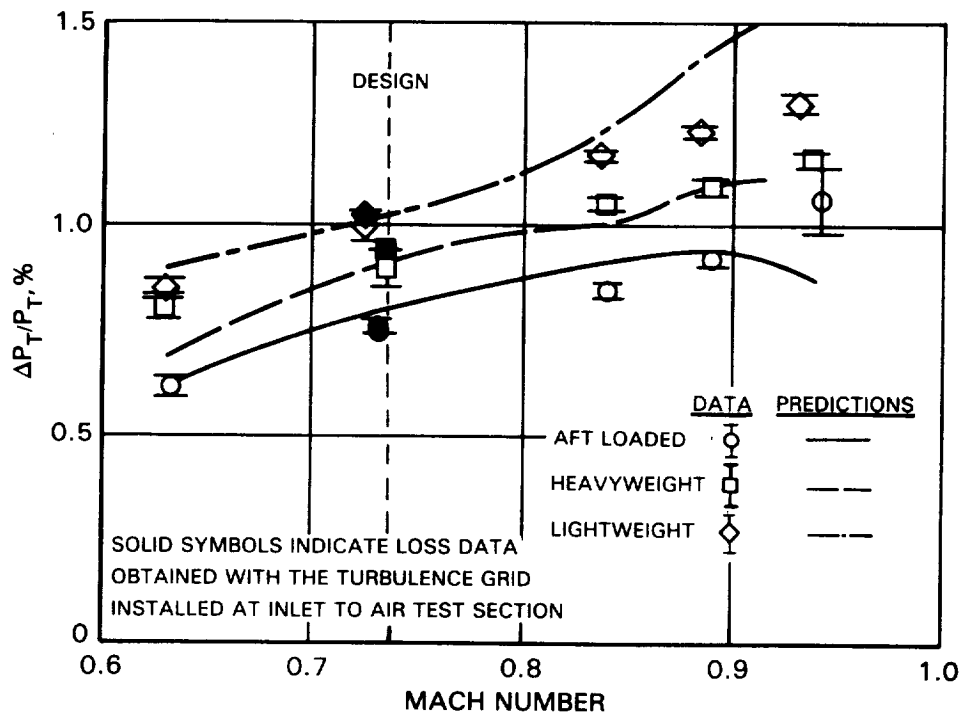


Figure 6-18 Baseline, Heavyweight, Lightweight - Predicted Versus Measured Mixed-Out Mid-Span Losses at Design Point Incidence, Variable Mach Numbers

6.3.3 Off-Design Loss

Mixed-out mid-span profile loss data for the three airfoil designs are compared to predictions in Figure 6-19 over a range of incidence angles with fixed exit Mach number. Agreement between predictions and data is good over the entire range. The data indicate that the profile loss for the 'aft-loaded' baseline airfoil is lower than either the 'heavyweight' or 'lightweight' designs for positive incidence angles whereas all airfoil sections show almost equal losses for large negative incidence angles.

Gap-averaged secondary loss data were obtained for the 'aft-loaded' baseline and 'lightweight' designs at three incidence angles. These data are plotted in Figures 6-20 and 6-21. These figures indicate a significant difference in the shapes of the loss curves for these two airfoils. Integrated secondary loss data (shown in Table 6-IV) for the 'aft-loaded' and the 'lightweight' airfoils indicate that losses were the same for the design and negative incidences whereas secondary losses for positive incidences were higher. The 'lightweight' airfoil showed a slower increase in secondary losses with negative incidence than the 'aft-loaded' design. Secondary losses for the 'lightweight' airfoil design at positive incidence are about 15 percent higher than at the design incidence. Secondary losses for the 'aft-loaded' design at positive incidence are about 30 percent higher than at design incidence. The 'aft-loaded' airfoil consistently showed lower magnitudes for the secondary losses as compared to the 'lightweight' design. It is not obvious by inspection which design yields the lower overall secondary loss. Integrating the curves yielded the loss values listed in Table 6-IV. These data clearly indicate the lower secondary loss characteristics of the baseline design. The Pratt & Whitney Aircraft cascade correlations are in reasonable agreement with

the data except for the 'lightweight' airfoil operating at positive incidence where it overestimates the loss by about 50 percent. The method of Dunham and Came (Appendix B - Reference 4) considerably overestimates the losses while the method of Mukhtarov and Krichakin (Appendix B - Reference 5) consistently underestimates them.

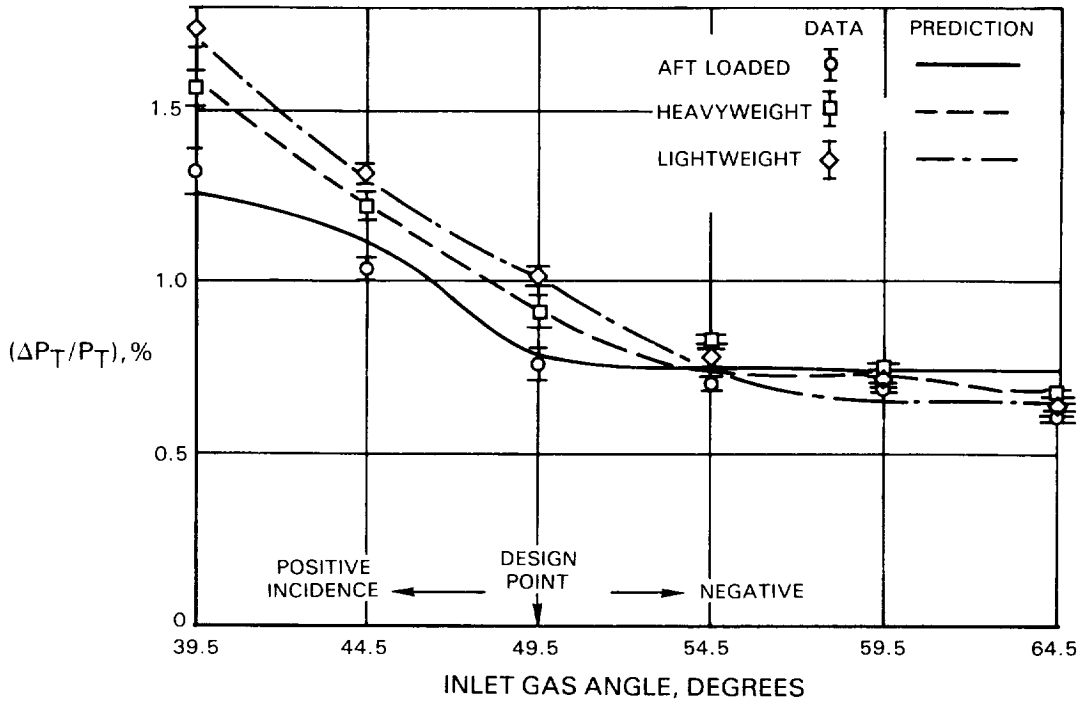


Figure 6-19 Aft-Loaded, Heavyweight, Lightweight - Predicted Versus Measured Mixed-Out Profile Loss Over Range of Incidence, Fixed Exit Mach Number $0.72 \pm .02$

TABLE 6-IV

SECONDARY LOSS DATA VERSUS PREDICTIONS FROM VARIOUS CORRELATIONS
LOSSES $\Delta P_T/P_T$ (Percent)

<u>Cascade</u>	<u>Data</u>	<u>P&WA Cascade Correlation</u>	<u>Dunham & Came</u>	<u>Mukhtarov & Krichakin</u>
Aft-Loaded				
(Design)	0.68	0.735	1.56	0.53
(Negative)	0.676	0.643	1.38	0.49
(Positive)	0.873	1.062	1.76	0.57
Lightweight				
(Design)	0.802	0.963	1.56	0.53
(Negative)	0.808	0.711	1.40	0.49
(Positive)	0.926	1.412	1.82	0.57

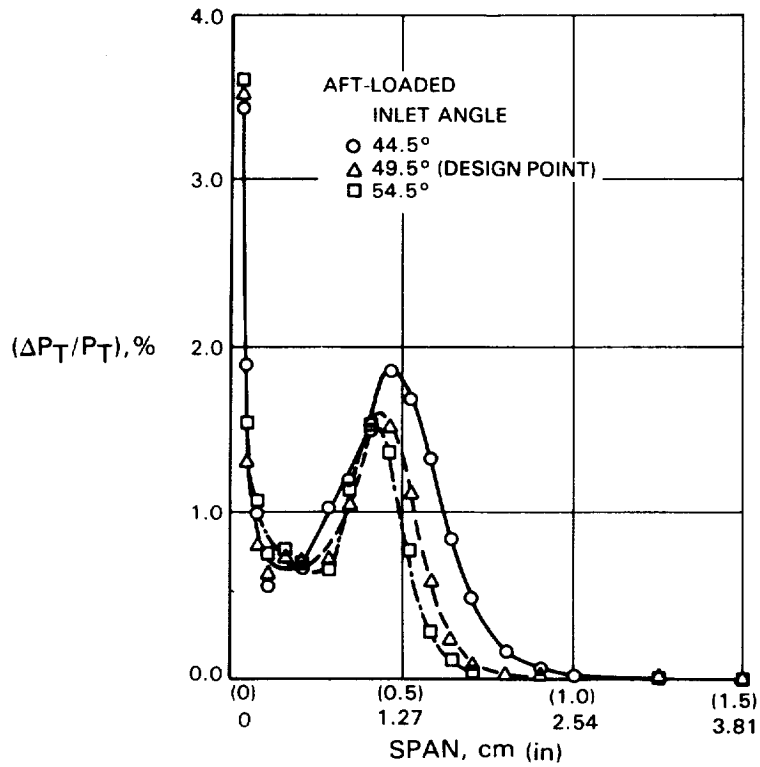


Figure 6-20 'Aft-Loaded' Baseline - Predicted Versus Measured Gap-Averaged Secondary Loss Over Range of Incidence, Fixed Exit Mach Number $0.72 \pm .02$

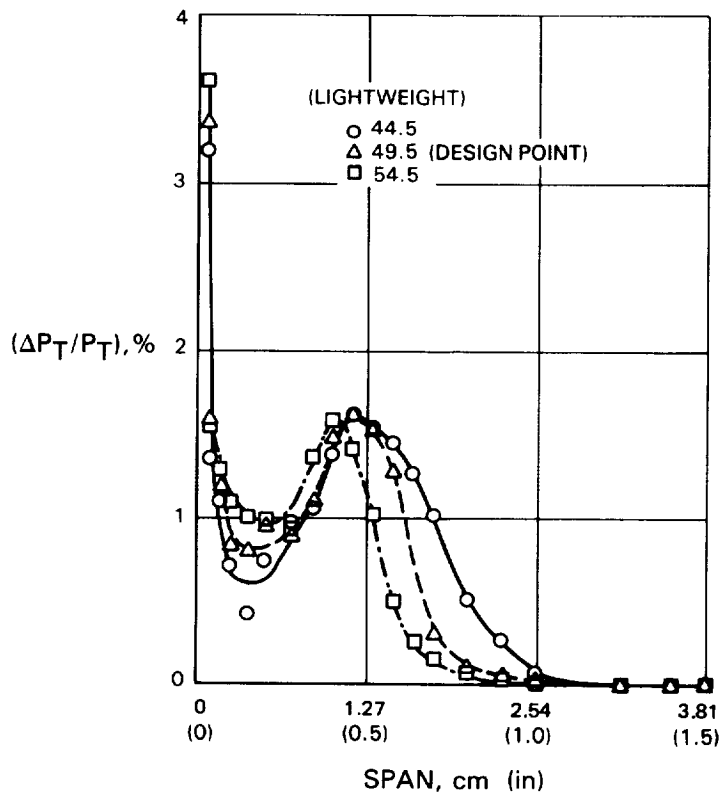


Figure 6-21 Lightweight - Predicted Versus Measured Gap-Averaged Secondary Loss Over Range of Incidence, Fixed Exit Mach Number $0.72 \pm .02$

6.4 Cascade Vs. Boundary Layer Tunnel Tests

As a part of the Energy Efficient Engine low-pressure turbine program, an experimental study was conducted where the suction surfaces of the 'aft-loaded' and 'heavyweight' airfoils were simulated in a large scale, low speed boundary layer tunnel. Detailed measurements of boundary layer velocity profiles were obtained under the influence of the two simulated pressure distributions. These results are described by Sharma, Wells, Schlinker, and Bailey (Appendix B - Reference 6) and in NASA CR-165338, PWA-5594-141. Results from this study indicate that the Reynolds number based on momentum loss thickness for the two simulated airfoils were about the same in the exit plane. This would indicate that the suction surfaces of the two airfoils would generate about the same losses. However, loss data from the present cascade tests indicate that the 'heavyweight' airfoil generates about 17 percent higher losses than the 'aft-loaded' airfoil (see Figure 6-19 for design incidence). This apparent paradox can be explained by examination of the pressure distributions on the suction surfaces of the two airfoils and the two simulated pressure distributions.

One of the features of the airfoil suction surface pressure distribution not simulated in the Boundary Layer Tunnel Investigation was the leading edge overspeed region. Potential flow analysis for the 'aft-loaded' and the 'heavyweight' airfoils shown in Figures 6-15(a) and 6-16(a) indicate that the 'heavyweight' airfoil has a larger overspeed region than the 'aft-loaded' airfoil. Different loss magnitudes generated by the 'heavyweight' airfoil in the cascade could result from a difference in the pressure distribution in the overspeed region for this airfoil as opposed to the 'aft-loaded' airfoil. This conclusion is substantiated by the fact that the difference in losses between the two airfoils decreases as these airfoils operate at higher inlet angles as shown in Figure 6-19. The extent of the leading edge overspeed region for the two airfoils is almost identical at higher inlet gas angles.

From the above discussion it could be concluded that when the leading edge overspeed is accounted for, the cascade test and large scale boundary layer tunnel test results are consistent. Further studies, directed towards understanding the influence of airfoil leading edge overspeed on the performance of turbine cascades, are required before some definite conclusions can be formulated with respect to its application in turbine designs.

SECTION 7.0 SUMMARY OF RESULTS

7.1 Surface Static Pressure Data Versus Pratt & Whitney Aircraft Potential Flow Prediction Method

Surface static pressure data for negative incidences are in good agreement with Pratt & Whitney Aircraft potential flow predictions for all of the five sets of airfoils used in the present investigation.

Predictions of static pressure distribution by the Pratt & Whitney Aircraft prediction method for the leading edge region of airfoils operating at zero or positive incidence are in relatively poor agreement with the measured data. In general, the depth of the leading edge overspeed is overpredicted and the length of the overspeed region is underpredicted. This disagreement between the measured data and predictions is due to the presence of separation bubbles in the leading edge region, these bubbles interact with the potential flow and change the local pressure distributions. Viscous-inviscid interaction analytical models, capable of handling these leading edge overspeed regions, are not generally available for analysing flows in cascades. For one of the test conditions (see Figure 6-4) a bubble (displacement surface) was added to the airfoil surface and potential flow analysis conducted on the modified airfoil surface. Improved agreement between the data and predictions was obtained through this procedure.

7.2 Loss Assessment

7.2.1 Low Camber Vane

The measured profile loss of 0.52 percent differential pressure at design point condition was fairly well predicted by the Pratt & Whitney Aircraft profile loss prediction method. Variation of profile losses with incidence is also fairly well predicted by the Pratt & Whitney Aircraft transitional boundary layer calculation procedure.

The measured off-design incidence performance at constant exit Mach number showed the vane section to have a negative incidence range of 8 degrees and a positive incidence range of 12 degrees as defined by the point where the loss level is 50 percent above the design point loss.

The measured secondary loss of 0.56 percent differential pressure at design point conditions was in good agreement with predictions obtained from the Pratt & Whitney Aircraft secondary loss correlation. Available endwall loss correlations of Dunham and Came (Appendix B - Reference 4) and Mukhtarov and Krichakin (Appendix B - Reference 5) both underestimated the losses.

7.2.2 Transonic 'Aft-Loaded' vs. Subsonic 'Squared-Off' for Root Section

Measured mid-span loss data for both airfoils show that minimum losses are obtained when the airfoils are operating at -12 degrees incidence. 'Squared-off' airfoil has higher mid-span losses (about 18 percent more) than the

'aft-loaded' airfoil at design point. Similar results are obtained for the test conducted to evaluate the influence of Mach numbers (0.78 to 0.94) on losses at design point incidence for these two airfoils. Measured profile loss for the "aft-loaded" airfoil is lower than or equal to that of the "squared off" airfoil over the incidence range tested.

Profile losses predicted by Pratt & Whitney Aircraft profile loss prediction method are in good agreement with the data over the entire range of Mach numbers and incidences.

The secondary losses measurements show that the 'squared-off' airfoil has about 13 percent more loss than the 'aft-loaded' airfoil at the design incidence and Mach number. Measured secondary losses were found to be in good agreement with the Pratt & Whitney Aircraft cascade loss correlation whereas Dunham and Came correlation overestimated the losses and Mukhtarov and Krichakin correlation underestimated them.

7.2.3 'Aft-Loaded' Versus 'Heavyweight' and 'Lightweight' Design for the Mean Section

Measured mid-span total pressure loss data at design incidence and over the entire range of Mach numbers (0.63 to 0.94) investigated in the present test show the 'aft-loaded' baseline airfoil to have the lowest pressure loss while the lightweight airfoil has the highest loss. Compared to the 'aft-loaded' baseline airfoil at design Mach number and incidence, the 'lightweight' design airfoil has a pressure loss that is 34 percent higher while the 'heavyweight' design airfoil is 21 percent higher. Highest profile losses for the 'lightweight' airfoil are possibly due to the larger overspeeds in the leading edge regions of the airfoil at the design point. A redesign of the 'lightweight' airfoil with reduced leading edge overspeed is likely to reduce the profile losses and make it more competitive in performance to the 'aft-loaded' airfoil design.

Measured mid-span total pressure loss data at design Mach number and over an incidence range of $+10^\circ$ to -15° investigated in the present test again show that the 'aft-loaded' airfoil has the lowest loss of the three airfoil packs. The data indicate that the profile loss for the aft loaded airfoil is lower than either the heavyweight or lightweight airfoil for positive incidence whereas all airfoil sections show almost equal losses for negative incidence angles.

No significant influence of the installation of turbulence screens at inlet to the cascade test section was observed on the airfoil mid-span losses.

Measured secondary loss data were found to be in reasonable agreement with the predictions (except for the 'lightweight' airfoil at positive incidence) obtained from Pratt & Whitney Aircraft cascade secondary loss correlation. Dunham and Came (Appendix B - Reference 4) correlations always overestimate secondary losses while Mukhtarov and Krichakin (Appendix B - Reference 5) always underestimate losses.

The overall results of this current study indicate that the 'aft-loaded' airfoil design generates lower losses than the 'squared-off' airfoil design, thus substantiating Pratt & Whitney Aircraft's "design philosophy" for the Energy Efficient Engine low-pressure turbine component.

APPENDIX A-1

COORDINATES FOR LOW CAMBER VANE AIRFOIL*

<u>X/BX</u>	<u>YL/BX</u>	<u>YU/BX</u>
0.0	2.53924	2.53924
0.01650	2.50318	2.56985
0.03300	2.47732	2.57418
0.04950	2.45147	2.57109
0.06600	2.42562	2.55956
0.08250	2.39977	2.54681
0.09900	2.37392	2.53395
0.11550	2.34807	2.52098
0.13200	2.32222	2.50790
0.14850	2.29636	2.49471
0.16500	2.27051	2.48141
0.20625	2.20589	2.44764
0.24750	2.14126	2.41313
0.28875	2.07663	2.37782
0.33000	2.01200	2.34169
0.37125	1.94737	2.30469
0.41250	1.88274	2.26678
0.45375	1.81811	2.22790
0.49500	1.75347	2.18799
0.53625	1.68884	2.14698
0.57750	1.62420	2.10479
0.61875	1.55956	2.06133
0.66000	1.49492	2.01649
0.70125	1.43028	1.97016
0.74250	1.36564	1.92217
0.78375	1.30099	1.87235
0.82500	1.23634	1.82048
0.86625	1.17169	1.76628
0.90750	1.10703	1.70940
0.94875	1.04236	1.64939
0.99000	0.97769	1.58570
1.03125	0.91303	1.51776
1.07250	0.84834	1.44504
1.11375	0.78364	1.36717
1.15500	0.71892	1.28396
1.19625	0.65419	1.19550
1.23750	0.58943	1.10208
1.27875	0.52468	1.00417
1.32000	0.45985	0.90233
1.36125	0.39496	0.79712
1.40250	0.32998	0.68909
1.44375	0.26487	0.57871
1.48500	0.19953	0.46637
1.50150	0.17332	0.42097
1.51800	0.14695	0.37533
1.53450	0.12043	0.32946
1.55100	0.09382	0.28340
1.56750	0.06684	0.23714
1.58400	0.03955	0.19070
1.60050	0.01148	0.14410
1.61700	0.01507	0.09734
1.63350	0.01963	0.05044
1.65000	0.00001	0.00001

* - Divide each number shown in the above three columns by 1.65 to reflect the actual rig size.

APPENDIX A-2

COORDINATES FOR SUBSONIC 'SQUARED-OFF' AIRFOIL*

<u>X/BX</u>	<u>YL/BX</u>	<u>YU/BX</u>
0.0	1.11362	1.11362
0.01480	1.08924	1.14126
0.02960	1.08622	1.15850
0.04440	1.09196	1.17524
0.05920	1.10402	1.19146
0.07400	1.11518	1.20716
0.08880	1.12550	1.22233
0.10360	1.13504	1.23695
0.11840	1.14386	1.25103
0.13320	1.15198	1.26456
0.14800	1.15946	1.27751
0.18500	1.17554	1.30739
0.22200	1.18816	1.33357
0.25900	1.19761	1.35594
0.29600	1.20406	1.37440
0.33300	1.20765	1.38887
0.37000	1.20842	1.39925
0.40700	1.20639	1.40549
0.44400	1.20154	1.40754
0.48100	1.19376	1.40537
0.51800	1.18292	1.39896
0.55500	1.16879	1.38832
0.59200	1.15105	1.37346
0.62900	1.12924	1.35443
0.66600	1.10270	1.33128
0.70300	1.07065	1.30406
0.74000	1.03295	1.27288
0.77700	0.99079	1.23781
0.81400	0.94554	1.19897
0.85100	0.89808	1.15648
0.88800	0.84887	1.11044
0.92500	0.79828	1.06098
0.96200	0.74650	1.00827
0.99900	0.69369	0.95239
1.03600	0.63997	0.89351
1.07300	0.58546	0.83176
1.11000	0.53017	0.76729
1.14700	0.47424	0.70025
1.18400	0.41769	0.63077
1.22100	0.36053	0.55900
1.25800	0.30283	0.48507
1.29500	0.24463	0.40911
1.33200	0.18593	0.33125
1.36800	0.16232	0.29960
1.36160	0.13863	0.26769
1.37640	0.11489	0.23549
1.39120	0.09106	0.20303
1.40600	0.06719	0.17031
1.42080	0.04322	0.13735
1.43560	0.01921	0.10414
1.45040	0.00491	0.07070
1.46520	0.01500	0.03702
1.48000	0.00000	0.00000

* - Divide each number shown in the above three columns by 1.48 to reflect the actual rig size.

APPENDIX A-3

COORDINATES FOR TRANSONIC 'AFT-LOADED' AIRFOIL*

<u>X/BX</u>	<u>YL/BX</u>	<u>YU/BX</u>
0.0	0.91975	0.91975
0.01480	0.89536	0.94832
0.02960	0.89234	0.96690
0.04440	0.89808	0.98475
0.05920	0.90917	1.00186
0.07400	0.91956	1.01827
0.08880	0.92931	1.03401
0.10360	0.93846	1.04907
0.11840	0.94701	1.06350
0.13320	0.95502	1.07728
0.14800	0.96251	1.09045
0.16500	0.97305	1.12073
0.22200	0.99271	1.14738
0.25900	1.00370	1.17057
0.29600	1.01216	1.19038
0.33300	1.01819	1.20695
0.37000	1.02189	1.22033
0.40700	1.02329	1.23059
0.44400	1.02239	1.23778
0.48100	1.01920	1.24191
0.51800	1.01369	1.24301
0.55500	1.00577	1.24108
0.59200	0.99535	1.23611
0.62900	0.98229	1.22806
0.66600	0.96639	1.21690
0.70300	0.94742	1.20257
0.74000	0.92501	1.18498
0.77700	0.89870	1.16405
0.81400	0.86794	1.13967
0.85100	0.83238	1.11167
0.88800	0.79243	1.07990
0.92500	0.74913	1.04415
0.96200	0.70335	1.00416
0.99900	0.65567	0.95963
1.03600	0.60647	0.91020
1.07300	0.55601	0.85562
1.11000	0.50447	0.79588
1.14700	0.45194	0.73118
1.18400	0.39857	0.66192
1.22100	0.34443	0.58859
1.25800	0.28961	0.51176
1.29500	0.23413	0.43196
1.33200	0.17904	0.34966
1.36680	0.15545	0.31613
1.36160	0.13278	0.28232
1.37640	0.11002	0.24820
1.39120	0.08716	0.21382
1.40600	0.06423	0.17920
1.42080	0.04122	0.14435
1.43560	0.01816	0.10929
1.45040	0.00499	0.07404
1.46520	0.01499	0.03860
1.48000	0.00000	0.00000

* - Divide each number shown in the above three columns by 1.48 to reflect the actual rig size.

APPENDIX A-4

COORDINATES FOR HEAVYWEIGHT AIRFOIL*

<u>X/BX</u>	<u>YL/BX</u>	<u>YU/BX</u>
0.0	1.11362	1.11362
0.01480	1.08924	1.14218
0.02960	1.08622	1.16074
0.04440	1.09197	1.17852
0.05920	1.10287	1.19553
0.07400	1.11277	1.21179
0.08880	1.12174	1.22730
0.10360	1.12986	1.24206
0.11840	1.13718	1.25610
0.13320	1.14374	1.26941
0.14800	1.14960	1.28200
0.18500	1.16132	1.31039
0.22200	1.16915	1.33444
0.25900	1.17332	1.35427
0.29600	1.17397	1.36994
0.33300	1.17114	1.38155
0.37000	1.16484	1.38917
0.40700	1.15509	1.39287
0.44400	1.14186	1.39272
0.48100	1.12530	1.38876
0.51800	1.10555	1.38105
0.55500	1.08285	1.36963
0.59200	1.05742	1.35456
0.62900	1.02949	1.33585
0.66600	0.99928	1.31355
0.70300	0.96699	1.28767
0.74000	0.93272	1.25826
0.77700	0.89663	1.22531
0.81400	0.85891	1.18886
0.85100	0.81935	1.14892
0.88800	0.77833	1.10550
0.92500	0.73583	1.05860
0.96200	0.69190	1.00821
0.99900	0.64658	0.95435
1.03600	0.59992	0.89705
1.07300	0.55198	0.83637
1.11000	0.50275	0.77248
1.14700	0.45230	0.70555
1.18400	0.40065	0.63579
1.22100	0.34781	0.56345
1.25800	0.29384	0.48876
1.29500	0.23870	0.41193
1.33200	0.18244	0.33321
1.36900	0.15964	0.30123
1.36160	0.13665	0.26900
1.37640	0.11349	0.23652
1.39120	0.09016	0.20380
1.40600	0.06663	0.17086
1.42090	0.04296	0.13770
1.43560	0.01912	0.10434
1.45040	0.00489	0.07078
1.46520	0.01500	0.03704
1.48000	0.00000	0.00000

* - Divide each number shown in the above three columns by 1.48 to reflect the actual rig size.

APPENDIX A-5

COORDINATES FOR LIGHTWEIGHT AIRFOIL*

<u>X/BX</u>	<u>YL/BX</u>	<u>YU/BX</u>
0.0	1.22129	1.22129
0.01480	1.19692	1.24725
0.02960	1.19390	1.26122
0.04440	1.19963	1.27473
0.05920	1.21000	1.28777
0.07400	1.21954	1.30033
0.08880	1.22831	1.31242
0.10360	1.23637	1.32401
0.11840	1.24376	1.33510
0.13320	1.25050	1.34568
0.14800	1.25664	1.35574
0.18500	1.26946	1.37862
0.22200	1.27894	1.39813
0.25900	1.28527	1.41417
0.29600	1.28859	1.42664
0.33300	1.28895	1.43546
0.37000	1.28638	1.44055
0.40700	1.28081	1.44186
0.44400	1.27212	1.43934
0.48100	1.26015	1.43293
0.51800	1.24461	1.42264
0.55500	1.22507	1.40845
0.59200	1.20097	1.39038
0.62900	1.17146	1.36844
0.66600	1.13603	1.34270
0.70300	1.09554	1.31318
0.74000	1.05156	1.27997
0.77700	1.00515	1.24315
0.81400	0.95690	1.20280
0.85100	0.90719	1.15902
0.88800	0.85625	1.11193
0.92500	0.80425	1.06162
0.96200	0.75134	1.00821
0.99900	0.69760	0.95185
1.03600	0.64311	0.89262
1.07300	0.58792	0.83067
1.11000	0.53210	0.76611
1.14700	0.47571	0.69908
1.18400	0.41877	0.62969
1.22100	0.36130	0.55805
1.25800	0.30334	0.48429
1.29500	0.24495	0.40852
1.33200	0.18612	0.33084
1.36800	0.16247	0.29926
1.36160	0.13875	0.26741
1.37640	0.11497	0.23527
1.39120	0.09111	0.20287
1.40600	0.06722	0.17020
1.42080	0.04324	0.13727
1.43560	0.01922	0.10410
1.45040	0.00488	0.07068
1.46520	0.01499	0.03702
1.48000	0.00001	0.00001

* - Divide each number shown in the above three columns by 1.48 to reflect the actual rig size.

APPENDIX B - REFERENCES

1. Stewart, W.L., Whitney, W.J., and Wong, R.Y.: 'A Study of Boundary Layer Characteristics of Turbomachine Blade Rows and Their Relation to Overall Blade Loss,' Trans. ASME, Journal of Basic Engineering, September 1960, pp. 588-592.
2. Langston, L.S., Nice, M.L., and Hooper, R.M.: 'Three-Dimensional Flow Within a Turbine Cascade Passage,' Journal of Engineering For Power, Trans. ASME, Vol. 99, No. 1, January 1977.
3. Kopper, F.C., Milano, R., and Vanco, M.: 'An Experimental Investigation of Endwalls Profiling in a Turbine Vane Cascade,' Paper presented at the AIAA/SAE/ASME 16th Joint Propulsion Conference, June 30 - July 2, 1980, Hartford, Connecticut.
4. Dunham, J., and Came, P.M., 'Improvement to the Ainley-Mathieson Method of Turbine Performance Prediction,' Journal of Engineering for Power, Trans. ASME, July 1976.
5. Mukhtarov, M.Kh., and Krichakin, V.I.: 'Procedure for Estimating Flow Section Losses in Axial Flow Turbines When Calculating Their Characteristics,' Teploenergetika, 1969, 18 (7) pp. 76-79.
6. Sharma, O.P., Wells, R.A., Schlinker, R.H., and Bailey, D.A., 'Boundary Layer Development on Turbine Airfoil Suction Surfaces,' ASME Gas Turbine Paper No. 81-GT-204, Paper presented at 1981 Gas Turbine Conference in Houston Texas, March 1981.

Also:

Gardner, W.B., 'Energy Efficient Engine Low-Pressure Turbine Boundary Layer Program Technology Report,' NASA CR-165338, PWA-5594-141, April 1981.

APPENDIX C
LIST OF SYMBOLS

<u>SYMBOL</u>	<u>DESCRIPTION</u>
BX	Axial chord
P	Static Pressure
P _T	Total Pressure
Re _{BX}	Reynolds number based on axial chord and exit conditions
X	Axial distance
α, β	Air angle measured from tangential directions (see Figure 3.5)

DISTRIBUTION LIST

GOVERNMENT AGENCIES

NASA Headquarters
600 Independence Ave., SW
Washington, D.C. 20546
Attention: RTP-6/R.S. Colladay
RTP-6/C.C. Rosen
RTM-6/L. Harris
RRP-6/J. Facey
Library

NASA-Lewis Research Center
21000 Brookpark Road
Cleveland, OH 44135
Attention: D. L. Nored

C. C. Ciepluch
J. W. Schaefer
P. G. Batterton
G. K. Sievers
Library
Report Control Office
Tech Utilization Office
M. A. Beheim
M. J. Hartmann
R. A. Rudey
R. A. Weber
W. C. Strack
T. P. Moffitt
J. E. Rohde
A. Long
W. M. Braithwaite
L. Reid
AFSC Liaison Office
Army R&T Propulsion Lab

MS 301-2
MS 301-4 (20 copies)
MS 301-4
MS 301-4
MS 301-2
MS 60-3 (2 copies)
MS 5-5
MS 3-19
MS 3-5
MS 5-7
MS 86-5
MS 500-127
MS 501-10
MS 77-2
MS 77-2
MS 500-305
MS 500-208
MS 5-9
MS 501-3
MS 302-2

DISTRIBUTION LIST (Continued)

NAVAL AIR Propulsion Test Center
Trenton, NJ 08628
Attention: J. J. Curry
A. A. Martino

U.S. Naval Air Test Center
Code SY-53
Patuxent River, MD 20670
Attention: E. A. Lynch

USAVRAD Command
PO Box 209
St. Louis, MO 63166
Attention: Robert M. Titus (ASTIO)

Department of Transportation
NASA/DOT Joint Office of Noise Abatement
Washington, D.C. 20590
Attention: C. Foster

Federal Aviation Administration
Noise Abatement Division
Washington, D.C. 20590
Attention: E. Sellman AEE-120

Environmental Protection Agency
1835 K Street, NW
Washington, D.C. 20460
Attention: J. Schettino
J. Tyler

Environmental Protection Agency
2565 Plymouth Road
Ann Arbor, MI 48105
Attention: R. Munt

Federal Aviation Administration
12 New England Executive Park
Burlington, MA 18083
Attention: Jack A. Sain, ANE-200

ENGINE MANUFACTURERS

Curtiss Wright Corporation
Woodridge, NJ 07075
Attention: S. Lombardo
S. Moskowitz

Detroit Diesel Allison Div. G.M.C.
P.O. Box 894
Indianapolis, IN 46206
Attention: W. L. McIntire

Cummins Engine Co.
Technical Center
500 S. Poplar
Columbus, IN 47201
Attention: J. R. Drake

AVCO/Lycoming
550 S. Main Street
Stratford, CT 06497
Attention: H. Moellmann

Detroit Diesel Allison Div. G.M.C.
333 West First Street
Dayton, Ohio 45402
Attention: F. H. Walters

The Garrett Corporation
AIRResearch Manufacturing Co.
Torrance, CA 90509
Attention: F. E. Faulkner

The Garrett Corporation
AIRResearch Manufacturing Co.
402 S. 36 Street
Phoenix, AZ 85034
Attention: Library

General Electric Co./AEG
One Jimson Road
Evendale, Ohio 45215
Attention: R. W. Bucy (3 copies)
T. F. Donohue

Pratt & Whitney Aircraft Group/UTC
Government Products Division
P.O. Box 2691
West Palm Beach, FL 33402
Attention: B. A. Jones

The Garrett Corporation
AIRResearch Aviation Co.
19201 Susana Road
Compton, CA 90221
Attention: N. J. Palmer

DISTRIBUTION LIST (Continued)

AIRResearch Manufacturing Co.
111 South 34th Street
P.O. Box 5217
Phoenix, AZ 85010
Attention: C. E. Corrigan
(93-120/503-4F)

Williams Research Co.
2280 W. Maple Road
Walled Lake, MI 48088
Attention: R. VanNimwegen
R. Horn

Teledyne CAE, Turbine Engines
1330 Laskey Road
Tolendo, Ohio 43612
Attention: R. H. Gaylord

General Electric Co./AEG
1000 Western Ave.
Lynn, MA 01910
Attention: R. E. Neitzel

Pratt & Whitney Aircraft Group/UTC
Commercial Products Division
East Hartford, CT 06108
Attention: W. Gardner
I. Mendelson

AIRFRAME MANUFACTURERS

Boeing Commercial Airplane Co.
P.O. Box 3707
Seattle, WA 98124
Attention: P. E. Johnson MS 9H-46
D. C. Nordstrom MS 73-01

Boeing Aerospace Co.
P.O. Box 3999
Seattle, WA 98124
Attention: D. S. Miller MS 40-26
H. Higgins

The Boeing Co., Wichita Division
Wichita, KS 67210
Attention: D. Tarkelson

Douglas Aircraft Company
McDonnell Douglas Corp.
3855 Lakewood Boulevard
Long Beach, CA 90846
Attention: R. T. Kawai Code 36-41
M. Klotzsche

Lockheed California Co.
Burbank, CA 91502
Attention: J. F. Stroud, Dept. 75-42
R. Tullis, Dept. 75-21
J. I. Benson

General Dynamics Convair
P. O. Box 80847
San Diego, CA 92138
Attention: S. Campbell, MZ 632-00

Rockwell International
International Airport
Los Angeles Division
Los Angeles, CA 90009
Attention: A. W. Martin

Gates Learjet Corp.
P. O. Box 7707
Wichita, KS 67277
Attention: E. Schiller

McDonnell Aircraft Co.
McDonnell Douglas Corp.
P. O. Box 516
St. Louis, MO 63166
Attention: F. C. Claser Dept. 243

Lockheed Georgia Co.
Marietta, GA 30060
Attention: H. S. Sweet

Grumman Aerospace Corp.
South Oyster Bay Road
Bethpage, New York 11714
Attention: C. Hoeltzer

Airlines

American Airlines
Maint. & Engr. Center
Tulsa, OK 74151
Attention: W. R. Neeley

Eastern Airlines
International Airport
Miami, FL 33148
Attention: A. E. Fishbein

Delta Airlines, Inc.
Hartsfield-Atlanta International Airport
Atlanta, GA 30320
Attention: C. C. Davis

DISTRIBUTION LIST (Continued)

TransWorld Airlines
605 Third Avenue
New York, NY 10016
Attention: A. E. Carrol

Pan American World Airways, Inc.
JFK International Airport
Jamica, NY 11430
Attention: J. G. Borger
A. MacLarty

United Airlines
San Francisco International Airport
Maint. Operations Center
San Francisco, CA 94128
Attention: J. J. Overton

Hamilton Standard
Bradley Field
Windsor Locks, CT 06096
Attention: P. J. Dumais, MS 1A-3-1
A. T. Reiff, MS 1-2-2

Fluidyne Engineering Corp.
5900 Olson Memorial Highway
Minneapolis, MN 55422
Attention: J. S. Holdhusen

Rohr Corporation
P.O. Box 878
Foot & H Street
Chula Vista, CA 92012
Attention: Library

Solar Division
International Harvester
2200 Pacific Highway
San Diego, CA 92112
Attention: Library

Pennsylvania State University
Department of Aerospace Engineering
233 Hammond Building
University Park, Pennsylvania 16802
Attention: Dr. B. Lakshminarayana

Gas Dynamics Laboratories
Aerospace Engineering Building
University of Michigan
Ann Arbor, MI 48109
Attention: Dr. C. W. Kaufmann

Massachusetts Inst. of Technology
Dept. of Astronautics & Aeronautics
Cambridge, MA 02139
Attention: Jack Kerrebrock

Massachusetts Inst. of Technology
Dept. of Structural Mechanics
Cambridge, MA 02139
Attention: James Mar

Westinghouse Electric Corp.
P.O. Box 5837
Beulah Road
Pittsburgh, PA 15236
Attention: Library

University of Tennessee
Space Institute
Tullahoma, TN 37388
Attention: Dr. V. Smith

TRW Equipment Group
TRW Inc.
23555 Euclid Ave.
Cleveland, OH 44117
Attention: I. Toth

Aerospace Corporation
R & D Center
Los Angeles, CA 90045
Attention: Library

George Shevlin
P.O. Box 1925
Washington, D.C. 20013

Brunswick Corporation
2000 Brunswick Lane
Deland, FL 32720
Attention: A. Erickson

Iowa State University
Department of Mechanical Engineering
Ames, Iowa 50011
Attention: Dr. Patrick Kavanagh

Detroit Diesel Allison
PO Box 894
Indianapolis, Indiana 46206
Attention: Mr. Robert Delanie
Speed Code U29A